Integrative investigation of plant long-distance electric signaling: a spatial, analytical, and optogenetic dissection

Inaugural dissertation

for the attainment of the title of doctor
in the Faculty of Mathematics and Natural Sciences
at the Heinrich Heine University Düsseldorf

presented by

Juan Camilo Barbosa Caro
from Bogotá, Colombia

Düsseldorf, 02/2025

from the institute for Molecular Physiology
at the Heinrich Heine University Düsseldorf

Published by permission of the
Faculty of Mathematics and Natural Sciences at
Heinrich Heine University Düsseldorf

Supervisor: Prof. Dr. Wolf B. Frommer
Co-supervisor: Dr. Michael M. Wudick

Date of the oral examination: 19.05.2025

STATUTORY DECLARATION

I, Juan Camilo Barbosa Caro, solemnly declare under oath that the present dissertation was prepared by me independently and without any improper external assistance, in compliance with the "Principles for Ensuring Good Scientific Practice at Heinrich Heine University Düsseldorf."

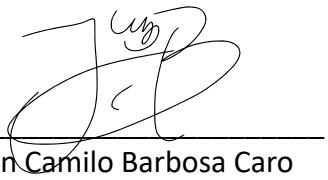

_____

Juan Camilo Barbosa Caro

06.2.2025, Düsseldorf

Summary

Plants can generate a systemic response to local damage. The coordination of that response in unstimulated tissue requires information delivery from the wounded site. The defense response-initiating signal is known as Slow Wave Potential (SWP), which is recorded as a membrane potential (V_m) depolarization and an increase in cytosolic calcium concentration ($[Ca^{2+}]_{cyt}$).

In the model plant *Arabidopsis thaliana,* multiple proteins have been identified to underlie the SWP. Notably, two members of the ligand-sensitive ion channel GLutamate Receptor-like (GLR) family, GLR3.3 and GLR3.6, are collectively necessary for initiating the SWP. Also, the Mechanosensitive of Small conductance-like channel (MSL) 10 contribute to a full length SWP signal.

This dissertation aims to understand the mechanisms underlying SWP propagation and generation. To elucidate molecular mechanisms in signal generation we aimed to identify a possible feedback loop between $[Ca^{2+}]_{cyt}$ and MSL10. Furthermore, we enhanced SWP quantification by mathematically assessing multiple signal components. We used this increased analytical resolution to develop and validate a high-throughput protocol for reverse genetic screening of SWP generation-involved genes.

Propagation of the SWP is explained by three hypotheses. (I) Chemical propagation - wound-related molecules are transported through the vasculature to intact leaves. (II) mechanical or hydraulic propagation - the rupture of the plant vasculature generates abrupt decompression along the system, i.e., a propagating mechanical stimulus. (III) green cable hypothesis - the vasculature can sustain self-propagating electric signals which support SWP spread, analog to neuronal signal propagation.

To elucidate the SWP propagation mechanism, we initiated by experimentally testing the green cable hypothesis. To assert the capacity of depolarization activated, self-propagating signals, we used channelrhodopsins - genetically encoded molecular tools

that allow precise control of V_m and $[Ca^{2+}]_{cyt}$. We determined that V_m depolarization does not generate self-propagating signals, but $[Ca^{2+}]_{cyt}$ does initiate an electric wave that propagates at SWP-comparable speed.

Furthermore, to determine the contribution of such self-propagating signals to SWP transmission, we combined increased analytical and spatial resolution to compare the arrival time of molecular components and of the SWP. We could resolve that different components of the SWP propagate at different speed along the petiole. Remarkably, the molecular cues arrive simultaneously with the first SWP component, hinting that the chemical propagation hypothesis is the leading transmission mechanism.

Table of contents

Introduction

Plants defend themselves against herbivorous attacks. As physical avoidance of the attacker is often unattainable, plants can coordinate within minutes a systemic production of defense molecules that deter herbivores from their action. Namely, resistance to herbivory depends on a group of regulatory lipids known as jasmonates (Howe and Jander, 2008; Browse, 2009). Communication of a local event to the rest of the plant within minutes is fast in the plant context (Lacombe and Achard, 2016). This is the case of a wounding event, where the transmission of information is achieved via rapidly propagating electric signals (Meyer and Weisenseel, 1997; Förster *et al.*, 2019; Farmer *et al.*, 2020; Fromm and Lautner, 2007). Wounding-induced cell depolarization is tightly linked to the increase of cytosolic calcium ($[Ca^{2+}]_{cyt}$), which can propagate systemically (Fisahn *et al.*, 2004) that, in turn, induces the defensive response (Ding *et al.*, 2024).

The systemic, long-distance electric signal in plants is known as a Slow Wave Potential (SWP). This depolarizing signal can be recorded from the surface of the tissue, and is generated in response to wounding and heat, for instance (Fisahn *et al.*, 2004; Stanković and Davies, 1996; Stanković *et al.*, 1997). In the model plant *Arabidopsis thaliana*, the SWP can be observed in leaves with direct vascular connection to the wounded leaf (Mousavi *et al.*, 2013). Locally, only seconds after the onset of the wound-induced electric signal, the $[Ca^{2+}]_{cyt}$ increases (Nguyen *et al.*, 2018), likely via influx through the Glutamate Receptor-Like (GLR) channels 3.3 and 3.6 (Mousavi *et al.*, 2013; Stephens *et al.*, 2008; Green *et al.*, 2021). Absence of GLR3.3 and GLR3.6 hinder SWP initiation and render the plants more vulnerable to herbivory.

Other proteins have been identified to underlie the SWP. The anion-permeable, mechanosensitive channel MSL10 is necessary for full activation of the signal (Moe-Lange *et al.*, 2021), while the proton pump AHA1 is important for the signal to return to baseline (Kumari *et al.*, 2019). However, further identification of proteins involved in this signal has proven challenging as the SWP, also known as variation potential, is a signal of highly

variable shape. Therefore, it is particularly troublesome to match a gene mutation with a change in shape of an inherently irregular signal.

Alongside the identification of proteins contributing to SWPs, understanding how this signal rapidly travels from the wounded site is an ongoing research effort. Three main hypotheses try to explain the transmission of the SWP. An early proposed chemical transmission hypothesis (Ricca, 1926), that has resurfaced after a century in the *Arabidopsis* SWP context (Gao *et al.*, 2023; Bellandi *et al.*, 2022), proposes that the transmission of this signal occurs by rapid propagation of bioactive molecules. Two main mechanisms attempt to explain how this chemical movement overcomes simple diffusion: bulk flow (Bellandi *et al.*, 2022), and turbulent diffusion (Vodeneev *et al.*, 2015). Another SWP transmission hypothesis is based on hydraulic propagation, which suggests that wound-induced vasculature rupture generates a pressure collapse that is rapidly perceived in distant, intact, vascular bundles (Malone, 1996; Malone and Stankovic, 1991; Moe-Lange *et al.*, 2021).

Thirdly, the electric propagation hypothesis is explained in the green cable theory, and proposes that electric signals can travel independently, in a self-propagating fashion, through specialized phloem cells (Hedrich *et al.*, 2016a; Hedrich and Becker, 1994). This theory is based on the occurrence in plants of component elements analogous to those that sustain animal Action Potentials (AP). The AP is a self-propagating, long distance electric signal that serves as rapid information carrying unit in neurons and muscles (de Bakker *et al.*, 2021; Barnett and Larkmann, 2007). The properties of an AP in plants have been thoroughly studied in fresh water algae Charophytes, and in the carnivorous plant *Dionaea muscipula* (Beilby, 2007; Brownlee, 2022). However, the AP studied in the model plant *Arabidopsis thaliana* has not been biophysically characterized, rendering the evaluation of this propagating hypothesis in the context of wound-induced SWPs an ungrounded task.

In this work, I present a comprehensive dissection of what is known about the *Arabidopsis* SWP, aiming to understand the phenomenon from two main aspects: propagation and

generation. This separation of concepts is essential as they are in constant interplay but are fundamentally different. Generation refers to the cellular process and molecular actors that sustain the observed signal, while propagation is the mechanism by which the generation process occurs over distance (Vodeneev *et al.*, 2015). For example, in the case of self-propagating APs, propagation and generation are inherently linked by a self-generating process, while in the case of mere chemical signaling, propagation happens by simple diffusion of a signaling molecule, and generation by receptor recognition of that molecule and transduction into an intracellular signal.

What we know about the molecular components underlying SWPs, and the mechanism of SWP propagation is thoroughly reviewed in chapter 1. Subsequently, I aimed to experimentally characterize the AP in *Arabidopsis* by means of versatile optogenetic tools, newly available in plants (Zhou *et al.*, 2021; Ding *et al.*, 2024). Particularly I am addressing the following questions: Is the *Arabidopsis* leaf tissue electrically excitable? Is the increase in $[Ca^{2+}]_{cyt}$ a consequence or an initiator of electric signaling? How can we transfer and compare what we know about the *Dionaea* AP to the *Arabidopsis* SWP? In chapter 2, I address these questions and the implications that the answers might have on SWP generation and propagation. Lastly, in chapter 3, I present an initial effort to understand unknown aspects of SWP generation. Namely, the characterization of the proposed feedback loop between $[Ca^{2+}]_{cyt}$ and MSL10 (Moe-Lange *et al.*, 2021), and a screening to identify new proteins underlying *Arabidopsis* long-distance electric signal.

Chapter 1 – Revisiting plant electric signaling: Challenging an old phenomenon with novel discoveries

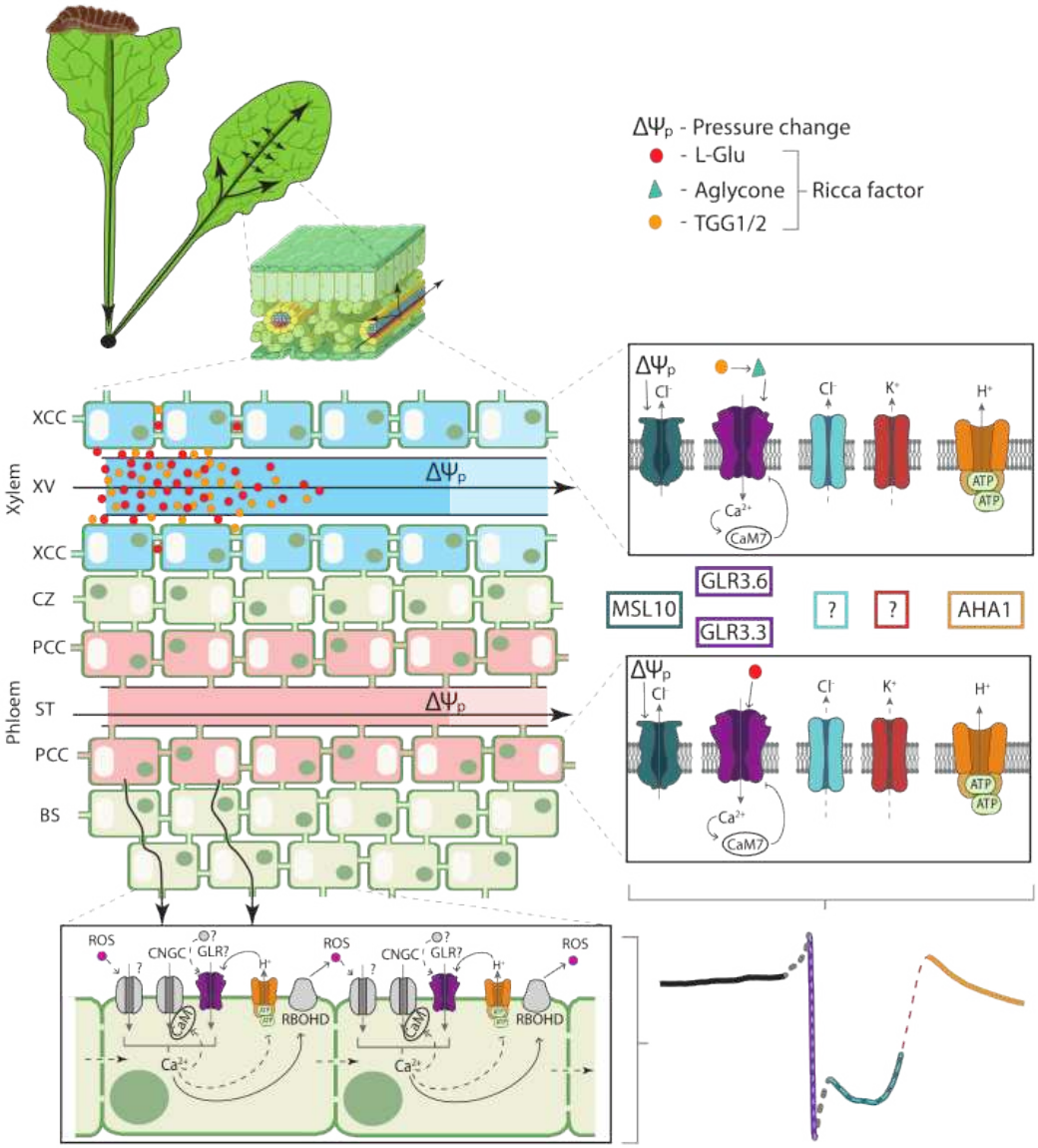

Status: Published

Journal: Current Opinion in Plant Biology

Contribution to this chapter: This chapter was written by Juan Camilo Barbosa-Caro with editorial assistance of Michael Wudick.

Available online at www.sciencedirect.com

ScienceDirect

Current Opinion in Plant Biology

ELSEVIER

Review

Revisiting plant electric signaling: Challenging an old phenomenon with novel discoveries

Juan Camilo Barbosa-Caro[1] and Michael M. Wudick[1,2]

Abstract

Higher plants efficiently orchestrate rapid systemic responses to diverse environmental stimuli through electric signaling. This review explores the mechanisms underlying two main types of electric signals in plants, action potentials (APs) and slow wave potentials (SWPs), and how new discoveries challenge conventional neurophysiological paradigms traditionally forming their theoretical foundations. Animal APs are biophysically well-defined, whereas plant APs are often classified based on their shape, lacking thorough characterization. SWPs are depolarizing electric signals deviating from this shape, leading to an over-simplified classification of plant electric signals. Indeed, investigating the generation and propagation of plant APs and SWPs showcases a complex interplay of mechanisms that sustain self-propagating signals and internally propagating stimuli, resulting in membrane depolarization, cytosolic calcium increase, and alterations in reactive oxygen species and pH. A holistic understanding of plant electric signaling will rely on unraveling the network of ion-conducting proteins, signaling molecules, and mechanisms for signal generation and propagation.

Addresses

[1] Heinrich Heine University Düsseldorf, Faculty of Mathematics and Natural Sciences, Institute for Molecular Physiology, 40225 Düsseldorf, Germany

[2] Heinrich Heine University Düsseldorf, Faculty of Mathematics and Natural Sciences, Cluster of Excellence on Plant Sciences, 40225 Düsseldorf, Germany

Corresponding author: Wudick, Michael M. (wudick@hhu.de)

Current Opinion in Plant Biology 2024, **79:**102528

This review comes from a themed issue on **Cell biology and cell signalling 2024**

Edited by **Arun Sampathkumar** and **Masayoshi Nakamura**

For complete overview of the section, please refer the article collection - Cell biology and cell signalling 2024

Available online 28 March 2024

https://doi.org/10.1016/j.pbi.2024.102528

Keywords:

Plant electrical signaling, Action potential, Slow wave potential, Long-distance signaling.

Introduction

Plants encounter diverse environmental stimuli, leading to the generation of both local and plant-wide responses. To achieve effective systemic responses, plants engage in long-distance, inter-tissue communication, requiring the relay of the initial trigger over extended distances.

This process may involve chemical cues, including phytohormones, peptides, amino acids, or RNA molecules [1–3]. These signaling compounds are transported through the apoplasm of the vasculature or symplasmically through plasmodesmata, which serve as plant cell–cell contact sites [4]. The propagation speed of these signals varies, with rates of around a few µm/s for non-vascular propagation and 0.02–0.04 cm/s for mass flow in the vasculature [4]. In situations requiring immediate responses, such as during herbivore attack, the systemic transmission of signals and subsequent responses occur at rates equal to or faster than those associated with vascular mass flow (Table 1). This fast transmission is associated with electric signaling events, of which we will focus on action potentials (APs) and slow wave potentials (SWPs) here. In animals, APs are characterized by the "all-or-nothing" principle, constant speed and amplitude, voltage dependency, and refractory period. In plants, however, the classification of electric signals has been historically phenomenological, categorizing signals by shape, but not biophysically, as APs. While any other propagating, long-lasting, depolarizing, and slow signal is typically labeled as SWP [5,6].

Plant APs have been mainly associated with rapid movements during lobe closure in Venus flytrap (*Dionaea muscipula*) or leaf movement in Mimosa (*Mimosa pudica*), but their existence has also been proposed in various other species [5,18,24,29–32]. While APs in *Mimosa* or *Dionaea* can be readily recorded with extracellular electrodes, the detection of signals classified as APs in other vascular plants usually relies on intracellular recordings with aphids. This suggests that the AP is cell-specific and may be obscured by the activity of surrounding cells, when recorded with surface electrodes. Though the mechanisms governing the rapid propagation of plant electric signals remain a topic of ongoing discussion that has been enriched by recent discoveries, yet the fundamental phenomena comprising AP and

Table 1

Comparison of electrical signal transmission speeds in diverse plant systems [7–28].

System	Stimulus	Signal readout	Speed (cm/s)	Reference
14–21-day-old wheat (*Triticum aestivum*) leaf	leaf tip burning	water pressure - leaf shape change by optical coherence microscopy (OCM)	~ 1500	[5]
Dionaea muscipula	sensory hair touch	surface potential	10 - 40	[6]
		$[Ca^{2+}]_{cyt}$ increase	2 – 5.3	[7]
Chara braunii	extracellular voltage pulse	intracellular membrane potential via impalement	1.5 ± 0.07	[8]
Nitella mucronata	extracellular voltage pulse	intracellular membrane potential via impalement	0.69 ± 0.01	[9]
Mimosa pudica	touch	surface potential	0.55 ± 0.04	[10]
		$[Ca^{2+}]_{cyt}$ increase	0.56 ± 0.07	
	wound	surface potential	0.43 ± 0.04	
		$[Ca^{2+}]_{cyt}$ increase	0.41 ± 0.05	
4–5-week-old Arabidopsis leaf 13	leaf 8 wound	surface potential	0.16 ± 0.05	[11]
			0.17 ± 0.02	[12]
			~ 0.18	[13]
			~ 0.11	[14]
		$[Ca^{2+}]_{cyt}$ increase	0.15 ± 0.05	[11]
		NaFluo dye propagation	~ 0.15	[15]
22–25-day-old *Helianthus annuus*	1-2 V stimulus at plant base	extracellular membrane potential – inserted electrodes	0.18 ± 0.02	[16]
5–6-week-old Arabidopsis leaf	9 V stimulus at leaf blade	surface potential	0.13 ± 0.03	[20]
6–7-week-old Arabidopsis leaf	2.5-18 V stimulus at leaf blade	intracellular membrane potential through aphid	0.08-0.19	[18]
14–day-old *Marchantia*	puncture wound	membrane depolarization	0.1 – 0.2	[19]
		$[Ca^{2+}]_{cyt}$ increase		
4–5-week-old Arabidopsis leaf	~38 mN mechanic stimulus	intracellular membrane potential through aphid	0.1 ± 0.015	[20]
14–21-day-old wheat (*Triticum aestivum*) leaf	leaf tip burn	surface potential	0.4 – 0.07 (deaccelerating)	[5]
22–25-day-old *Helianthus annuus*	leaf tip burn	surface potential – inserted electrodes	0.42 ± 0.01 – 0.08 ± 0.03	[16]
14-day-old *Vicia faba*	leaf tip burn	surface potential – inserted electrodes	0.1	[21]
Dionaea muscipula	leaf blade cut	$[Ca^{2+}]_{cyt}$ increase	0.12 ± 0.017	[7]
14-day-old *Marchantia* thallus	puncture wound	surface potential	0.1 – 0.2	[19]
		$[Ca^{2+}]_{cyt}$ increase		
2-week-old Arabidopsis leaf	caterpillar wound	$[Ca^{2+}]_{cyt}$ increase	~ 0.013	[11]
11–13-day-old Arabidopsis cotyledon	vasculature cut wound	$[Ca^{2+}]_{cyt}$ increase	0.01 - 0.05	[22]
9–10-day-old Arabidopsis cotyledon	puncture wound	$[Ca^{2+}]_{cyt}$ increase	~ 0.00075	[22]
Conocephalum conicum thallus	0.1-0.8 V stimulus in thallus	surface potential & intracelular membrane potential through impalement	n.d.	[23]
Stem, petioles, and leaf lamina of 4-leaf-stage *Solanum lycopersicum*	root-knot nematode (*Meloidogyne incognita*) infections	surface potential	n.d.	[24]
Leaves 1, 2, 3 of 5-day-old *Oryza sativa*	root ablation	surface potential	n.d.	[25]
Physcomitrium patens protonema & gametophyte	H_2O_2 (0.5 - 5 mM)	Intracellular membrane potential through impalement & $[Ca^{2+}]_{cyt}$ increase	n.d.	[26]
	glutamate (0.05 - 30 mM)	Intracellular membrane potential through impalement & $[Ca^{2+}]_{cyt}$ increase	n.d.	[27]

Species are color-coded, transmission speeds sorted from fast (black) to slow (gray). n.d. – not determined.

SWP are poorly understood and conceptually entangled. In this review, we propose an organization in terms of *generation* and *propagation* of APs and SWPs in order to understand the contribution of molecular actors to either type of signal. While *generation* is the result of the activation of ion-permeable membrane proteins that commonly causes the change in membrane potential and $[Ca^{2+}]_{cyt}$ increase (Figure 1a), *propagation* is the physical mechanism by which this channel activation progresses over distance enabling long-distance signaling (Figure 1b).

Rapid electric signals in plants

The exploration of rapid signal propagation in biological systems has its origins in electrophysiological experiments, pioneered by Luigi Galvani's frog-leg experiments in 1791 [33,34]. Following Darwin's suggestion, Burdon-Sanderson (1873) documented the first plant electric signal, triggered by the bending of sensitive hairs on the *Dionaea* leaf lobe [35,36].

The ground-breaking work of Hodgkin and Huxley in parallel to the work of Cole and Curtis on understanding the generation of electric signals in the electrically excitable single cells of squid (*Loligo*) and the charophyte alga *Nitella* solidified the understanding of biological electric signals as the movement of ions across living membranes [37–39] (Figure 1a). This concept laid the foundation to understand electric excitability in animal neurophysiology, which is the base of AP generation. However, in plants, the recognition of electric signaling in long-distance information transmission gained significant momentum only in the last decades through few seminal publications.

Data collected from excitable plants, including charophyte algae *Chara* or *Nitella*, or the vascular plants *Dionaea* and *Mimosa*, provided valuable mechanistic insights into plant APs and enabled the comparison between plant and animal systems. For instance, in *Mimosa*, APs triggered by mechanical stimulation of a leaflet induce depolarization, followed by an increase in $[Ca^{2+}]_{cyt}$ and leaflet closure. Recently, this mechanism was linked to deterrence of herbivorous attacks in *Mimosa* [12]. In *Dionaea*, rapid leaf closure is triggered by an increase in $[Ca^{2+}]_{cyt}$ [9,40], preceded by a depolarizing electric signal [8] proposed to be initiated by the mechanosensitive channel FLY Catcher 1 (*Dm*FLYC1) at the bending hinge of specialized sensitive hairs [41]. Interestingly, there seems to be a parallel in the observed sequence of events between leaf closure in these excitable plants and neuronal synaptic transmission in animals: stimulus, membrane depolarization, $[Ca^{2+}]_{cyt}$ increase, cellular response (Figure 1a–e). However, as our understanding of plant electrophysiology deepens, it becomes evident that its foundations diverge from animal neurophysiological paradigms.

Unlike APs, SWPs propagate slower and can be triggered by diverse stimuli [42,43] (Table 1). Wound-induced SWPs lead to the activation of defense mechanisms *via* production of jasmonates [44]. This possibly involves membrane depolarization-induced phase changes in chloroplastic lipids, which act as jasmonate precursors [45]. Importantly, these complex signals can propagate through dead tissue or artificial aqueous connections [15,17,42,46,47]. In excitable plants, SWPs coexist with APs in the same tissue with distinct kinetics and extend beyond the AP-generating leaf domain. For instance, when a *Dionaea* leaf is wounded or exposed to cold, both the AP-generating lobe and other parts of the leaf depolarize resulting in a non-AP signal [8,9]. In *Mimosa*, wounding the leaflets generates an SWP that appears to overlay with the AP [12,48]. Interestingly, wound-induced SWPs have been extensively observed in both vascular and non-vascular plants, even in those lacking the electric excitability seen in *Dionaea* and *Mimosa*. Such signals were reported in moss (*Physcomitrium*

patens), liverworts (*Conocephalum conicum* and *Marchantia polymorpha*), and the model dicot plant *Arabidopsis thaliana* [21,43,44,49].

Mechanisms of signal propagation

The key features of an animal AP are threshold-activation, constant amplitude and speed ("all-or-nothing"), self-propagation, and a post-stimulation inactivity phase (refractory period) [50] (Figure 1b–d). Such characteristics are the foundation of a self-propagating signal, stemming from its self-generating nature granted by the activity of voltage dependent channels [51]. More precisely, a local stimulus triggers an intensity-dependent depolarization that, upon surpassing a threshold, initiates a series of channel activation, deactivation, and inactivation events (Figure 1c).

In plants, AP-like signals have been reported, but whether they fulfill the mentioned animal AP characteristics remains unaddressed in many cases. For instance, APs observed in *Dionaea* and *Mimosa* appear to propagate through a comparable mechanism, and specific plant-voltage-dependent channels that may sustain this phenomenon have been suggested based on transcriptomic data [40]. However, in *Dionaea*, the AP amplitude and speed fluctuate, depending on the leaf's prior excitation events [8]. This contrasts with the constant amplitude, and stimulus-independency of neuronal action potentials [50], suggesting a fundamentally distinct mechanism in plants (Figure 1d). A theoretical approximation to plant-specific electric signaling mechanisms, based on ion-homeostats, was recently published and could be the biophysical foundation for plant APs [52].

Self-propagating APs in plants other than *Dionaea* or *Mimosa* have been proposed, but our fundamental understanding of the underlying mechanisms is incomplete. Specifically, a mechanically induced AP was documented in *Arabidopsis thaliana* [37]; however, a recent comprehensive re-evaluation revealed that these electric signals do not present the constant amplitude of a typical "all-or-nothing" AP [22].

In the same species, an AP can be triggered by a 2.5- to 18-V stimulus in the leaf blade [19,20]. Yet, the positive correlation of the electrical response speed and amplitude to the stimulus intensity, and the propagation speed similar to that of SWP (Table 1), suggest that it is likely more similar to a wound-induced SWP than an AP. The ability of vascular plants, beyond *Dionaea* and *Mimosa*, to generate self-propagating APs remains unsettled as the link between signal propagation and generation through voltage-dependent channels is unclear. Therefore, understanding propagating electric signals may require a conceptual framework that goes beyond an animal-AP-centric perspective.

Other propagation mechanisms have been proposed for SWPs. Particularly in Arabidopsis leaves and petioles, propagation of SWPs can be categorized into two multicomponent, not mutually exclusive mechanisms, which refute the initial SWP definition as hydraulically induced depolarizations [6]. The first involves a combination of coincidentally propagating stimuli—hydraulic and chemical. The second mechanism entails a self-propagating signal that includes membrane depolarization, changes in $[Ca^{2+}]_{cyt}$, and reactive oxygen species (ROS) [4,53–56] (Figure 1f).

Historically, the involvement of a signaling chemical called Ricca's factor was proposed to contribute to the propagation of electric $[Ca^{2+}]_{cyt}$ signals upon wounding [23]. Gao *et al.* recently suggested that aglycone, the metabolic product of the enzymes β-thioglucoside glucohydrolase 1 and 2 (TGG1 and 2), together with glutamate, could serve as the Ricca's factor in SWP in leaf-to-leaf propagation [17] (Figure 1f). The rapid propagation speed of the Ricca's factor (~0.15 cm/s) is too fast to be explained by simple diffusion (Table 1), leading to proposals of other mechanisms, such as vasculature transport by bulk flow, Taylor dispersion, or turbulent diffusion due to irregular xylem architecture [7,17,23].

Simultaneously, a hydraulic wave is hypothesized to occur in response to pressure collapse ($\Delta\Psi_p$) in damaged tissues [6,14]. This wave presumably acts as a vehicle for the propagation of Ricca's factor and may also serve as a stimulus—a hypothesis supported by the involvement of the Mechanosensitive channel of Small conductance-Like 10 (MSL10) in SWP generation [14] (Figure 1f).

In addition, and contrasting with the mobile stimuli mentioned so far, a self-propagating signal may persist through the interplay of membrane depolarization, $[Ca^{2+}]_{cyt}$ release, and changes in pH and ROS. Originally proposed to sustain responses to salt stress [57,58], these interconnected feedback loops are hypothesized to play a role in mediating some stage of the SWP propagation, possibly in the radial, plasmodesmata-dependent, slower transmission out of the vasculature [16] (Figure 1f), with comprehensive details provided in a recent review [4].

The presented propagation mechanisms may function differently, depending on tissue type, stimulus, and organism. For instance, recent research has shed light on how wound-induced, long-distance signal propagation occurs in *Marchantia polymorpha* [21], a liverwort belonging to the group of basic, non-vascular plants [43]. The kinetics and speed of the electric signal resemble those of wound-induced SWPs in Arabidopsis (Table 1). Given the phenomenological definition of the SWP as a non-AP-like signal [5,6], we raise the question of whether the long, variable, depolarizing signal observed

Figure 1

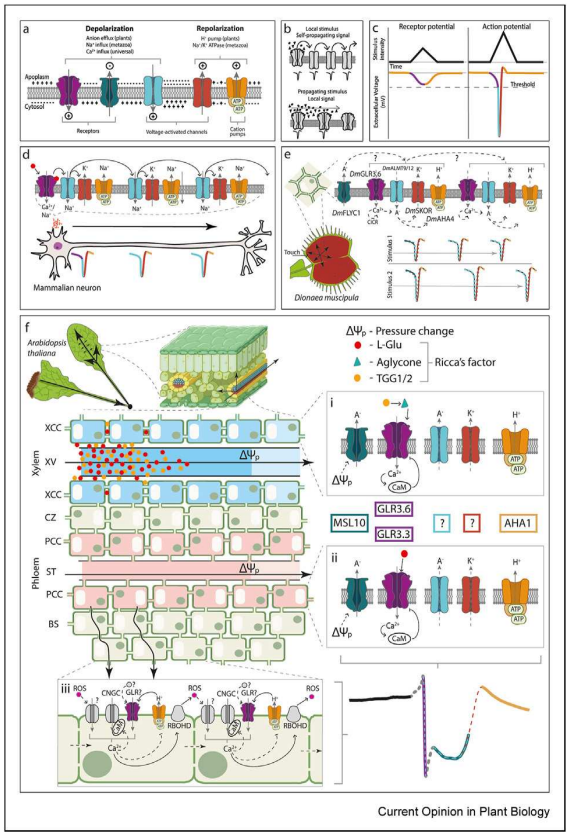

Comparison of conceptual and molecular bases of electrical signaling in neurons and plant cells. (**a**) Ion-permeable proteins sustain membrane-borne electric signals. Cation pumps (yellow) maintain a negative-charged cytosol and receptors, including chemical (purple) and mechanoreceptors (green), facilitate stimulus-induced ion fluxes. Voltage-dependent channels can lead to depolarization—less negative cytosol (blue), or hyperpolarization—more negative cytosol (red). Repolarization refers to a return to the resting negative-membrane potential. Color codes of ion-transporting proteins and traces correspond throughout the figure. (**b**) Non-decaying electric signal propagation. Top: Local stimulus causes depolarization, with signal reamplification via voltage-dependent channels. Bottom: propagating stimulus induces a non-self-propagating signal at each location. (**c**). Representation of extracellularly recorded membrane depolarization patterns (bottom) in response to a changing-intensity stimulus (top). A receptor potential is constituted by ion fluxes directly correlated to stimulus onset and offset. A neuronal AP is initiated by depolarizing beyond a threshold, at which voltage-dependent channels open, inducing further, stimulus-independent depolarization, and a propagating cascade of channel-gating events. (**d**) Mammalian neuron AP propagation: A ligand (red) induces a receptor potential surpassing the threshold, initiating the initial AP. Subsequent APs are independent of the initial receptor potential, maintaining constant speed and amplitude. (**e**) Representation of isometric AP propagation in *Dionaea* lobe. Top: Mechanosensitive *Dm*FLYC1 mediates an anion-sustained receptor potential upon trigger-hair stimulation. Downstream activated channels are hypothesized to be Ca^{2+}-permeable *Dm*GLR3.6, endoplasmic-reticulum-localized Ca^{2+}-induced Ca^{2+} release (CICR), Ca^{2+} -dependent anion channels *Dm*ALMT9/12, voltage-dependent K^+ channel *Dm*SKOR, and the proton pump *Dm*AHA4. Dashed lines: hypothesized relationships. Bottom: AP generation maintains a constant amplitude upon stimulation, with increased amplitude and propagation speed upon a second stimulation. (**f**) Propagation mechanisms of leaf-to-leaf wound-induced SWPs in Arabidopsis. Longitudinal transmission occurs through the vascular bundle. Molecular components and water potential change ($\Delta\Psi_p$) propagate along the XV, and XV/ST, correspondingly. (*i*) TGG1/2 propagate along the XV, generate aglycone and initiate a *At*GLR3.6-dependent signal. (*ii*) Glutamate mediates SWP generation through phloem-localized *At*GLR3.3. $\Delta\Psi_p$ propagating in the XV and ST is hypothesized to mechanically stimulate *At*MSL10, A^- – anions. Putative signal propagation outside of the vascular bundle depicted in (*iii*): Regulation of cation channels by respiratory burst oxidase homologs (RBOHs)-derived reactive oxigen species (ROS), or via other ligands for GLRs and cyclic-nucleotide-gated channels (CNGCs) is paralleled by H^+-pump-mediated proton efflux, forming regulatory circuits and resulting in cell-to-cell propagation of the signal, CaM – calmodulin. Putative contribution of proteins to the SWP is color-coded in the representative SWP trace (bottom-right). Solid and dashed lines represent proven and hypothesized interactions, respectively. Cell types of the vascular bundle: XCC – xylem companion cells, XV – xylem vessel, CZ – cambial zone, PCC – phloem companion cell, ST – sieve tube, BS – bundle sheath, TGG – thioglucoside glucohydrolase, AP – action potential; GLR – glutamate receptor–like; SWP – slow wave potential, *DmFLYC1 – mechanosensitive channel FLY Catcher 1*.

in *Marchantia* aligns with the SWP classification. We propose that it can be classified as such until mechanistic differences allow us to discern between different types of non-AP-like electric signals. The identification of SWP propagation in *Marchantia* implies that tissue signal transmission is an ancestral trait already present in non-vascular plants. From this, several questions emerge: (1) how do the vasculature-based propagation mechanisms in Arabidopsis align with the propagation of SWPs in a non-vascular plant? (2) Is the generation of wound-induced SWPs in *Marchantia* and Arabidopsis dependent on the same molecular players? (3) Are those molecular players in Arabidopsis confined to the vasculature, whereas in *Marchantia*, they are prevalent throughout the entire thallus? Identifying the protein families constituting the universal building blocks of signal generation across plant clades may provide insights into these questions and allow us to properly define and classify these signals.

Molecular actors in long-distance electric signaling

Various ion conductances contributing to plant APs have been identified pharmacologically. In *Dionaea*, lanthanum cations (La^{3+}), a blocker for Ca^{2+} channels, reduced membrane depolarization and $[Ca^{2+}]_{cyt}$ amplitude upon hair stimulation [8,40]. Additionally, Ca^{2+} uptake into the endoplasmic reticulum facilitated the repolarization phase [40]. Blocking K^+-permeable channels with tetraethylammonium ions confirmed that K^+-ion efflux from the cytoplasm is also involved in repolarization [8,40].

While no channels underlying ion fluxes have been genetically identified in *Dionaea*, a correlation was noted between lobe excitability and transcription abundance

Table 2

Open questions in the field of plant electrical signaling.

Context	Question
Classification of plant electrical signals is often heuristic.	Why are plant APs called APs? What are the common traits with animal APs? Can all the depolarizing, non-AP-like signals be classified as SWPs?
The biophysical foundations of AP and SWPs are different.	To what extent can knowledge developed in one system be translated to the other?
The role of anions and their transport proteins facilitating AP and SWP generation remains unexplored.	Which anion channels are involved in SWP or AP signal generation?
In *Dionaea* APs, propagation speed does not depend on the Ca^{2+} conductance [8].	Could the conductance mediating AP propagation be voltage-dependent and permeable to anions?
While the propagation of SWP does not seem to occur through a voltage-dependent mechanism [17], the activity of this type of mechanism cannot be discarded.	Are there voltage-sensitive feedback loops between the channels involved in SWP generation?
*At*GLR3.3 and 3.6 are considered to be active in the initial stage of the SWP as cation-permeable channels, also facilitating calcium influx [60].	How can desensitization of *At*GLR3.3 shorten the later SWP depolarization phase? Does this imply a feed-forward mechanism between *At*GLR3.3 and a downstream channel? Could GLRs permeate anions to also sustain the later phase of the SWP?
*At*GLR3.3 and 3.6 are in different cell types [13].	How are they interacting across different cell populations to generate the SWP?
Although the presence of *At*GLR3.3 and 3.6 at the plasma membrane of vascular cells cannot be completely ruled out, current data does not substantiate this localization [13].	How can a non−plasma membrane localized protein interact with apoplasmic ligands? How can internal membranes contribute to electric signaling?
Generation of APs in Arabidopsis, and vascular plants in general, is frequently considered, but assessing this capacity in the tissue is technically challenging.	Are plants, other than *Dionaea* and *Mimosa*, capable of generating a self-propagating, depolarization-initiated electric signal?
A crucial aspect of plant electrical signaling is whether the generated signal carries meaningful information for the plant. However, we only start to understand how plants decode electrical signals [45].	Does each type of SWP trigger the same intracellular response? If not, how is stimulus-specific information encoded and subsequently decoded by the recipient cells?

Abbreviations: AP = action potential; GLR = glutamate receptor−like; SWP = slow wave potential.

of certain genes, including those coding for the Ca^{2+}-permeable glutamate receptor−like 3.6 (*Dm*GLR3.6), the Cl^--permeable *Dm*ALMT9/12, the K^+-channel *Dm*SKOR, and the H^+-pump *Dm*AHA4 [40,59]. This molecular linkage suggests that these channels may play a role in the generation of the AP. In traditionally non-excitable higher plants, various molecular contributors to SWP generation have been identified. In Arabidopsis, *At*GLR3.3 and 3.6 are crucial for generating electric and $[Ca^{2+}]_{cyt}$ signals in response to leaf wounding [13,44]. This function is similarly observed in tomato (*Solanum lycopersicum*) with *Sl*GLR3.5 [25] and appears to be conserved in monocots, as demonstrated by the involvement in rice (*Oryza sativa*) of *Os*GLR3.4 [26].

Some of these Ca^{2+}-permeable channels can be regulated by glutamate, which implies this amino acid as a signaling molecule in SWP generation [16]. Challenges, such as the differential ligand interaction and cell-type expression pattern of the essential *At*GLR3.3 and 3.6 (Figure 1f), the requirement for high ligand concentration (μM-mM) for activation, and the constitutive non−fully closed gating state of the GLRs, complicate the direct comparison of GLRs with their animal counterparts as electric signaling initiators [60−62]. Recently, a regulatory feedback loop involving $[Ca^{2+}]_{cyt}$-dependent inhibition of *At*GLR3.3 by calmodulin 7 (*At*CaM7) was discovered, limiting SWP duration [63]. The anion-permeable mechanosensitive channel *At*MSL10, with a recently reported cryo-electron microscopy structure and gating mechanism [64], appears to sustain a later phase of the SWP [14]. This suggests a mechanical cue in signal generation, with anions involved in the subsequent depolarization phase (Figure 1f). Furthermore, repolarization might involve K^+-permeable channels, such as *At*AKT2 [19]. The proton pump *At*AHA1 has been demonstrated to contribute to this later SWP phase [65], indicating ATP-consuming H^+ efflux during this stage. Additionally, a

Table 2

Open questions in the field of plant electrical signaling.

Context	Question
Classification of plant electrical signals is often heuristic.	Why are plant APs called APs? What are the common traits with animal APs? Can all the depolarizing, non-AP-like signals be classified as SWPs?
The biophysical foundations of AP and SWPs are different.	To what extent can knowledge developed in one system be translated to the other?
The role of anions and their transport proteins facilitating AP and SWP generation remains unexplored.	Which anion channels are involved in SWP or AP signal generation?
In *Dionaea* APs, propagation speed does not depend on the Ca^{2+} conductance [8].	Could the conductance mediating AP propagation be voltage-dependent and permeable to anions?
While the propagation of SWP does not seem to occur through a voltage-dependent mechanism [17], the activity of this type of mechanism cannot be discarded.	Are there voltage-sensitive feedback loops between the channels involved in SWP generation?
*At*GLR3.3 and 3.6 are considered to be active in the initial stage of the SWP as cation-permeable channels, also facilitating calcium influx [60].	How can desensitization of *At*GLR3.3 shorten the later SWP depolarization phase? Does this imply a feed-forward mechanism between *At*GLR3.3 and a downstream channel? Could GLRs permeate anions to also sustain the later phase of the SWP?
*At*GLR3.3 and 3.6 are in different cell types [13].	How are they interacting across different cell populations to generate the SWP?
Although the presence of *At*GLR3.3 and 3.6 at the plasma membrane of vascular cells cannot be completely ruled out, current data does not substantiate this localization [13].	How can a non–plasma membrane localized protein interact with apoplasmic ligands? How can internal membranes contribute to electric signaling?
Generation of APs in Arabidopsis, and vascular plants in general, is frequently considered, but assessing this capacity in the tissue is technically challenging.	Are plants, other than *Dionaea* and *Mimosa*, capable of generating a self-propagating, depolarization-initiated electric signal?
A crucial aspect of plant electrical signaling is whether the generated signal carries meaningful information for the plant. However, we only start to understand how plants decode electrical signals [45].	Does each type of SWP trigger the same intracellular response? If not, how is stimulus-specific information encoded and subsequently decoded by the recipient cells?

Abbreviations: AP = action potential; GLR = glutamate receptor–like; SWP = slow wave potential.

of certain genes, including those coding for the Ca^{2+}-permeable glutamate receptor–like 3.6 (*Dm*GLR3.6), the Cl^--permeable *Dm*ALMT9/12, the K^+-channel *Dm*SKOR, and the H^+-pump *Dm*AHA4 [40,59]. This molecular linkage suggests that these channels may play a role in the generation of the AP. In traditionally non-excitable higher plants, various molecular contributors to SWP generation have been identified. In Arabidopsis, *At*GLR3.3 and 3.6 are crucial for generating electric and $[Ca^{2+}]_{cyt}$ signals in response to leaf wounding [13,44]. This function is similarly observed in tomato (*Solanum lycopersicum*) with *Sl*GLR3.5 [25] and appears to be conserved in monocots, as demonstrated by the involvement in rice (*Oryza sativa*) of *Os*GLR3.4 [26].

Some of these Ca^{2+}-permeable channels can be regulated by glutamate, which implies this amino acid as a signaling molecule in SWP generation [16]. Challenges, such as the differential ligand interaction and cell-type expression pattern of the essential *At*GLR3.3 and 3.6 (Figure 1f), the requirement for high ligand concentration (μM-mM) for activation, and the constitutive non–fully closed gating state of the GLRs, complicate the direct comparison of GLRs with their animal counterparts as electric signaling initiators [60–62]. Recently, a regulatory feedback loop involving $[Ca^{2+}]_{cyt}$-dependent inhibition of *At*GLR3.3 by calmodulin 7 (*At*CaM7) was discovered, limiting SWP duration [63]. The anion-permeable mechanosensitive channel *At*MSL10, with a recently reported cryo-electron microscopy structure and gating mechanism [64], appears to sustain a later phase of the SWP [14]. This suggests a mechanical cue in signal generation, with anions involved in the subsequent depolarization phase (Figure 1f). Furthermore, repolarization might involve K^+-permeable channels, such as *At*AKT2 [19]. The proton pump *At*AHA1 has been demonstrated to contribute to this later SWP phase [65], indicating ATP-consuming H^+ efflux during this stage. Additionally, a

ROS-centered propagation mechanism proposes the interaction of respiratory burst oxidase homolog D (*At*RBOHD), cyclic-nucleotide-gated channels (*At*CNGCs), *At*GLRs, and *At*AHAs (Figure 1f).

In *Marchantia*, Ca^{2+} and K^+ fluxes are essential for the initial depolarization phase of the SWP [21]. Contrasting with the repolarizing role of K^+ across taxa, it is puzzling how in *Marchantia* K^+ ions can trigger cell depolarization [43,50,60]. So far, the only SWP-related channel identified in *Marchantia* is *Mp*GLR. Its indispensability for signal propagation [21] highlights the conserved, central role of Ca^{2+} and GLRs in the depolarization phase of electric signals during plant evolution.

Conclusions

The field of plant electrophysiology has made important progress over the past 4 decades. In recent years, numerous significant discoveries from the past have been revisited and scrutinized using a wider array of molecular techniques now at our disposal. The integration of quantitative approaches, including modeling, has played a pivotal role in providing profound and fundamental insights into the subject matter. While affirming that, the role of GLRs and their correlation with increasing $[Ca^{2+}]_{cyt}$ is central across plant taxa; other channel families are consistently explored as key molecular actors. Our enhanced understanding may allow us to resolve key features in plant electric signaling and how they differ from the biophysical principles of neurophysiology. The heuristic classification of plant electric signals, primarily based on their shape and speed, appears oversimplified and problematic. This approach groups seemingly similar phenomena with potentially distinct underlying mechanisms, impeding an accurate description of diverse processes.

The development of plant-specific biophysical and electrophysiological paradigms is an opportunity and a task that the field is now facing. Embracing rigorous biophysical, mathematical, and theoretical approaches is crucial for this endeavor. Furthermore, the adoption of novel tools for approaching a mechanistic understanding of propagation and generation of electric signals is essential. These tools include multiarray electrode setups allowing for increased spatio-temporal resolution of the electrical signal, and optogenetic tools, enabling precise and non-invasive manipulation of the signaling process. As a result, a plant-tailored conceptual framework for electric signaling is emerging, raising with it countless new questions (Figure 1). In Table 2, we present some of the most immediate questions we identified in this exciting and promising field.

Author contributions

JB and MW wrote and edited the article.

Declaration of competing interest

The authors declare that they have no known competing financial interests or personal relationships that could have appeared to influence the work reported in this paper.

Data availability

No data was used for the research described in the article.

Acknowledgements

We apologize to colleagues whose studies were not included due to space limitation and thank Erwan Michard for valuable discussions and the reviewers for their constructive comments. Research in the authors' laboratory is supported by the Deutsche Forschungsgemeinschaft (DFG, German Research Foundation) under Germany's Excellence Strategy – EXC-2048/1 – Project-ID 390686111, and by the DFG Collaborative Research Center SFB 1208 – Project-ID 267205415. Figures were created with the help of www.biorender.com.

References

Papers of particular interest, published within the period of review, have been highlighted as:

* of special interest
** of outstanding interest

1. Zhang W, Thieme CJ, Kollwig G, Apelt F, Yang L, Winter N, Andresen N, Walther D, Kragler F: **tRNA-Related sequences trigger systemic mRNA transport in plants**. *Plant Cell* 2016, **28**:1237–1249.

2. Garg V, Kühn C: **What determines the composition of the phloem sap? Is there any selectivity filter for macromolecules entering the phloem sieve elements?** *Plant Physiol Biochem* 2020, **151**:284–291.

3. Lacombe B, Achard P: **Long-distance transport of phytohormones through the plant vascular system**. *Curr Opin Plant Biol* 2016, **34**:1–8.

4. Johns S, Hagihara T, Toyota M, Gilroy S: **The fast and the furious: rapid long-range signaling in plants**. *Plant Physiol* 2021, **185**:694–706.

5. Dziubińska H, Filek M, Koscielniak J, Trebacz K: **Variation and action potentials evoked by thermal stimuli accompany enhancement of ethylene emission in distant non-stimulated leaves of *Vicia faba* minor seedlings**. *J Plant Physiol* 2003, **160**: 1203–1210.

6. Stahlberg R, Cleland RE, Van Volkenburgh E: **Slow Wave Potentials — a propagating electrical signal unique to higher plants**. In *Communication in plants*. Edited by Baluška F, Mancuso S, Volkmann D, Springer Berlin Heidelberg; 2006: 291–308.

7. Vodeneev V, Orlova A, Morozova E, Orlova L, Akinchits E, Orlova O, Sukhov V: **The mechanism of propagation of variation potentials in wheat leaves**. *J Plant Physiol* 2012, **169**: 949–954.

8. ** Armada-Moreira A, Dar AM, Zhao Z, Cea C, Gelinas J, Berggren M, Costa A, Khodagholy D, Stavrinidou E: **Plant electrophysiology with conformable organic electronics: deciphering the propagation of Venus flytrap action potentials**. *Sci Adv* 2023, **9**, eadh4443.
In this paper, the authors use a revolutionary technique for a meticulous description of *Dionaea* AP propagation, revealing nuances that distinguish *Dionaea* APs from neuronal APs.

9. Suda H, Mano H, Toyota M, Fukushima K, Mimura T, Tsutsui I, Hedrich R, Tamada Y, Hasebe M: **Calcium dynamics during trap closure visualized in transgenic Venus flytrap**. *Nat Plants* 2020, **6**:1219–1224.

10. Tabata T, Sibaoka T: **Conduction velocity and blockage of action potential in Chara internodal cells**. *Plant Cell Physiol* 1987, **28**:1187–1194.

11. Umrath K: **Der Erregungsvorgang bei *Nitella mucronata***. *Protoplasma* 1933, **17**:258–300.

12. Hagihara T, Mano H, Miura T, Hasebe M, Toyota M: **Calcium-mediated rapid movements defend against herbivorous insects in *Mimosa pudica***. *Nat Commun* 2022, **13**: 6412.

13. Nguyen CT, Kurenda A, Stolz S, Chételat A, Farmer EE: **Identification of cell populations necessary for leaf-to-leaf electrical signaling in a wounded plant**. *Proc Natl Acad Sci USA* 2018, **115**:10178–10183.

14. Moe-Lange J, Gappel NM, Machado M, Wudick MM, Sies CSA, Schott-Verdugo SN, Bonus M, Mishra S, Hartwig T, Bezrutczyk M, *et al.*: **Interdependence of a mechanosensitive anion channel and glutamate receptors in distal wound signaling**. *Sci Adv* 2021, **7**.

15. Ricca U: **Transmission of stimuli in plants**. *Nature* 1926, **117**: 654–655.

16. Toyota M, Spencer D, Sawai-Toyota S, Jiaqi W, Zhang T, Koo AJ, Howe GA, Gilroy S: **Glutamate triggers long-distance, calcium-based plant defense signaling**. *Science* 2018, **361**: 1112–1115.

17. ** Gao Y-Q, Jimenez-Sandoval P, Tiwari S, Stolz S, Wang J, Glauser G, Santiago J, Farmer EE: **Ricca's factors as mobile proteinaceous effectors of electrical signaling**. *Cell* 2023, **186**: 1337–1351.e20.
This study provides compelling evidence that enzymatic glucosinolate breakdown contributes to SWP propagation and membrane depolarization, highlighting the role of protein transport in plant electrical signaling and establishing a link to the elusive Ricca's factor.

18. Dziubińska H, Trębacz K, Zawadzki T: **Transmission route for action potentials and variation potentials in *Helianthus annuus* L**. *J Plant Physiol* 2001, **158**:1167–1172.

19. Cuin T, Dreyer I, Michard E: **The role of potassium channels in *Arabidopsis thaliana* long distance electrical signalling: AKT2 modulates tissue excitability while GORK shapes action potentials**. *IJMS* 2018, **19**:926.

20. Favre P, Agosti RD: **Voltage-dependent action potentials in *Arabidopsis thaliana***. *Physiol Plantarum* 2007, **131**:263–272.

21. * Watanabe K, Hashimoto K, Hasegawa K, Shindo H, Tsuruda Y, Kupisz K, Koselski M, Wasko P, Trebacz K, Kuchitsu K: **Rapid propagation of Ca^{2+} waves and electrical signals in a liverwort *Marchantia polymorpha***. 2023, https://doi.org/10.1101/2023.10.16.562169.
This work broadens the taxonomic scope of wound-mediated signaling by exploring the SWP and its molecular components in a basal plant clade.

22. * Yang T-H, Chtelat A, Kurenda A, Farmer EE: **Mechanosensation in leaf veins**. *Sci Adv* 2023, **9**, eadh5078.
In this study, the authors systematically, meticulously, and objectively assess the mechanically induced AP-generating capacity of Arabidopsis leaves.

23. * Bellandi A, Papp D, Breakspear A, Joyce J, Johnston MG, de Keijzer J, Raven EC, Ohtsu M, Vincent TR, Miller AJ, *et al.*: **Diffusion and bulk flow of amino acids mediate calcium waves in plants**. *Sci Adv* 2022, **8**, eabo6693.
Here, the authors present data supporting a model based on apoplasmic diffusion and amino acid bulk-flow in local, wound-induced Ca^{2+}-wave transmission.

24. Dziubińska H, Paszewski A, Trębacz K, Zawadzki T: **Electrical activity of the liverwort *Conocephalum conicum:* the all-or-nothing law, strength-duration relation, refractory periods and intracellular potentials**. *Physiol Plantarum* 1983, **57**:279–284.

25. Wang G, Hu C, Zhou J, Liu Y, Cai J, Pan C, Wang Y, Wu X, Shi K, Xia X, *et al.*: **Systemic root-shoot signaling drives jasmonate-based root defense against nematodes**. *Curr Biol* 2019, **29**: 3430–3438.e4.

26. Yu B, Wu Q, Li X, Zeng R, Min Q, Huang J: **GLUTAMATE RECEPTOR-like gene *OsGLR3.4* is required for plant growth and systemic wound signaling in rice (*Oryza sativa*)**. *New Phytol* 2022, **233**:1238–1256.

27. Koselski M, Hoernstein SNW, Wasko P, Reski R, Trebacz K: **Long-distance electrical and calcium signals evoked by hydrogen peroxide in Physcomitrella**. *Plant Cell Physiol* 2023, **64**:880–892.

28. Koselski M, Wasko P, Derylo K, Tchorzewski M, Trebacz K: **Glutamate-induced electrical and calcium signals in the moss *Physcomitrella patens***. *Plant Cell Physiol* 2020, **61**:1807–1817.

29. Salvador-Recatalà V: **New roles for the GLUTAMATE RECEPTOR-LIKE 3.3, 3.5, and 3.6 genes as on/off switches of wound-induced systemic electrical signals**. *Plant Signal Behav* 2016, **11**, e1161879.

30. Salvador-Recatalà V, Tjallingii WF, Farmer EE: **Real-time, in vivo intracellular recordings of caterpillar-induced depolarization waves in sieve elements using aphid electrodes**. *New Phytol* 2014, **203**:674–684.

31. Macedo FCO, Dziubinska H, Trebacz K, Oliveira RF, Moral RA: **Action potentials in abscisic acid-deficient tomato mutant generated spontaneously and evoked by electrical stimulation**. *Acta Physiol Plant* 2015, **37**:207.

32. Rhodes DR, Tomlins SA, Varambally S, Mahavisno V, Barrette T, Kalyana-Sundaram S, Ghosh D, Pandey A, Chinnaiyan AM: **Probabilistic model of the human protein-protein interaction network**. *Nat Biotechnol* 2005, **23**:951–959.

33. Galvani L: **Aloysii Galvani De viribus electricitatis in motu musculari commentarius**. Ex Typographia Instituti Scientiarium; 1791.

34. Piccolino M: **Luigi Galvani and animal electricity: two centuries after the foundation of electrophysiology**. *Trends Neurosci* 1997, **20**:443–448.

35. Burdon-Sanderson JS: **I. Note on the electrical phenomena which accompany irritation of the leaf of *Dionaea muscipula***. *Proc Roy Soc Lond* 1873, **21**:495–496.

36. Feijó JA: **Bioelectricity in plants: from so simple a beginning**. *Bioelectricity* 2023, **5**:1–6.

37. Cole KS, Curtis HJ: **Electric impedance of Nitella during activity**. *J Gen Physiol* 1938, **22**:37–64.

38. Cole KS, Curtis HJ: **Electric impedance of the squid giant axon during activity**. *J Gen Physiol* 1939, **22**:649–670.

39. Hodgkin AL, Huxley AF: **The components of membrane conductance in the giant axon of *Loligo***. *J Physiol* 1952, **116**: 473–496.

40. Scherzer S, Böhm J, Huang S, Iosip AL, Kreuzer I, Becker D, Heckmann M, Al-Rasheid KAS, Dreyer I, Hedrich R: **A unique inventory of ion transporters poises the Venus flytrap to fast-propagating action potentials and calcium waves**. *Curr Biol* 2022, **32**:4255–4263.e5.

41. Procko C, Murthy S, Keenan WT, Mousavi SAR, Dabi T, Coombs A, Procko E, Baird L, Patapoutian A, Chory J: **Stretch-activated ion channels identified in the touch-sensitive structures of carnivorous Droseraceae plants**. *Elife* 2021, **10**, e64250.

42. Farmer EE, Gao Y-Q, Lenzoni G, Wolfender J-L, Wu Q: **Wound- and mechanostimulated electrical signals control hormone responses**. *New Phytol* 2020, **227**:1037–1050.

43. Kisnieriene V, Trębacz K, Pupkis V, Koselski M, Lapeikaite I: **Evolution of long-distance signalling upon plant terrestrialization: comparison of action potentials in Characean algae and liverworts**. *Ann Bot* 2022, **130**:457–475.

44. Mousavi SAR, Chauvin A, Pascaud F, Kellenberger S, Farmer EE: **GLUTAMATE RECEPTOR-LIKE genes mediate leaf-to-leaf wound signalling**. *Nature* 2013, **500**:422–426.

45. Morin H, Chételat A, Stolz S, Marcourt L, Glauser G, Wolfender J, Farmer EE: **Wound-response jasmonate dynamics in the primary vasculature**. *New Phytol* 2023, **240**:1484–1496.

46. ** Hagihara T, Toyota M: **Mechanical signaling in the sensitive plant *Mimosa pudica* L**. *Plants* 2020, **9**:587.

This study comprehensively links electric signaling to $[Ca^{2+}]_{cyt}$ increase in the leaflet-closing mechanism of *Mimosa*, providing experimental evidence supporting the anti-herbivory evolutionary advantage of this mechanism.

47. Houwink AL: **The conduction of excitation in *Mimosa pudica***. *Recl Trav Bot Neerl* 1935, **32**:51–91.

48. Sibaoka T: **Physiology of rapid movements in higher plants**. *Annu Rev Plant Physiol* 1969, **20**:165–184.

49. Koselski M, Trebacz K, Dziubinska H: **Vacuolar ion channels in the liverwort *Marchantia polymorpha*: influence of ion channel inhibitors**. *Planta* 2017, **245**:1049–1060.

50. Kandel ER, Schwartz James H, Jessell Thomas, Siegelbaum Steven A, Hudspeth AJ. ***Principles of neural science***. McGraw-Hill; 2013.

51. Bear MF, Connors BW, Paradiso MA: *Neuroscience: exploring the brain*: *Jones & Bartlett Learning*. 4th edition. Philadelphia: Wolters Kluwer; 2016:975 ISBN 9781451109542. https://search.worldcat.org/title/Neuroscience-:-exploring-the-brain/oclc/905677113.

52. Dreyer I, Li K, Riedelsberger J, Hedrich R, Konrad KR, Michard E: **Transporter networks can serve plant cells as nutrient sensors and mimic transceptor-like behavior**. *iScience* 2022, **25**, 104078.

53. Farmer EE, Gasperini D, Acosta IF: **The squeeze cell hypothesis for the activation of jasmonate synthesis in response to wounding**. *New Phytol* 2014, **204**:282–288.

54. Tinturier E, É Badel, Leblanc-Fournier N, Julien J: **Stem bending generates electrical response in poplar**. *Physiol Plantarum* 2021, **173**:954–960.

55. Hedrich R, Salvador-Recatalà V, Dreyer I: **Electrical wiring and long-distance plant communication**. *Trends Plant Sci* 2016, **21**:376–387.

56. Gilroy S, Białasek M, Suzuki N, Górecka M, Devireddy AR, Karpiński S, Mittler R: **ROS, calcium, and electric signals: key mediators of rapid systemic signaling in plants**. *Plant Physiol* 2016, **171**:1606–1615.

57. Evans MJ, Choi W-G, Gilroy S, Morris RJ: **A ROS-assisted calcium wave dependent on the *At*RBOHD NADPH oxidase and TPC1 cation channel propagates the systemic response to salt stress**. *Plant Physiol* 2016, **171**:1771–1784.

58. Choi WG, Toyota M, Kim S-H, Hilleary R, Gilroy S: **Salt stress-induced Ca^{2+} waves are associated with rapid, long-distance root-to-shoot signaling in plants**. *Proc Natl Acad Sci USA* 2014, **111**:6497–6502.

59. Hedrich R, Kreuzer I: **Demystifying the Venus flytrap action potential**. *New Phytol* 2023, **239**:2108–2112.

60. Simon AA, Navarro-Retamal C, Feijó JA: **Merging signaling with structure: functions and mechanisms of plant glutamate receptor ion channels**. *Annu Rev Plant Biol* 2023, **74**:415–452.

61. Mou W, Kao Y-T, Michard E, Simon AA, Li D, Wudick MM, Lizzio MA, Feijó JA, Chang C: **Ethylene-independent signaling by the ethylene precursor ACC in Arabidopsis ovular pollen tube attraction**. *Nat Commun* 2020, **11**:4082.

62. Ortiz-Ramírez C, Michard E, Simon AA, Damineli DSC, Hernández-Coronado M, Becker JD, Feijó JA: **GLUTAMATE RECEPTOR-LIKE channels are essential for chemotaxis and reproduction in mosses**. *Nature* 2017, **549**:91–95.

63. ** Yan C, Gao Q, Yang M, Shao Q, Xu X, Zhang Y, Luan S: **Ca^{2+}/calmodulin-mediated desensitization of glutamate receptors shapes plant systemic wound signalling and anti-herbivore defence**. *Nat Plants* 2024, https://doi.org/10.1038/s41477-023-01578-8.
This paper presents compelling evidence for a calmodulin-mediated desensitization of GLRs via its cytosolic C-terminus.

64. Zhang J, Maksaev G, Yuan P: **Open structure and gating of the Arabidopsis mechanosensitive ion channel MSL10**. *Nat Commun* 2023, **14**:6284.

65. Kumari A, Chételat A, Nguyen CT, Farmer EE: **Arabidopsis H^+-ATPase AHA1 controls slow wave potential duration and wound-response jasmonate pathway activation**. *Proc Natl Acad Sci USA* 2019, **116**:20226–20231.

Chapter 2 – Long-distance electric communication in *Arabidopsis thaliana*: optogenetic dissection and implications for wound response.

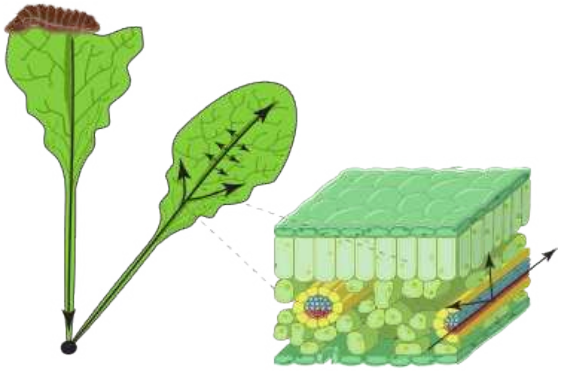

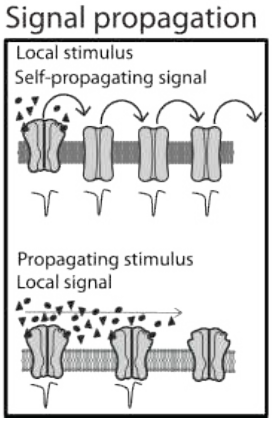

Status: In preparation

Journal: bioRxiv

Contribution to this chapter:

The experimental work and data analysis for figures 1,2,3,5,7 was acquired by Juan Camilo Barbosa-Caro.

Data for figure 4 was acquired by Juan Camilo Barbosa-Caro and Abdul Manan Dar, from the Laboratory of Organic Electronics at Linköping university in Sweden. Design and manufacturing of the multi-electrode arrays, and the base 3D design of the single leaf holder were performed by Abdul Manan Dar. Analysis of this raw data was performed by Juan Camilo Barbosa-Caro with guidance of Abdul Manan Dar.

Data for figure 6 was acquired together with Fatiha Atanjaoui, analysis of imaging raw data was performed by Fatiha Atanjaoui, and analysis of electrophysiological raw data was done by Juan Camilo Barbosa-Caro.

Statistical analysis and writing of this chapter were entirely done by Juan Camilo Barbosa-Caro.

Long-distance electric communication in *Arabidopsis thaliana*: optogenetic dissection and implications for wound response.

Juan Camilo Barbosa-Caro[1], Abdul Manan Dar[2], Fatiha Atanjaoui[1], Eleni Stavrinidou[2], Shiqiang Gao[4], Georg Nagel[4], Michael M. Wudick[1,3],

[1] Heinrich Heine University Düsseldorf, Faculty of Mathematics and Natural Sciences, Institute for Molecular Physiology, 40225 Düsseldorf, Germany.
[2] Laboratory of Organic Electronics, Department of Science and Technology, Linköping University, SE-601 74 Norrköping, Sweden.
[3] Heinrich Heine University Düsseldorf, Faculty of Mathematics and Natural Sciences, Cluster of Excellence on Plant Sciences, 40225 Düsseldorf, Germany.
[4] Department of Neurophysiology, Physiological Institute, University of Wuerzburg, Würzburg, Germany.

Abstract

Plants react systemically to local wounding by broadcasting a signal denominated Slow Wave Potential (SWP); a membrane potential (V_m) fluctuation and cytosolic calcium concentration ($[Ca^{2+}]_{cyt}$) increase. A possible mechanism of SWP propagation is hypothesized to be analogous to neuronal electric propagation of the Action Potential (AP). However, AP-sustaining membrane electric excitability has not been thoroughly asserted in vascular plants. We evaluate excitability of leaf tissue in *Arabidopsis thaliana*, and assert its possible contribution to SWP propagation. Excitability was tested by tight optogenetic control of transmembrane anion and Ca^{2+} fluxes. Complementarily, to assert the contribution of membrane excitability in SWP propagation, we increased the spatial and analytical resolution of the SWP recordings and, compared its propagation pattern to that of chemical cues. We determined that V_m depolarization does not generate self-propagating signals, but $[Ca^{2+}]_{cyt}$ does. We could resolve that different components of the SWP propagate at different speed along the petiole. Remarkably, the fastest SWP component occurs simultaneously with the arrival of molecular cues. Voltage insensitivity of the tissue, and concurrence of SWP and molecular cues onset, hint that chemical propagation is the leading transmission mechanism, and questions the role of hypothesized mechanical stimuli and Ca^{2+}-activated, self-propagating signals in SWP transmission.

Introduction

Plants can generate a systemic defense response against local herbivory attacks on a single leaf. To coordinate this organismic response, propagating signals are generated in the wounded leaf and induce metabolic changes in non-wounded ones. These signals can be recorded as a transient membrane potential (V_m) depolarization linked to a cytosolic calcium ($[Ca^{2+}]_{cyt}$) increase, and have been coined as Slow Wave Potential (SWP) (Mousavi *et al.*, 2013).

In *Arabidopsis*, some underlying molecular actors that sustain the SWP have been identified. Notably, mutation of two members of the Glutamate Receptor-Like (GLR) family, *GLR3.3* and *GLR3.6*, abolishes the SWP and the associated $[Ca^{2+}]_{cyt}$ increase (Mousavi *et al.*, 2013). The knockout of the anion-conductive, Mechanosensitive channel of Small conductance-Like 10 (MSL10) induces a shorter SWP (Moe-Lange *et al.*, 2021), and the knockout of the proton pump AHA1 leads to a prolonged SWP (Kumari et al., 2019). The knockout of the K^+ channel AKT2 also prolongs the electric signal duration generated by 9 V application to the leaf blade (Cuin *et al.*, 2018), yet likely representing a different type of wounding stimulus (Barbosa-Caro and Wudick, 2024). This information can be used to generate a simplistic model in which the initial depolarization observed in SWPs is mediated by fluxes of Ca^{2+} and anions, while the subsequent repolarization is mediated by H^+ and K^+ (Barbosa-Caro and Wudick, 2024).

Despite the identification of some molecular actors, our understanding of wound-induced SWPs is largely phenomenological given our limited understanding of the physiologically-relevant cues that comprise a wound stimulus in plants. Essential is the dissection of the physical phenomena that compose a wound, and which of these are significant in the transduction to membrane voltage, and $[Ca^{2+}]_{cyt}$ changes.

Recent research has focused on understanding biophysical mechanisms of generation, transduction, and propagation of the SWP. Three possible propagation means are

considered so far. 1 - a chemical stimulus that propagates and triggers local signals on its path, experimentally tested by (Gao *et al.*, 2023). 2 – a hydraulic wave, hypothesized to be generated by the collapse of the static turgor in vascular bundles (Gao *et al.*, 2023), measured with a speed 4 orders of magnitude higher than the SWP (Vodeneev *et al.*, 2012; Alarcon and Malone, 1994). 3 – a self-propagating electric wave, initiated by an initial stimulus and self-generated by the activity of endogenous membrane proteins in phloem cells (Fromm & Lautner, 2007; Hedrich et al., 2016a).

The electric propagation hypothesis, however, lacks comprehensible evidence in the context of plant wound responses. The existence of a propagating electric wave is based on the capacity of the signal to be self-generating, in other words, to have a voltage stimulus generate a voltage response. A mechanism observed in the generation of action potentials (AP) in animal neurons (reviewed in Barbosa-Caro2024). Proper experimental characterization of self-propagating electric signals in vascular plants has been technically challenging due to the difficulty of non-invasively manipulating the membrane potential of cells *in planta*.

Given this, interpretation of electric signals in vascular plants was established with the characterization of APs in the ancestral *Characeae* algal family (Pupkis *et al.*, 2022; Lapeikaite *et al.*, 2020; Fromm and Lautner, 2007). Experiments in chara allowed to establish a model in which the single cell membrane potential can be manipulated to generate an AP identified by its canonical characteristics: I) an “all-or-nothing” response characterized by a membrane potential threshold at which an autonomous, self-generating AP is triggered. II) constant amplitude of the all-or-nothing signal. III) a refractory period in which the system cannot generate a new AP (Barnett and Larkmann, 2007; Barbosa-Caro and Wudick, 2024). For an electric signal to fit into the category of action potential, these specific characteristics must be identified.

In vascular plants, transient electric signals can be easily recorded in excitable species, such as the Venus flytrap *Dionaea muscipula* and the *Mimosa pudica*. However, their

classification as APs largely relies on their highly consistent shape, while other AP-specific criteria have not been thoroughly assessed *in planta* (Barbosa-Caro and Wudick, 2024; Armada-moreira *et al.*, 2023; Huang and Hedrich, 2023). Moreover, tangential evidence suggests that the signal recorded in excitable species is an electrically-triggered signal, similar to the AP in chara and in animal neurons, as multiple depolarizing stimuli converge in generating the stereotypical AP. It is known that wounding events (Marhavý et al., 2019), touch (Yang *et al.*, 2023)(yang2023), cold exposure (Vodeneev *et al.*, 2006), methanol application (Tran *et al.*, 2018), and intense light stimulation (Koselski *et al.*, 2008), can generate local, transient depolarization events in plant tissue, and in the case of *Dionaea* result in the generation of a stereotypical AP (Armada-moreira *et al.*, 2023; Iosip *et al.*, 2020; Trebacz and Sievers, 1998; Pavlovič *et al.*, 2017).

The mechanistic understanding of the AP in characean algae and *Dionaea* sets the ground to hypothesize that SWPs have a self-propagating, AP component. Despite these abundant references to *Dionaea* and characean APs in our mechanistic understanding of *Arabidopsis* SWPs, the capacity of *Arabidopsis* to generate self-propagating electric signals, and of *Dionaea* to generate wound-induced SWPs has not been conclusively addressed.

In this work I aim to determine the capacity of *Arabidopsis* leaves to sustain self-propagating electric signals, and the contribution of electric transmission to the propagation of SWPs. Complementarily, I will test the capacity of *Dionaea* to generate SWPs and APs in different developmental stages to shed light on the potential interplay of these signals.

Results

Electric excitability in AP generation

The tools to study APs in algae involve impalement electrodes that allow tight control of the membrane potential of the cell, and quantification of the fundamental AP characteristics: excitation threshold, self-propagation, and refractory period (Pupkis *et al.*, 2022; Beilby, 2007). However, in vascular plants the use of such intracellular electrodes is invasive and technically limited given their electrically coupled, multicellular nature.

The technical challenge to use intracellular electrodes also applies to *in vivo* manipulation of neuronal activity in mammalian systems. This challenge was overcome with the development of genetically encoded, light-activated, ion-permeable, membrane proteins known as channelrhodopsins, which modulate the cells' electrical state (Nagel *et al.*, 2002). These optogenetic tools allow non-invasive control of membrane potential with high cellular and temporal precision (reviewed in Fenno *et al.*, 2011). Recently, this optogenetic technique has become available in plants, allowing to determine the contribution of specific ions to biotic and abiotic stress responses (Ding *et al.*, 2024), stomatal closure (Huang *et al.*, 2021), and plant growth (Zhou *et al.*, 2021).

To assess whether the *Arabidopsis* leaf can generate an AP, we investigated its ability to produce a threshold-dependent, electric transient in response to depolarization.

To investigate voltage-dependent excitability, we used the Anion ChannelRhodopsin 1 (ACR1) to generate a precise, non-invasive, depolarizing stimulus. Depolarization by ACR1 is induced by light and sustained by the endogenous electrochemical gradient of the cells, hence preventing undesired wounding artifacts caused by electrodes or severe stimulation from external voltage generators (Cuin *et al.*, 2018; Stanković and Davies, 1996).

The ACR1, under the control of the *UBIQUITIN10* promoter (pUBQ10), was expressed in Col-0 *Arabidopsis thaliana* plants. This optogenetic tool was shown to localize to the

plasma membrane in *Nicotiana tabacum* pollen tubes, and in the heterologous system *Xenopus laevis* oocytes. In *Nicotiana* epidermal cells, ACR1 is observed in the membrane system, and generates light-activated currents of 100 mV in amplitude (Zhou *et al.*, 2021). The depolarization is induced by anion efflux upon green light (λ = 535 nm) stimulation (Govorunova *et al.*, 2015). Light onset generates a rapid depolarization with an amplitude that increases dose-dependently with the intensity of the light stimulus. Upon maximum stimulation of 1050 μW/mm^2 for 200 ms, depolarization reaches a maximum amplitude of -72.29 ± 0.90 mV (Mean±SEM, n=16) (Figure 1b).

The observed sigmoidal dose-response curve of the depolarization response (Figure 1a). contradicts the hypothesis of a voltage-dependent, threshold-conditioned AP. More detailed, if an autonomous cellular response to voltage existed, the dose-response would abruptly saturate at a specific stimulus intensity, representing the threshold.
Instead, the observed dose-response curve gradually reaches a saturating plateau, indicating that the tissue reached its maximum ACR1-mediated depolarization limit. This maximal depolarization is in the range of the maximum amplitude of endogenous electric responses (-71.97 ± 1.73, n = 10) (Figure 4), thus indicating that the depolarization spans the physiological voltage range but does not trigger an autonomous response.

This behavior suggests that the stimulated tissue either cannot generate voltage-triggered APs, or that any APs generated by few cells are masked by the large-scale depolarization of the whole tissue. To test this "masking hypothesis", we used the *MSL10* promoter (pMSL10) to exclusively drive *ACR1* expression in the cell population considered to be the active electric transmitters in the electric transmission theory, and to other SWP-related cell types.

The maximum depolarization of pMSL10:ACR1 plants was obtained with blue light at 1050 μW/mm^2 for 1 s, and it only resulted in an average amplitude of -1.08 ± 0.06 mV (n=14) (Figure 1b). This depolarization is an order of magnitude smaller than that

observed in equally stimulated pUBQ10:ACR1 plants, and wound-induced SWPs. While a smaller depolarization is expected due to fewer cells expressing the ACR1, it remains unclear if those individual cells are depolarized to the hypothesized threshold.

Alternatively, to further investigate the potential masking of the AP by the strong ACR1-mediated depolarization, we hypothesized that an AP must propagate along the petiole, and can be recorded in unstimulated areas at a later time point. To test this, we placed a second electrode 6 mm away from the stimulation site. ACR1-mediated depolarization was generated but no depolarization event was perceived in the distal electrode, indicating that no propagating electric signal was triggered by ACR1-driven tissue depolarization (Figure 1c).

Interestingly, when naïve, unstimulated plants were exposed to a maximum-intensity light stimulus for the first time, the repolarization phase was significantly longer (2.85 ± 0.96 s) than in any subsequent stimuli (0.96 ± 0.34 s). The prolonged repolarization observed only upon the first stimulus suggests voltage-dependent activation of hyperpolarizing channels, or deactivation of depolarizing channels. Notably, the initial stimulus failed to trigger an autonomous, propagating response (Figure 1d).

As cell-borne depolarization alone is insufficient to generate an AP in *Arabidopsis*, we hypothesized that additional components may be required. In contrast, membrane depolarization alone is sufficient to trigger a characean AP, as it induces the required voltage-dependent $[Ca^{2+}]_{cyt}$ increase that subsequently generates the AP (Kisnieriene *et al.*, 2019; Beilby, 2007). Based on this observation, we hypothesized that the simultaneous occurrence of depolarization and a $[Ca^{2+}]_{cyt}$ increase is essential for triggering a self-generating transient in *Arabidopsis*.

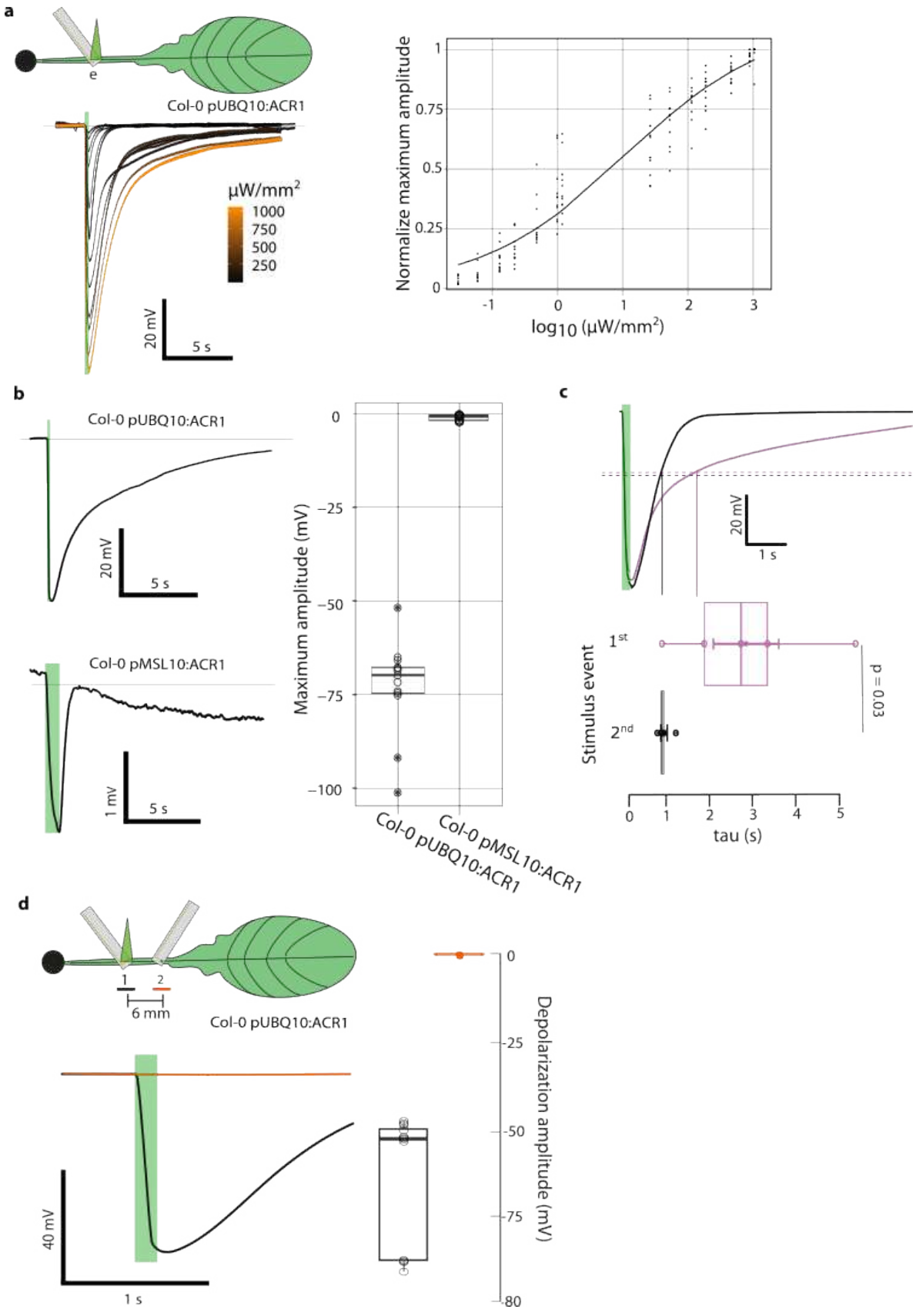
a
e
Col-0 pUBQ10:ACR1
µW/mm²
1000
750
500
250
20 mV
5 s
Normalize maximum amplitude
log10 (µW/mm²)
b
Col-0 pUBQ10:ACR1
20 mV
5 s
Col-0 pMSL10:ACR1
1 mV
5 s
Maximum amplitude (mV)
Col-0 pUBQ10:ACR1
Col-0 pMSL10:ACR1
c
20 mV
1 s
Stimulus event
1st
2nd
p = 0.03
tau (s)
d
1
2
6 mm
Col-0 pUBQ10:ACR1
40 mV
1 s
Depolarization amplitude (mV)

Figure 1. Surface potential recordings of *Arabidopsis thaliana* expressing ACR1. (**a**) Electric response from plants expressing ACR1 from a *UBQ10* promoter, stimulated by 535 nm light at increasing power densities for a duration of 200 ms. The dose-response curve describes a sigmoidal curve (n=11). (**b**) Electric response to 1050 μW/mm^2 light stimulus for 200 ms (top) or 1 s (bottom). Depolarization amplitude (±SEM) when ACR1 is expressed either from the *UBQ10* (-72.74 ± 0.94 mV, n=13), or MSL10 promoter (-1.08 ± 0.06mV n=14). (**c**) Repolarization time to 37% of maximum depolarization in a naïve plant upon the first (1st) and second (2nd) 200 ms stimulation. The stimuli are separated by 15 s. (**d**) Electric response at the stimulated electrode (black) and at non-stimulated electrode (orange) placed 6 mm apart. The amplitude (±SEM) of the electric transient at the stimulated electrode is -34.08 ± 1.90 mV (n=12); at the non-stimulated electrode -1.03 ± 0.06 mV (n=12). Statistical tests were done with Whitney-Mann U test.

Ca^{2+} in AP generation

To test whether depolarization and changes in $[Ca^{2+}]_{cyt}$ can trigger a stimulus-independent transient, we employed the Ca^{2+}-permeable channelrhodopsin XXM (Ding *et al.*, 2024), expressed under the control of the *UBQ10* promoter and targeted to the plasma membrane. Stimulation of XXM with blue light (peak λ = 470 nm) for 1 s induced Ca^{2+} influx to the cytosol, simultaneously driving membrane depolarization of around -19.33 ± 0.88 mV (n=9) (Figure 2a). Although XXM has been shown to be also permeable also to Na2+ (Duan et al., 2019), Ding et al. (2024) showed that under physiological conditions this conductance is negligible. Consequently, the currents observed *in planta* are primarily carried by Ca^{2+}.

Successive stimulation of pUBQ10:XXM Col-0 plants with increasing light intensities for 1 s produced progressively larger depolarization events, following an exponential dose-response curve (Figure 2a). The lack of a saturating plateau may result from the relatively low stimulation intensity of 1160 $\mu W/mm^2$, compared to the 5000 $\mu W/mm^2$ required for maximal XXM activation (Duan *et al.*, 2019).
Interestingly, despite non-maximal XXM activation, in 10 % of the measurements we observed an endogenous transient that occurred after the offset of the XXM-stimulating light stimulus (Figure 2a-bottom). Since this transient persists after light stimulus offset, we hereafter refer to it as an autonomous transient. Its infrequent occurrence suggests that the sequential stimulation steps increased the $[Ca^{2+}]_{cyt}$, presumably inactivating the Ca^{2+}-sensitive mechanism that initiates the autonomous transient. In other words, the responsive cells were brought into a refractory period, where generation of an autonomous response is temporary abolished.

To verify the excitability and refractory property of pUBQ10:XXM plants, we challenged leaves of previously unstimulated plants with 1160 $\mu W/mm^2$ blue light. Remarkably, naïve plants evoked self-generating electric transients upon full activation of XXM.
Overall, we recorded autonomous transients 91% of the time; 23% with 1 s pulses and 68% with 10 s pulses (n=22) (Figure 2b), suggesting that the stimulus intensity is sub-

threshold but its integration over time increases the response rate. These data also showcase the refractory property of this system. Every time an autonomous transient is generated, a second pulse within the next minute generates only the XXM-mediated depolarization, without triggering another autonomous transient (Figure 2b).

As previously stated, stimulus-independency and a refractory period are hallmark properties of an AP. To assess the possible self-propagating capacity of this $[Ca^{2+}]_{cyt}$ -triggered response, we placed a second electrode 6 mm away from the stimulation site. Upon optogenetic stimulation near the first electrode, we observed a time-delayed, smaller autonomous transient at the distal, unstimulated electrode, which propagated at a speed of 0.11 ± 0.01 cm/s (n=14) (Figure 2c). A simultaneous depolarization is observed at both the stimulated and distal electrodes during the light onset, similar to that seen in Col-0 plants expressing pUBQ10:ACR1. This simultaneous response is likely due to light scattering from the source to the distal electrode, as it persists even when the petiole is severed between the electrodes (Figure 3).
The dampening of the transient amplitude over distance could be a property of the tissue, or could be due to the inherent limitation of the recording setup. As the morphology of the tissue changes underneath both electrodes, the surface potential could be perceived differently although it remains intracellularly constant.

The Ca^{2+}-triggered electric transient fulfills some of the canonical properties of an animal AP: it is self-generating, propagates, and presents a refractory period. However, its amplitude is not held constant over distance, potentially hinting at fundamental differences between the generation mechanism of animal and plant APs.
Having established that membrane depolarization is not sufficient, and $[Ca^{2+}]_{cyt}$ increase is necessary for AP generation in *Arabidopsis*, we aimed to identify its contribution to signal generation in the physiological context of a wounding event.

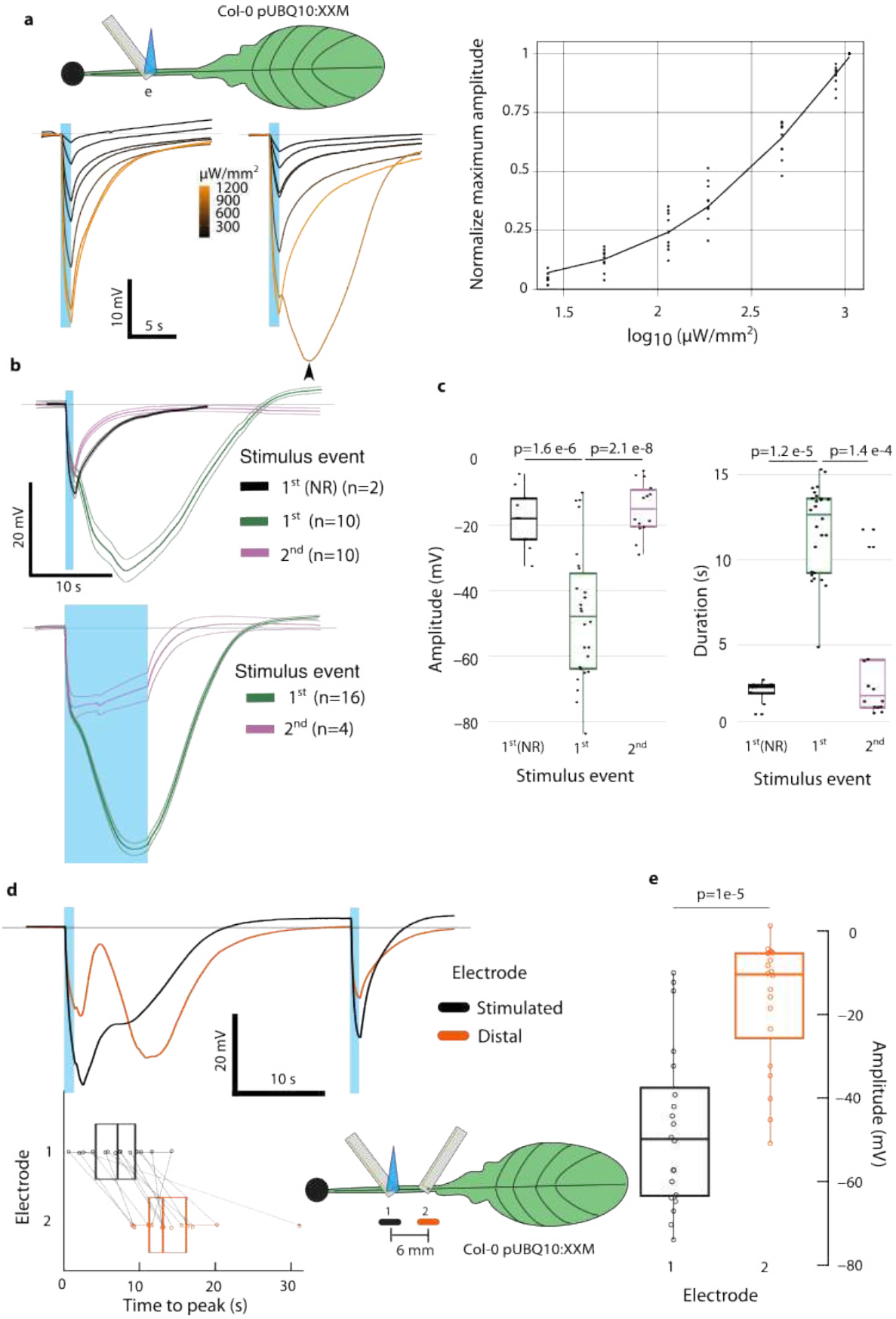
a
Col-0 pUBQ10:XXM
e
µW/mm²
1200
900
600
300
10 mV
5 s
Normalize maximum amplitude
log10 (µW/mm²)
b
Stimulus event
1st (NR) (n=2)
1st (n=10)
2nd (n=10)
20 mV
10 s
Stimulus event
1st (n=16)
2nd (n=4)
c
p=1.6 e-6
p=2.1 e-8
Amplitude (mV)
1st(NR)
1st
2nd
Stimulus event
p=1.2 e-5
p=1.4 e-4
Duration (s)
1st(NR)
1st
2nd
Stimulus event
d
Electrode
Stimulated
Distal
20 mV
10 s
Electrode
Time to peak (s)
6 mm
Col-0 pUBQ10:XXM
e
p=1e-5
Amplitude (mV)
Electrode

Figure 2. Surface potential recordings of *Arabidopsis thaliana* expressing XXM.
(**a**) Electric response from plants expressing XXM from a the *UBQ10* promoter stimulated by 470 nm light at increasing power densities for a duration of 1 s. The dose-response curve follows an exponential trend. Left - representative traces of the light response used for generating the dose-response curve. Right - traces present an autonomous electric transient after stimulus offset (black arrowhead). (**b**) Mean ± SEM traces of the electric response of naïve plants to a 1 s, 1160 μW/mm^2 light stimulus. The black trace represents the light-dependent response without an autonomous response (NR), the green trace shows both the light-dependent and autonomous responses, and the purple trace depicts the response to a 2nd light stimulus 15 s after the first. Top - stimulation with 1 s, bottom with 10 s light pulse. (**c**) Quantification of amplitude and duration of all the electric responses represented in (**b**). (**d**) Electric response at the stimulated (black) and at non-stimulated electrode (orange) placed 6 mm apart. Top - Representative trace of autonomous, propagating transient generated by 1 s light pulse, a second pulse fails to generate an autonomous response. Bottom left – latency between light stimulus onset and depolarization peak at stimulated (7.34 ± 0.17 s) and distal (12.85 ± 0.36 s) electrodes. **(e)** Amplitude of the autonomous depolarization at stimulated (-47,39 ± 0.97 mV) and distal (-17,24 ± 0.77 mV) electrodes (n=20). Statistical tests were done with Whitney-Mann U test.

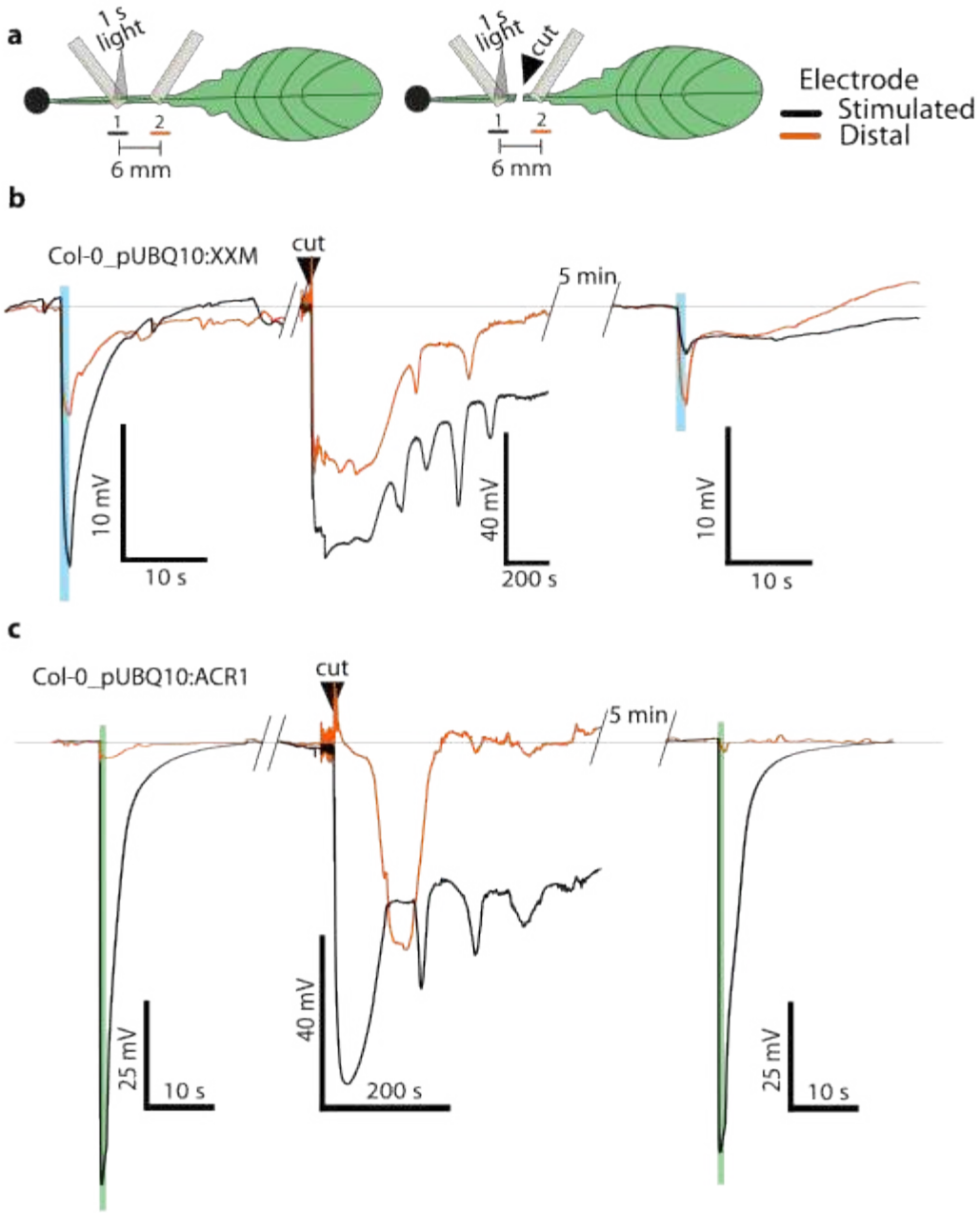

Figure 3. Dual-electrode surface potential recordings on *Arabidopsis thaliana* expressing optogenetic tools. (**a**) Left - illustration of the experimental setup for investigation of signal propagation along the petiole. Right – petiole severed in between the two recording electrodes. (**b**) Representative trace of Col-0 plants expressing pUBQ10:XXM stimulated for 1 s with 1160 µW/mm^2 blue light (blue rectangle) before (left trace) and after (right trace) the petiole cut (middle trace). (**c**) Representative trace of a Col-0 plant expressing pUBQ10:ACR1 stimulated for 1 s with 1050 µW/mm2 green light (green rectangle) before (left trace) and after (right trace) the petiole cut (middle trace).

Identifying the AP as part of the SWP in *Arabidopsis*

To investigate the potential involvement of an AP component in the complex SWP kinetics, we aimed to enhance the spatial and analytical resolution of the SWP recording to capture its propagating properties. To this end, we induced the SWP by locally wounding leaf 8 and recorded at the surface of the leaf 13 petiole using a custom-designed Multi-Electrode Array (MEA) featuring 32 electrodes arranged in 3 rows and 11 columns (Figure 4 a).

We observed that the SWP is not a uniform signal, but exhibits significant variations along the longitudinal axis of the petiole (Figure 4a). This variation in signal shape could result from differences in arrival of stimuli, varying expression of stimulus-transducing proteins, or a constant signal being differently detected by the surface electrodes, due to heterogeneous morphology of the signal-generating tissue. Regardless, our findings reveal that the high variability of the SWP, traditionally referred to as variation potential, arises not only from the genetic background, as previously assumed, but also from the specific recording location at the petiole and leaf.

In order to characterize and quantify the transformation of the signal along the petiole, we standardized the wounding procedure of the plants using grip plyers and 3D printed surfaces, and also increased the analytical resolution by quantifying 8 parameters from the SWP traces (Atanjaoui et al., submitted – chapter 3). While quantitative characterization of the SWP has typically focused on the pronounced, downward depolarization phase, it is preceded by a smaller, upward hyperpolarization phase, that has yet to be studied. By quantifying multiple parameters of both phases (Figure 4b), we identified differences in their propagation behaviors.

Notably, the depolarization and hyperpolarization phases exhibit distinct propagation speeds. The depolarization phase propagates acropetally at 0.26 ± 0.02 cm/s, consistent with published values for SWP propagation speeds (Figure 4g). In contrast, at the 100 Hz sampling rate used for recording, the hyperpolarization phase appears to initiate

simultaneously across the recorded area (Figure 4c). This intriguing disparity in propagation dynamics suggests that the hyperpolarization and depolarization phases might be mediated by different underlying mechanisms.

We hypothesized that the apparently immediate hyperpolarization propagation could result from either a hydraulic pressure wave or electrical influence originating from a distant source. To test these hypotheses, we initially aimed to investigate whether the massive depolarization of a wounded leaf could simultaneously influence some cells in the distal leaf by electrotonic conductivity (Armada-moreira *et al.*, 2023), and induce a macroscopic hyperpolarizing reaction through depolarization-activated K^+ channels (Adem *et al.*, 2020; Hosy *et al.*, 2003; Ache *et al.*, 2000). To verify this, we simultaneously recorded the electric response in the wounded leaf 8 with a single electrode, and in the receiving leaf 13 with the MEA. To assure that electrotonic conductivity was possible through the tissue, we inserted a silver wire into the petiole of leaf 13, whit which we generated a sinusoidal pulse every 15 s as beacon to test for electric connectivity between both leaves (Figure 5a).

The sinusoidal beacon signal could be recorded simultaneously in both leaves, contrasting with the leaf 8 depolarization, which was not perceived in the receiving leaf, and peaked before leaf 13 hyperpolarization (Figure 5b). The exogenous beacon was recorded simultaneously in both leaves, with an expected, slight amplitude dampening resulting from passive electrotonic transmission through the tissue. This suggests that, although electrotonic transmission between plants is possible, massive wound-induced depolarization is not passively transmitted. The pathway for electrotonic transmission of the beacon pulse could the apoplasm or the symplasm through plasmodesmata (Van Bel and Ehlers, 2005; Van Bel *et al.*, 2014). We determined that electrotonic transmission of the beacon occurred through the apoplasmic syncytium as the signal is disseminate even through scalded, dead tissue connected only by the xylem (Gao *et al.*, 2023) (Figure 5c-d).

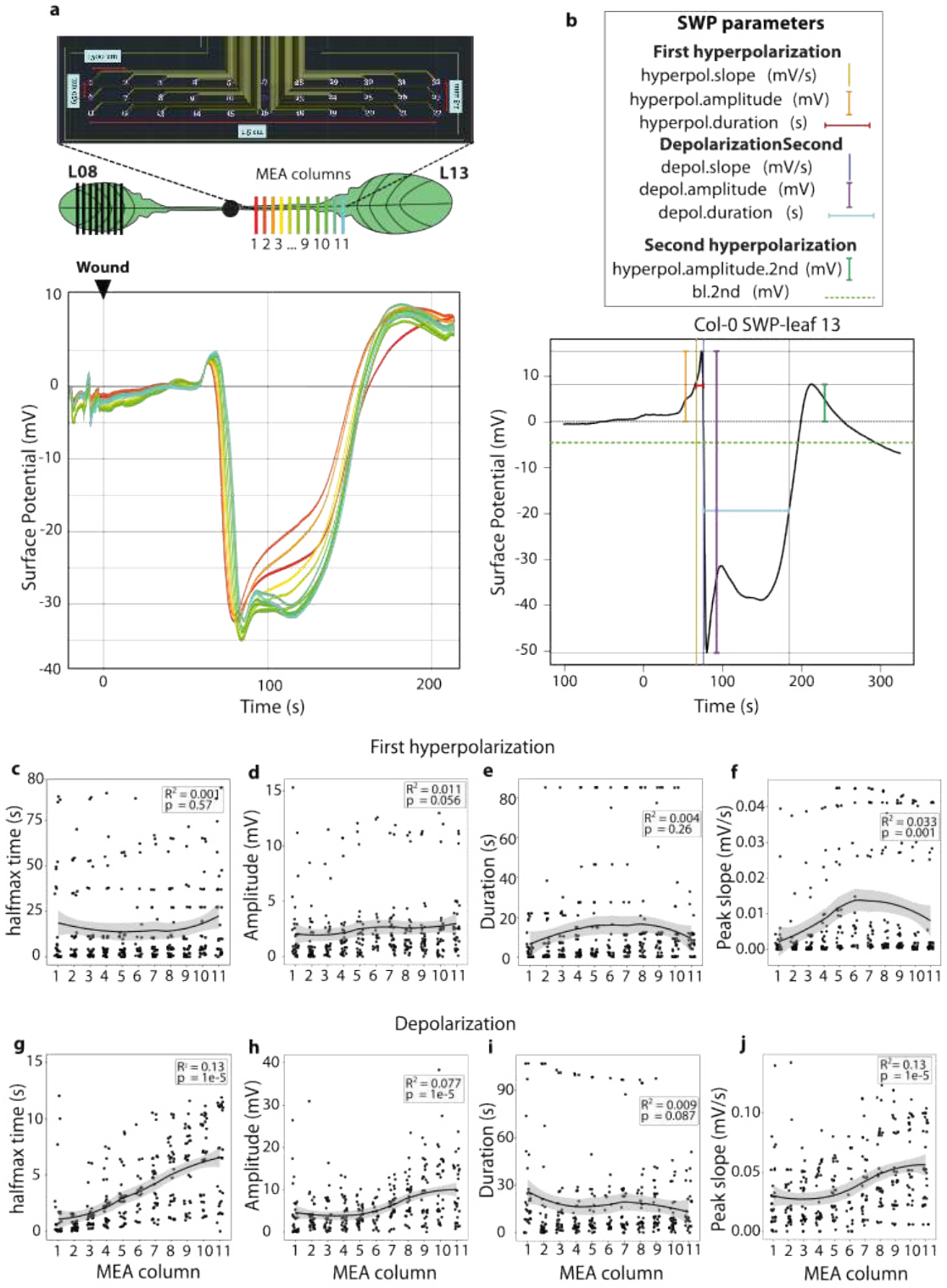
a
L08
MEA columns
L13
1 2 3 ... 9 10 11
Wound
Surface Potential (mV)
Time (s)
b
SWP parameters
First hyperpolarization
hyperpol.slope (mV/s)
hyperpol.amplitude (mV)
hyperpol.duration (s)
DepolarizationSecond
depol.slope (mV/s)
depol.amplitude (mV)
depol.duration (s)
Second hyperpolarization
hyperpol.amplitude.2nd (mV)
bl.2nd (mV)
Col-0 SWP-leaf 13
Surface Potential (mV)
Time (s)
First hyperpolarization
c
halfmax time (s)
R² = 0.001
p = 0.57
d
Amplitude (mV)
R² = 0.011
p = 0.056
e
Duration (s)
R² = 0.004
p = 0.26
f
Peak slope (mV/s)
R² = 0.033
p = 0.001
Depolarization
g
halfmax time (s)
R² = 0.13
p = 1e-5
h
Amplitude (mV)
R² = 0.077
p = 1e-5
i
Duration (s)
R² = 0.009
p = 0.087
j
Peak slope (mV/s)
R² = 0.13
p = 1e-5
MEA column

Figure 4. Recording of *Arabidopsis* SWP with increased spatial and analytical resolution. (**a**) Top - multi electrode array (MEA) used to simultaneously record the surface potential at 32 points along the petiole of a plant wounded in the leaf 8 (L08). Numbered lines in leaf 13 (L13) represent the position of the 11 electrodes displayed in the trace. Bottom – representative trace of the SWP recorded with the MEA. Only 1 channel per column is displayed for clarity (*i.e.*, the mid-row electrodes). (**b**) Illustration of the parameters quantified by the semi-automated signal analysis pipeline developed.
Parameters quantified at the first hyperpolarization phase (**c-f**) and from the depolarization phase (**g-j**) are displayed in scatter plots over the longitudinal position on the petiole to determine change along the propagation axis. Insets display the R^2 and the p value of a Pearson correlation between both variables, n=10.

The sinusoidal beacon signal could be recorded simultaneously in both leaves, contrasting with the leaf 8 depolarization, which was not perceived in the receiving leaf, and peaked before leaf 13 hyperpolarization (Figure 5b). The exogenous beacon was recorded simultaneously in both leaves, with an expected, slight amplitude dampening resulting from passive electrotonic transmission through the tissue. This suggests that, although electrotonic transmission between plants is possible, massive wound-induced depolarization is not passively transmitted. The pathway for electrotonic transmission of the beacon pulse could the apoplasm or the symplasm through plasmodesmata (Van Bel and Ehlers, 2005; Van Bel *et al.*, 2014). We determined that electrotonic transmission of the beacon occurred through the apoplasmic syncytium as the signal is disseminate even through scalded, dead tissue connected only by the xylem (Gao *et al.*, 2023) (Figure 5c-d).

This observation highlights a remarkable electric compartmentalization of endogenous membrane depolarization in plants, despite the existence of an apoplasmic electric syncytium. Furthermore, the SWP simultaneous hyperpolarization of leaf 13 during the SWP occurs only after the massive depolarization in leaf 8, refuting the hypothesis that the hyperpolarization phase is generated by distal electric influences.

Focusing on the depolarization phase, it exhibits distinct kinetic changes. Initially presenting a single peak following sharp depolarization, the wave progressively develops a second peak as it propagates acropetally (Figure 4a). Despite this transformation, the duration of the depolarization phase remains constant (66.37 ± 3.51 s, n = 9) (Figure 4c), which is significantly longer than the duration of the AP (11.48

± 0.14 s, n = 5). This suggests that the AP-generating mechanism may only partially contribute the SWP generation. Furthermore, towards the acropetal region, the slope of the SWP depolarization slope becomes shallower (Figure 4j) as the broader, second peak develops – a kinetic characteristic reminiscent of the Ca^{2+}-triggered AP described.

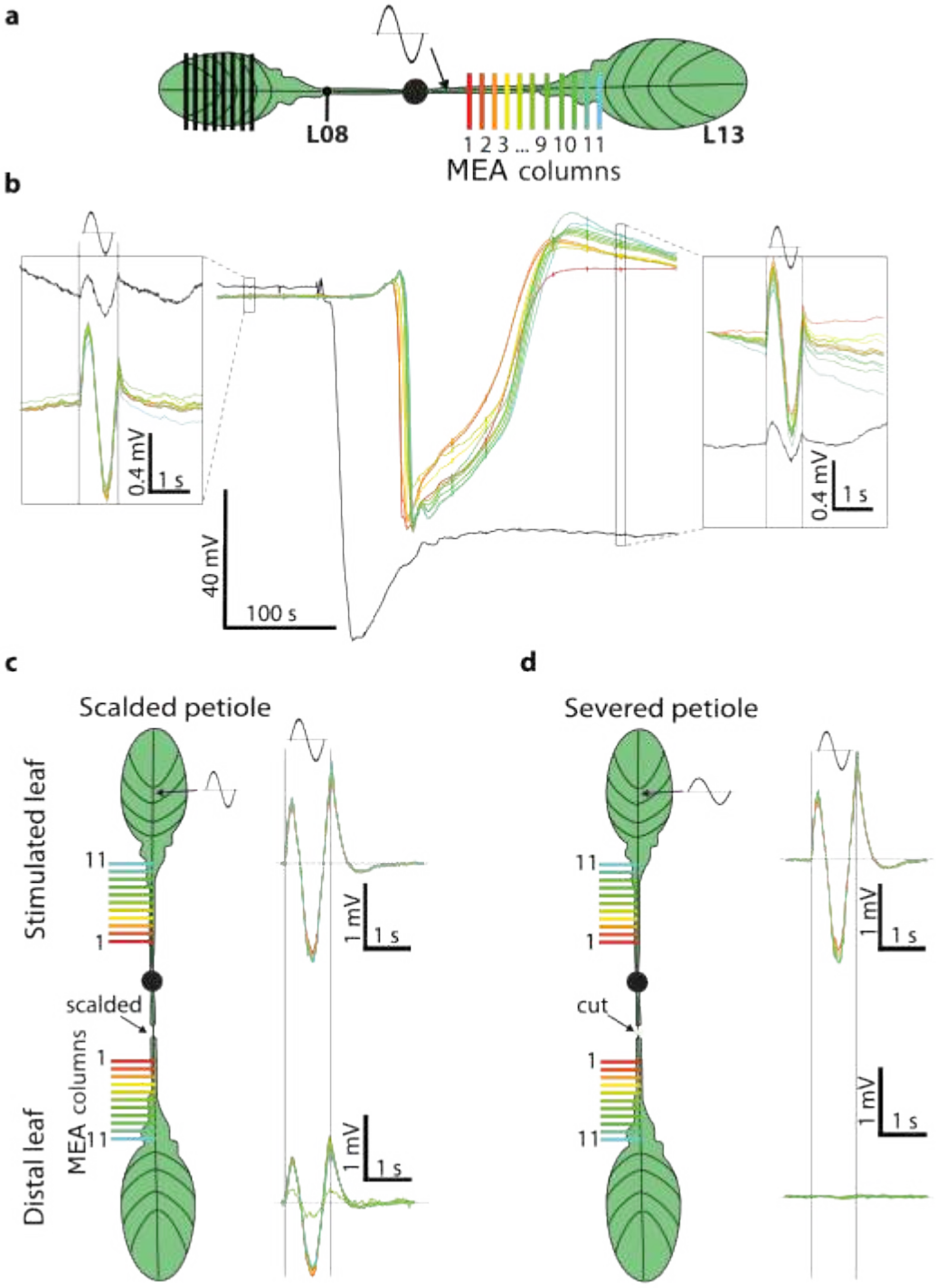

Figure 5. Electrotonic transmission of an SWP and a computer-generated sine wave. (**a**) Illustration of experimental setup. Black point on leaf 8 (L08) represents the recording electrode. Numbered lines in leaf 13 (L13) represent the position of the 11 electrodes displayed in the respective colored traces. Arrow in leaf 13 indicates point of wire insertion for generation of a sine wave of 10 mV amplitude, period 1 s. (**b**) Representative leaf 13 traces (colored traces) of an SWP generated upon leaf 8 wounding (recorded as black trace) while a sine pulse is generated every 15 s. Insets are a zoom into the first pulse before the

SWP and last pulses after. Propagation of the sine wave from the stimulated leaf to a distal leaf that was scalded one day before recording (**c**), and the same scalded leaf severed after the first recording (**d**). Illustration of experimental setup. Numbered lines represent the position of the 11 electrodes displayed in the trace.

The contribution of the AP to the SWP remains unclear, since it is entangled with the chemical and mechanical mechanisms hypothesized to sustain signal propagation and generation. In an attempt to understand the interplay between these mechanisms, we compared the arrival times of the depolarization and hyperpolarization phases at the petiole with the bulk flow.

The simultaneous onset of the initial hyperpolarization could be explained by the synchronous stimulation of the entire tissue. The mechanical propagation hypothesis suggests that a rapidly propagating pressure wave could result in simultaneous excitation along the tissue (Vodeneev *et al.*, 2012; Moe-Lange *et al.*, 2021). If a hydraulic wave initiates the hyperpolarization, we would expect this phase of the SWP to precede the arrival of the wounding-induced bulk flow, which carries the chemical cues (Gao *et al.*, 2023; Bellandi *et al.*, 2022).
To test this hypothesis, we loaded the leaf to be wounded with the fluorescent label Atto 514, and, following wounding, simultaneously recorded the arrival of the chemical and electrical signals at the receiving leaf (Figure 6a).

Using Atto 514 fluorescence increase as a reference, the onset of the hyperpolarization occurs almost immediately, while the onset of the depolarization is delayed by nearly 10 s (Figure 6b,c,f). This indicates that the bulk flow, represented by the movement of Atto 514, arrives within the same time range as the onset of the hyperpolarization, and precedes the depolarization.

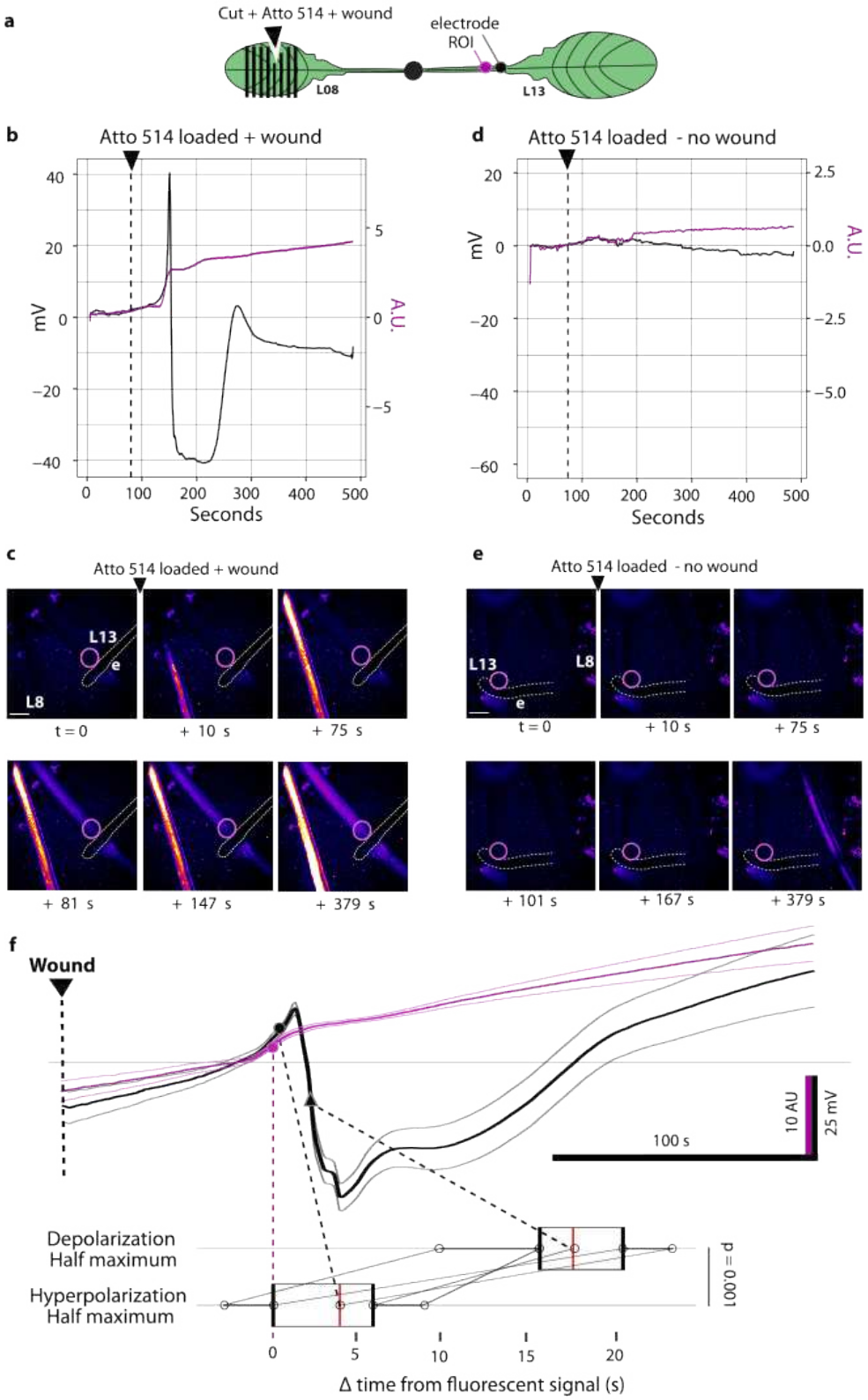
a
Cut + Atto 514 + wound
electrode
ROI
L08
L13
b
Atto 514 loaded + wound
mV
A.U.
Seconds
d
Atto 514 loaded - no wound
mV
A.U.
Seconds
c
Atto 514 loaded + wound
L13
e
L8
t = 0
+ 10 s
+ 75 s
+ 81 s
+ 147 s
+ 379 s
e
Atto 514 loaded - no wound
L13
L8
e
t = 0
+ 10 s
+ 75 s
+ 101 s
+ 167 s
+ 379 s
f
Wound
10 AU
25 mV
100 s
Depolarization
Half maximum
Hyperpolarization
Half maximum
p = 0.001
Δ time from fluorescent signal (s)

Figure 6. Simultaneous recording of fluorochrome Atto 514 and SWP propagation in *Arabidopsis* leaves. (**a**) Illustration of experimental setup. Atto 514 was loaded on leaf 8 (L08) through a marginal cut excluding the midvein prior to wounding. SWP and Atto 514 fluorescence intensity were correspondingly recorded at the ROI and electrode in the petiole of leaf 13 (L13). (**b**) Representative traces of fluorescent imaging (purple) and surface potential recordings (black) on leaf 13 after cutting, fluorochrome addition, and wounding, or no wounding (**d**). (**c**,**e**) Representative images of the traces on **b** and **d**. Electrode (e) is outlined by white dotted line; purple circle is the ROI for intensity quantification. (**f**) Mean ± SEM traces of the simultaneous surface potential recordings (black), and pixel intensity (purple) illustrated in **b** and **c**. Boxplots show the time difference between the fluorescence increase at half maximum (purple dotted line) and the half maximal time of the hyperpolarization (left black dotted line) and depolarization (right black dotted line). Points in the boxplots corresponding to the same plant are connected. p value determined by a student T-test, n=5.

Although the determination of the fluorochrome arrival time is constrained by detection limits, and the movement of Atto 514 does not provide information about the effective concentration of physiologically relevant molecules, its early arrival emphasizes the significance of the chemical propagation hypothesis in SWP transmission and generation. Moreover, it allows us to propose that the AP might be generated at the later phase of SWP depolarization.

As reported in *Nitella*, amino acids can modulate the properties of APs (Lapeikaite *et al.*, 2020). We hypothesize that the chemical cues carried by the bulk flow precede the AP and can modulate its kinetics, potentially integrating it into what we observe as SWP. To test the wound-mediated modulation of the AP, we studied the effect of wounding on the kinetics of the archetypal plant AP, the *Dionaea* AP.

Co-occurrence of AP and SWP in *Dionaea muscipula*

The *Dionaea* AP has provided important mechanistic insights into electric signals in plants. However, wound-induced, long-distance electric signals in this model have not been investigated. Here, we characterized the SWP generation capacity of the Venus flytrap, identified the different propagation domains of AP and SWP, and explored how wounding can modulate the AP.

We simultaneously recorded the surface potential on the vein at the base of the lobe and at the petiole (Figure 7a). The electric signal generated by hair stimulation is restricted to the lobe, with only a hyperpolarization (< 1 mV) observed in the petiole during the repolarization phase of the lobe AP, consistent with findings reported by Pavlovic et al. (2017) (Figure 7b).

Once the lobe is closed, it is wounded by compression for 3 s, similar to the procedure used for *Arabidopsis* SWP generation. Immediately upon compression, a transient, slow depolarization initiates both in the lobe and the petiole. This wound-induced depolarization is accompanied only in the lobe by a series of 11 ± 1 (n=5) consecutive APs that occur during and after the release of the compression stimulus. The initial frequency of these APs is 0.74 ± 0.03 Hz and decreases to 0.19 ± 0.01 Hz until the activity ceases. Notably, this spontaneous activity is not recorded in the petiole, where only the SWP is observed (Figure 7b).

The spatial segregation of the AP and SWP suggests that their generation is potentially supported by different molecular mechanisms. To determine whether the molecular actors required for AP generation are also necessary for SWP generation, we wounded the lobe of immature, non-AP-generating, stage V plants (Scherzer, Huang, *et al.*, 2022). As expected, these juvenile plants did not generate APs upon wounding, while an SWP was observed both in the lobe and petiole (Figure 7e). This discovery suggests that, in *Dionaea*, the mechanisms underlying AP generation may not be required for SWP generation.

Considering that the characean AP can be modulated by amino acids, and the possibility that the $[Ca^{2+}]_{cyt}$-triggered AP in *Arabidopsis* might be modulated by wounding-related molecules during the SWP generation, we examined the effect of this crush-wounding in *Dionaea* AP kinetics. We observed that the amplitude of the wound-induced APs diminishes, while their duration increases from 420 ± 5 ms for the touch-induced APs to 740 ± 3 ms for the spontaneous wound-induced APs (Figure 7d). In addition to changes in amplitude and duration, the shape of the APs also shifts: the depolarization phase becomes bimodal and is preceded by a hyperpolarization phase, mimicking the *Arabidopsis* SWP (Figure 7c). This alteration in AP shape suggests that the AP-generating mechanism is sensitive to wound-mediated modulation.

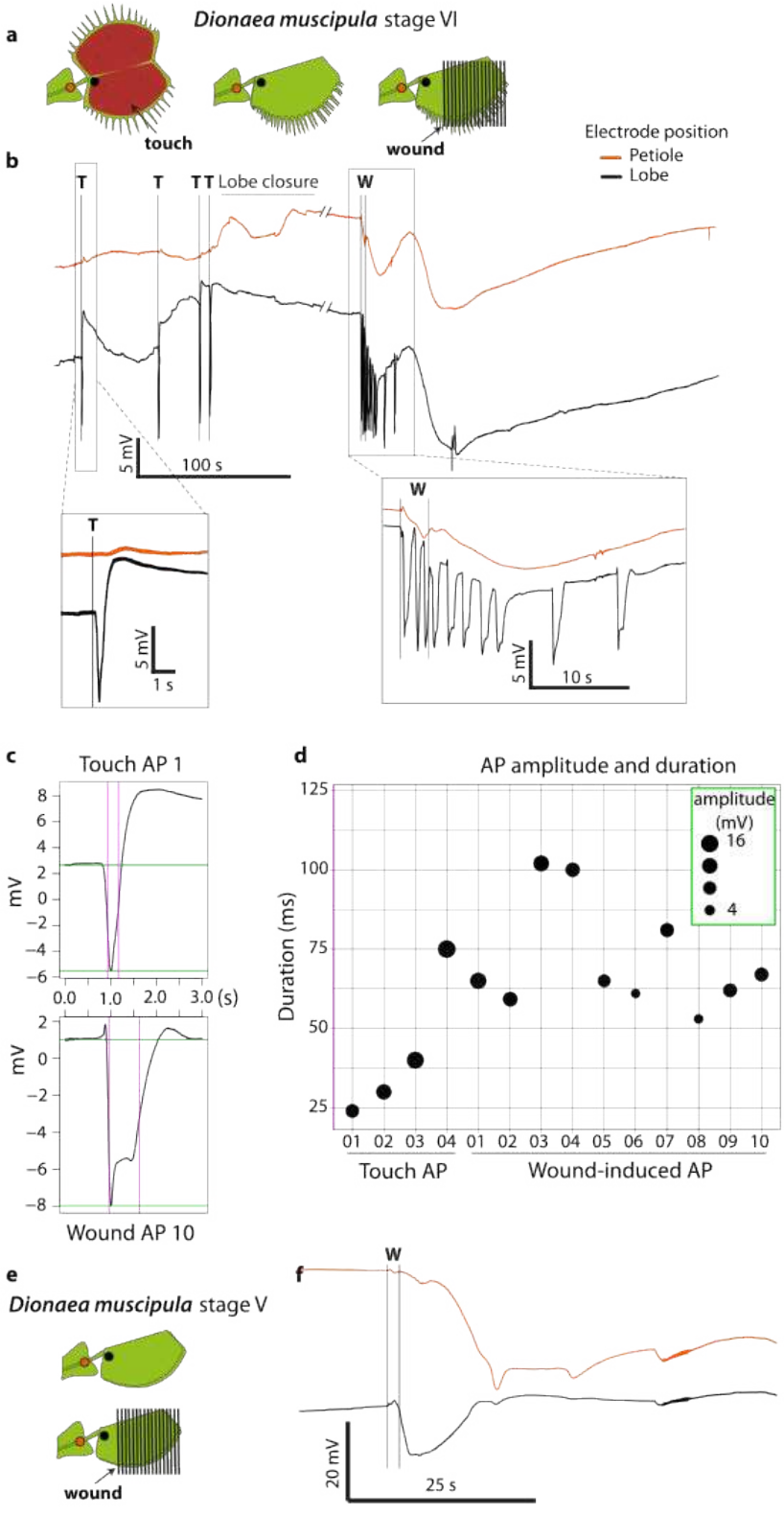
a
Dionaea muscipula stage VI
touch
wound
b
Electrode position
Petiole
Lobe
T
T
T T Lobe closure
W
5 mV
100 s
T
5 mV
1 s
W
5 mV
10 s
c
Touch AP 1
mV
0.0 1.0 2.0 3.0 (s)
mV
Wound AP 10
d
AP amplitude and duration
amplitude (mV)
16
4
Duration (ms)
125
100
75
50
25
01 02 03 04 01 02 03 04 05 06 07 08 09 10
Touch AP
Wound-induced AP
e
Dionaea muscipula stage V
wound
f
W
20 mV
25 s

Figure 7. Surface potential recordings of *Dionaea muscipula* plants. (**a**) Illustration of the experimental setup. Electrodes were placed at the base of the lobe (black dot) and at the petiole (orange dot) of adult stage VI plants. Electrode position color corresponds to the trace color. (**b**) Representative traces of touch (T)-induced APs and a 3 s lobe compression wound (W)-induced response. Rectangles represent zoomed-in views of the respective traces. (**c**) Illustration of the quantification of the amplitude (green lines) and duration (purple lines) for the first touch-induced AP and the last, wound-induced, spontaneous AP. (**d**) Scatter plot of amplitude vs duration of all the APs from **b**. (**e**) Illustration of the experimental setup. Electrodes were placed at the base of the lobe (black dot) and at the petiole (orange dot) of adult stage V plants. (**f**) Electrodes positioned at the base of the lobe and at the petiole of juvenile stage V plants. Representative trace of a 3 s compression wound (W)-induced response.

Discussion

In this work we provide a fundamental and detailed characterization of the AP-generating mechanism in *Arabidopsis thaliana*, revealing that plant APs are $[Ca^{2+}]_{cyt}$ -dependent and constitute a tunable response, unlike the voltage-dependent, highly stereotypical APs in animal systems (Barnett and Larkmann, 2007). Connecting this knowledge to the physiological context of wound-induced SWPs, we propose a synergistic operation between the $[Ca^{2+}]_{cyt}$-dependent AP, and the bulk flow of Ricca's factors (Bellandi *et al.*, 2022; Gao *et al.*, 2023), that contributes to the SWP generation. This supports the hypothesis that the AP does not function as a signaling cascade initiator, but rather as a mechanism of signal amplification downstream of the initiating chemical stimulus propagated by the bulk flow.

Arabidopsis AP in SWP propagation

Despite the proposition of AP as signaling entity in a variety of plant physiological phenomena (Pyatygin *et al.*, 2008; Fromm and Lautner, 2007), their fundamental characteristics have only been well-characterized in Characean algae: voltage-dependent initiation, determined stimulus threshold, duration, amplitude and refractory period (Beilby, 2007; Barnett and Larkmann, 2007; Lapeikaite *et al.*, 2019; Pupkis *et al.*, 2022).

Here, we demonstrate that *Arabidopsis* leaves generate a signal that fulfills some key characteristics of an AP. It is a self-propagating transient, initiated by a stimulus threshold, and has a refractory period. The *Arabidopsis* AP differs from the canonical AP definition in that its amplitude and duration are variable, and its initiation critically depends on an increase of $[Ca^{2+}]_{cyt}$, while membrane depolarization alone is insufficient.

This reliance on $[Ca^{2+}]_{cyt}$ aligns with the Characeaen model (Beilby, 2007). However, unlike Characean algae, in which voltage-dependent $[Ca^{2+}]_{cyt}$ increase occurs (Lapeikaite *et al.*, 2020; Lapeikaite *et al.*, 2019), membrane depolarization is insufficient to activate the AP in *Arabidopsis*. This difference suggests that the electrically triggered $[Ca^{2+}]$ conductance of the Characean family is missing in *Arabidopsis.* Rendering the $[Ca^{2+}]$ increase in the SWP likely activated by chemical rather than electric stimulation, which inherently suggests a slower signal propagation (Vodeneev *et al.*, 2015). This differential signal activation could also explain why the speeds of the *Arabidopsis* AP (0.11 cm/s), and SWP (0.11 – 0.19 cm/s) (Gao *et al*., 2023; Nguyen *et al*., 2018; Toyota *et al*., 2018, reviewed in Barbosa-Caro & Wudick 2024) are slower than the Characean AP (0.70 – 4.4 cm/s) (Tabata and Sibaoka, 1987; Umrath, 1932; Beilby, 2007).

Additionally, using a higher spatial resolution MEA, we report that the hyperpolarization initiates simultaneously along the petiole area recorded, while the depolarization propagates at the speeds consistent with those reported for SWPs. We show that the propagation of Atto 514 in the vasculature precedes the depolarization, with the hyperpolarization and the fluorochrome arrival occurring simultaneously within our detection limit. This sequence of events was determined with a single point measurement at the acropetal end of the petiole. However, at more basipetal points, the bulk flow could potentially precede the hyperpolarization, assuming that our detection limit allows identification of a propagating fluorescent front.

We could not resolve whether the bulk flow arrives before or simultaneously with the hyperpolarization, but in both cases it certainly precedes the SWP-associated $[Ca^{2+}]_{cyt}$ increase (Moe-Lange *et al.*, 2021). This suggests that SWP-relevant molecules may arrive before the AP mechanism is activated. Additionally, coincidence of chemical cues arrival and the SWP initiation leave little space for the hypothesized hydraulic propagation to act as a SWP initiator. In more detail, if an immediate hydraulic wave as measured in wheat by (Vodeneev *et al.*, 2012) occurs, it could (i) generate a response in the distal leaf through an electrically silent transduction mechanism, (*ii*) it could be

delayed in the node between leaves, which can work as an information relay, and arrive at the same time or after the chemical cues, contributing to the SWP after its initiation, (*iii*) it could have no effect on the receiving cells, or (*iv*) it could simply not occur in *Arabidopsis*. Altogether, the role of hydraulic signal transmission in the SWP remains unresolved in *Arabidopsis* and warrants further investigation.

We therefore propose that the SWP transmission mechanism in the *Arabidopsis* vasculature is driven by the rapid propagation of Ricca's factors, likely sustained by bulk flow, turbulent diffusion, or aided by a hydraulic mechanism (Gao *et al.*, 2023; Bellandi *et al.*, 2022; Vodeneev *et al.*, 2012). This mechanism would exclude instantaneous rapid pressure waves or self-propagating APs as primary contributors to propagation.

To address the possibility that the fluorochrome propagation differs from that of the SWP-relevant molecules glutamate and aglycone (Gao *et al.*, 2023), and considering the limitations of a single-point observation, it is essential to resolve the propagation patterns of these ligands. This analysis should be referenced against the hyperpolarization and depolarization propagation dynamics along the petiole for a comprehensive understanding of their spatiotemporal relationships.

Arabidopsis AP in SWP generation

Given that the AP mechanism does not initiate the SWP, we propose that it could function as a signal amplifier. While the *Arabidopsis* AP amplitude (-50 mV) is similar to the SWP, its duration (13 s) is much shorter than that of the SWP duration (100 s). Additionally, we observed that the duration of the *Dionaea* AP can be significantly increased by a massive wounding in the lobe, while small wounds only generate a stereotypical, single AP (Pavlovič *et al.*, 2017). Notably, the AP amplitude decrease reported here is drastically stronger than shape modulations previously described in the Characean algae, where exogenous application of amino acids prolonged the AP

(Lapeikaite *et al.*, 2020; Lapeikaite *et al.*, 2019), or in *Dionaea*, where sequential trigger-hair touch events cause bigger and faster APs (Armada-moreira *et al.*, 2023; Moe-Lange *et al.*, 2021).

We hypothesize that, similar to the *Dionaea* AP, the *Arabidopsis* AP can be modulated in the context of systemic wound response. We propose that the SWP in the non-wounded leaf is initiated by the onset of the bulk flow carrying GLR-activating ligands. This induces an initial $[Ca^{2+}]_{cyt}$ increase that summons the AP machinery, whose shape could be modulated into a longer transient by wound-related molecules. Experimental validation is needed to determine whether the kinetics of the *Arabidopsis* AP can be modulated by wounding, and to identify such potential AP-modulating moieties.

Furthermore, the mechanical and chemical stimuli precede the observed MSL10 activity window. To elaborate, after the GLR3.3/GLR3.6-dependent initiation of the SWP, MSL10 is necessary for its full development. Predicted putative EF-hands ($[Ca^{2+}]_{cyt}$-binding, regulating domains) in MSL10 suggest a $[Ca^{2+}]_{cyt}$-dependent regulatory role in this mechanosensor (Moe-Lange *et al.*, 2021). Additionally, the mechanical stimulus, if it occurs at all, hypothesized to result from distal massive wounding would propagate orders of magnitude faster (Vodeneev *et al.*, 2012) than the observed SWP initiation.
Considering that the mechanical and chemical stimuli precede MSL10 activity, the regulatory role of $[Ca^{2+}]_{cyt}$ in MSL10 function becomes increasingly relevant. This raises the possibility that the MSL10 might contribute to the generation of the $[Ca^{2+}]_{cyt}$ -initiated AP.

Alternatively, it is remarkable that the propagation speed of the SWP and the AP in *Arabidopsis* coincide with that of the self-propagating Reactive Oxygen Species (ROS) wave discovered by Miller et al. (2009). The 0.14 cm/s propagating ROS wave can be generated by mechanical wounding, and has been linked to the activation of electric and $[Ca^{2+}]_{cyt}$ transients (Miller *et al.*, 2009; Mittler *et al.*, 2011; Gilroy *et al.*, 2014; Gilroy *et al.*, 2016). The *Arabidopsis* AP reported here could be sustained by this propagating

mechanism. This could suggest that the activity of $[Ca^{2+}]_{cyt}$ increase, but not membrane depolarization alone, can initiate the propagating ROS-$[Ca^{2+}]_{cyt}$ positive feedback loop, which can tangentially be observed as an electric wave.

These hypotheses render the AP observed in Col-0 plants expressing pUBQ10:XXM an ideal system to directly investigate the functional interplay between MSL10, $[Ca^{2+}]_{cyt}$,and ROS in the propagation of long distance signals.

Evolutionary remarks

Electric signals are usually associated to a demand for fast information transmission in response to rapidly changing stimuli (Fromm and Lautner, 2007; Pyatygin *et al.*, 2008). This fully corresponds to the mobile, quickly responsive nature of animals, but in plants it is essential to ask how fast is *fast*?

Here we propose that the SWP is more likely propagated by chemical diffusion, supported by bulk flow, turbulent diffusion or potentially aided by a hydraulic wave. The demand for a fast response in the case of plant wound signaling could be fulfilled by such physical phenomena, which initiate a complex cascade of biological processes that amplify or encode the signal. This raises the fundamental question of how is the observed electric signal biologically relevant.

Electric signals undeniably play key roles in plant biology, regulating processes such as stomatal dynamic regulation (Stange *et al.*, 2010; Geiger *et al.*, 2010; Papanatsiou *et al.*, 2019; Hosy *et al.*, 2003; Blatt and Thiel, 1994; Meyer *et al.*, 2010), root nutrient uptake homeostasis (Hedrich and Geiger, 2017; Wang *et al.*, 2021; Dreyer *et al.*, 2022). In these processes membrane potential directly regulates the activity of membrane proteins. But membrane electric sensitivity as an initiation mechanism of propagating signals has only been observed in the Characean AP (Beilby, 2007). Similarly, in the *Dionaea* AP, an electric cue is only assumed to be the initiator, as the mechanosensitive membrane

protein expressed in the hinge of the lobe sensing hairs is permeable to chloride upon membrane stretch (Procko *et al.*, 2020), which would translate to membrane depolarization upon trigger-hair bending *in planta.* However, it is still necessary to identify whether the electric signal precedes the $[Ca^{2+}]_{cyt}$ increase. And if so, which voltage-sensitive proteins link these events that orchestrate insect-catching-fast lobe closure (Suda et al., 2020).

Furthermore, the evolutionary context highlights the unique nature of the rapid *Dionaea* AP. Carnivory in angiosperms is rare, occurring only in about 800 of the nearly 290,000 living species (~ 0.2%) (Christenhusz and Byng, 2016; Ellison and Adamec, 2018). Among the carnivorous angiosperm taxa, carnivory is a polyphyletic trait - it is not shared with a common ancestor. Specifically, the most frequent trapping mechanisms are passive and evolved multiple independent times; flypaper traps emerged five times while pitcher traps three times. In stark contrast, only two active trapping mechanisms exist, and they evolved only once in two different taxonomical orders. One is the aquatic, microorganism-catching bladder in the genus *Utricularia*, and the other is the snapping leaf trap of *Dionaea* (Albert *et al.*, 1992). This evolutionary singularity of the *Dionaea* trapping mechanism, tightly linked to its capacity of generating APs, motivates us to ask how far can we extrapolate to other vascular plants the physiological mechanisms that support the *Dionaea* AP.

We propose that, based on the broader, plant-specific AP definition presented here, the occurrence of APs is a polyphyletic, broad spread phenomenon among plants, including characean algae and *Dionaea*. Besides these two conspicuous cases, the AP underlying mechanism in other plants is probably cryptic, diverse, and likely voltage-independent and slow, as shown in *Arabidopsis.*

In contrast, the wide-spread occurrence of the SWP in response to wounding is conspicuous and has been reported in a multiplicity of plant clades:-*Arabidopsis*, *Vicia faba* (Dziubińska, 2003), *Helianthus annus* (Dziubińska *et al.*, 2001), *Triticum aestivum*

(V. Vodeneev et al., 2012), *Oryza sativa* (Yu *et al.*, 2022), and the primitive liverwort *Marchanti polimorpha* (Sanmartín *et al.*, 2024; Watanabe *et al.*, 2023), and in *Dionaea* (Figure 7). Besides being a phenomenon broadly found in taxonomy, the SWP is also broadly occurring in the *Dionaea* tissue. It propagates out of the AP-generating tissue, and occurs even in the immature, non-AP-generating, developmental stage (Figure 7b,e). This raises the question whether the SWP supporting mechanisms is conserved among the multiple clades, and whether some SWP molecular actor could be the base for *Dionaea* AP evolution.

To answer this, and all the questions ahead in the field of plant electric signaling, it is necessary to continue a thorough molecular and biophysical investigation to identify the underlying components that sustain the AP and SWP in different species. It is essential to stand on the assumption that the stablished animal and the *Dionaea* models are an invaluable electrophysiological framework, but many aspects of general plant biology and physiology depart from these models and require new and creative paradigms.

Materials and methods

Plant growth condition

Arabidopsis thaliana plants for SWP recordings were grown for 5-6 weeks at 22 °C, 60% humidity, ~120 µmol $m^{-2}s^{-1}$ light intensity, and 10/14 h light/dark photoperiod. Leaves 8 and 13 were counted as described in (Atanjaoui *et al*., submitted). *Arabidopsis* plants expressing the pUBQ10:ACR1, pUBQ10:XXM, and pMSL10:ACR1 constructs were grown for 4-5 weeks in a 16/8 h light/dark photoperiod, at 22 °C, 60% humidity, under 4 µmol $m^{-2}s^{-1}$ red light (λ_{peak} = 660 nm), and 1 µmol $m^{-2}s^{-1}$ blue light (λ_{peak} = 390 nm). These growth conditions apply for all the experiments.

Cloning of the optogenetic tools cloning and Arabidopsis transformation

The optogenetic tools were obtained from Georg Nagel's group. ACR1 tagged with a YFP, and the retinol-producing dioxigenase (Ret) are in the pCambia backbone under the *UBIQUITIN10* promoter and the *RBC* terminator. Basta resistance for plant selection under the 35S promoter and kanamycin resistance for bacterial selection (annex2). The change to the *MSL10* promoter was done with the Greengate system. The promoter was cloned from *Arabidopsis* genomic DNA and added overhangs for insertion into the corresponding Greengate module. The primers used can be found in (table 1). The final vector, with ACR1 under the *MSL10* promoter and *UBQ10* terminator, has an RFP seed coat label for plant selection and spectinomycin for bacterial selection (annex2). The XXM-Ret was cloned into a pRB40 backbone, expressed under the *UBQ10* promoter and terminator, followed by the Ca^{2+} reporter jR-GECO1/a. It has Plant resistance to Basta under the 35S promoter, and bacterial resistance to spectinomycin (annex2). Channelrhodopsins, Ret, and jR-GECO1/a are separated from each other by a P2A cleaving sequence.

Optogenetic light stimulation

For stimulation of optogenetics tools, the high-power LED light sources M530F3 and the M470F4 (Thorlabs, Germany) were used for ACR1- and XXM-expressing plants, respectively. Light was guided through an optic fiber (M76L01, Thorlabs) to a collimator (CFC5-A, Thorlabs), and focused on a 2 mm diameter circle. Positioning was guided, and light further restrained from scattering with a 3D printed, custom-designed cone coupled to the collimator (annex1). All manipulation and recording was done in a recording faraday cage under red light (λ_{peak} = 600 nm).

Leaf manipulation – wounding, scalding, sine wave generation

For SWP recording, the leaf 8 is placed in the wounding device (Atanjaoui,submitted) (annex 1). Briefly, plants were left to rest for 10-15 minutes after setting up. A stable baseline was recorded on leaf 13 for 90 s, followed by a 3 s compression wounding event with a grip wrench. Corrugated wounding surfaces attached to the grip wrench were custom-designed and 3D printed (annex 1). For petiole scalding, leaves were placed in the 3D printed holder (annex 1c) and approx. 200 µl of boiling water were dropped on the middle of the petiole the day before the experiment. For sine wave generation, a 0.25 mm diameter silver wire, previously chloridized for at least 1 h in 13% bleach, was inserted into the petiole or leaf blade of the stimulated leaf. The wire was connected to the pulse generator output of the headstage of the ME2100-system (Multichannel Systems, Germany). A sine wave with peak-to-peak amplitude of 10 mV, and period of 1 s was generated.

Custome-made printed electrode manufacturing

All materials were deposited using a flatbed sheet-fed screen-printing system (DEK Horizon 03iX) onto polyethylene terephthalate (PET) plastic substrates, such as Polifoil Bias from Policrom Screen. Standard polyester mesh-based screens were employed for all printing steps. The initial conductive layers, including conductors and contact pads, were printed using silver ink (Ag 5000, DuPont) on the flexible PET substrate. These contact pads serve as probing surfaces for subsequent electrical measurements.

Following this, the electrode material, PEDOT:PSS (Clevios SV3, Heraeus), was patterned at the end of the silver contact pads. Both silver and PEDOT:PSS layers were dried at 120 °C for 5 minutes. Finally, A UV-curable insulating layer (5018, DuPont) was screen-printed over the device, leaving the electrode areas containing PEDOT:PSS exposed. This layer was UV-cured to provide electrical insulation while allowing electrode functionality through the open areas.

Surface potential recording – individual electrodes

Plants were acclimated for a minimum of 1 hour in the recording room under 120 µmol $m^{-2}s^{-1}$ white light for Col-0 plants or red light (600 nm) for Col-0 plants expressing channelrhodopsins, at ~22°C. The pot was submerged 3-4 cm deep in MS/2 solution. An Ag/AgCl electrode was chloridized and used as ground electrode placed in the solution. Recording was done with custom-made printed electrode. To bridge the electrodes and the tissue, a of drop PSSNa electrolyte (in deionized water, PSSNa 50% w/v, D-Sorbitol 10%, NaCl 0.1 M, glycerol 5% w/v). Experiments were initiated only after a stable baseline of at least 5 minutes was observed. When leaves were severed in electric transmission experiments a second ground was attached to the to-be-severed leaf tip with a 1 mm diameter Ag/AgCl electrode (World Precision Instruments) bridged with 3 M KCl in 2% (w/v) agar. Data acquisition was done with dual-channel amplifiers (NPI Instruments EXT-02F amplifiers, World Precision Instruments LabTrax data acquisition digital converter, iWorx LabScribe 4 data acquisition software). Gain was set to the minimum for all experiments, and offset was manually adjusted to zero after mounting electrodes.

Fabrication of multi-electrode array

A 23 µm-thick polyethylene terephthalate (PET) foil (Mylar Plastic Film, RS article number: 785-0782, Germany) was laser-cut into circular substrates with a diameter of 10 cm using a laser (Trotec Speedy 300 flexx laser engraver Fiber: 20 W). The PET substrates were cleaned with deionized (DI) water and acetone, followed by vacuum baking at 120 °C for 90 s. To facilitate adhesion between the PET substrate and a 4-inch

glass wafer, a 20 µm-thick polydimethylsiloxane (PDMS) adhesion layer (Sylgard 184, Dow Corning, mixed at a 10:1 ratio) was spin-coated at 4000 rpm for 30 s and cured overnight on a hotplate at 70 °C. Metallization was patterned using the lift-off technique. The negative AZ nLOF 2020 photoresist was spin-coated at 3000 rpm, followed by soft baking and post-exposure baking at 110 °C for 90 s. Ultraviolet (UV) exposure was conducted using a Suss MA6 DUV Mask Aligner, and development was carried out in AZ 300 MIF developer. A 5 nm chromium (Cr) adhesion layer was deposited via thermal evaporation, followed by the deposition of a 150 nm gold (Au) layer using a high-vacuum Glovebox metal evaporator. The lift-off process was completed by immersing the samples in an acetone bath for 2 hours. To electrically insulate the metal lines, the substrate was encapsulated with SU-8 2010 (MicroChem). Openings of active areas were created using wet etching in mr-Dev 600 developer (Microresist Technology). To enhance signal recording quality, platinum (Pt) was electrochemically deposited on the gold electrodes using a three-electrode electrochemical setup with a 0.8 wt% chloroplatinic acid solution in DI water. A platinum mesh served as the counter electrode, and a silver/silver chloride (Ag/AgCl) electrode was used as the reference. All chemicals were used as received from Sigma-Aldrich unless otherwise specified.
This protocol was developed and executed by the Stavrinidou's lab at Linkoping University, Sweden.

Surface potential recording – multi-electrode array (MEA)

All recordings were carried out in a Faraday cage and plants were prepared as mentioned above. The leaf to be recorded was secured in a 3D printed, custom-designed holder (annex 1). PSSNa electrolyte was applied over the MEA, gently scraped away with a glass coverslip allowing the electrolyte to be deposited only in the indentures where the electrodes are. It was then placed on the petiole and a lid of the holder was gently pressed over it to ensure contact. Data was acquired at 1000 Hz sampling rate, down sampled to 100 Hz for analysis, with the ME2100-system (Multichannel Systems, Germany).

Bulk flow fluorescent imaging and simultaneous surface potential recording

A plant was positioned under a stereomicroscope (see more below) and an electrode was placed on leaf 13, as described above for single electrode measurements, but using a 1 mm diameter Ag/AgCl electrode (World Precision Instruments) that was bridged with 3 M KCl in 2% (w/v) agar.

The surface potential recording was initiated first, followed by imaging acquisition after 10 s. A cut was made on leaf 8, perpendicular to the midvein, extending from the broadest side of the leaf to 2-3 mm away from the mid vein. Immediately after cutting, 10 µl of Atto 514 fluorochrome solution (1 mM, Silwett 0.25%) was applied on the cut. Sixty seconds later, leaf 8 was wounded by compression. Quantitative imaging was performed using a Zeiss AxioZoom.V16 zoom microscope equipped XCite Xyilis XT720L light source (AHF, L56-720), 1× objective lens (PlanNeoFluar Z 1×/0.25 NA, FWD 56 mm, Zeiss), and a Hamamatsu ORCA Flash4.0 CMOS camera. Zoom magnification was set to 10x, and pixel binning was set to 2 × 2. For Atto 514 acquisition, a 500/25-nm excitation filter was used with a 515 dichroic and 535/35-nm emission filter. Manual circular Regions of interest (ROIs) were used for quantification in Fiji (Fiji is just imageJ), and analysed with the surface potential recordings using R (version 4.3.2).

Data manipulation and statistical analysis

Raw traces were smoothed by applying a Savitzky-Golay filter with a 3-frame window, or 7-9 frames for imaging-synchronized recordings. The time at the depolarization half maximum was used to determine occurrence of an event. The half maximum was calculated using peak-to-peak maxima for SWPs and optogenetically induced transients. Duration was calculated as the time from the initial half maximum, to the time of the returning half maximum. The second half maximum was independently calculated from the interval between the depolarization and repolarization peaks. All additional SWP parameters were calculated as described previously (Atanjaoui et al., submitted). Multichannel systems HDF5 raw data was initially opened in Python using the package McsPyDataTools. This and all the other raw data were further analyzed using R (version 4.3.2).

3D designs and printing

All the printed parts used were designed in Fusion 360 (v2.0.19941), sliced with PrusaSlicer (version 2.8.1), and printed with PLA in a Prusa Mini, using a layer height of at most 0.1 mm (annex 1). All the STL designs are accessible at https://github.com/jucbca/Plant-ephys/tree/main/3D%20designs.

Primer name	sequence
JB050-pMSL10>pGGA.fwd	GCTTGGTCTCAACCTAACGAGTGACAATGAATGGCATAT
JB051-pMSL10>pGGA.rev	ATTCGGTCTCATGTTTCCAATGCTACTACCATCCAATT

Table 1. List of primers used for MAL10 promoter cloning with overhangs fitting pGGC000 Greengate module.

Acknowledgements

We are grateful to Nicoline Gappel, Lisa Schöll, Waldemar Seidel and Marcel Pfaff for precious technical assistance. This work was supported by the Deutsche Forschungsgemeinschaft (DFG, German Research Foundation) under Germany's Excellence Strategye EXC-2048/1e Project-ID 390686111, and by the DFG Collaborative Research Center SFB 1208e Project-ID 267205415.

Annex 1. Holding devices for MEA recordings and optogenetic stimulation. (**a**) Setup of an *Arabidopsis* plant for MEA recordings of SWPs on leaf 13 and wounding device for compression wounding of leaf 8. (**b**) Setup for recording ACR1-driven responses with an MEA in the stimulated leaf 13 (right) and unstimulated leaf 12 (left). Light stimulation is confined by a coupled cone. (**c**) 3D designs of the leaf-MEA holder, the collimator coupled cone and the attachments for the compression-wounding device.

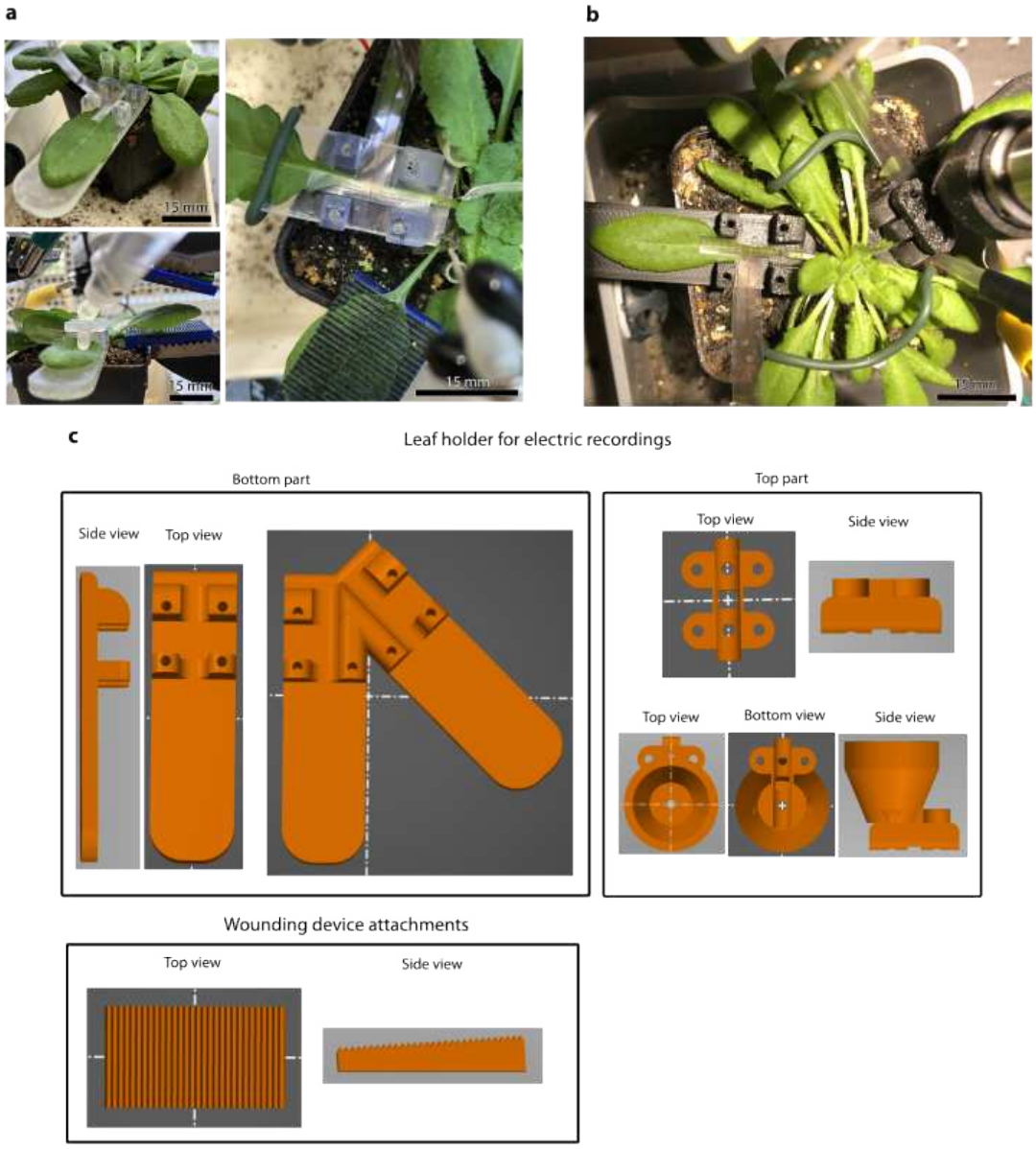
a
15 mm
15 mm
15 mm
b
c
Leaf holder for electric recordings
Bottom part
Side view
Top view
Top part
Top view
Side view
Top view
Bottom view
Side view
Wounding device attachments
Top view
Side view


A
B

Annex 2. Vector maps of plasmids containing the optogenetic tools ACR1 and XXM.

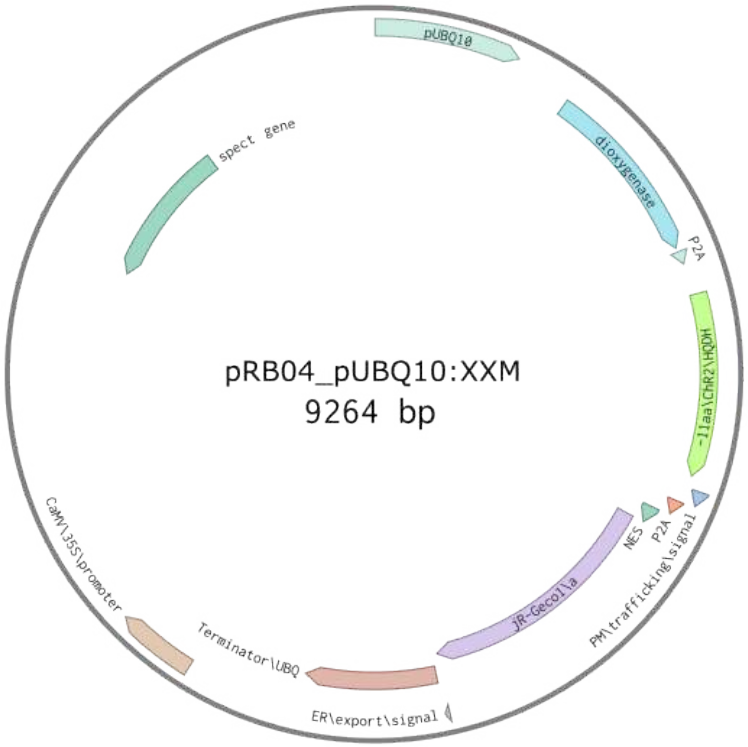

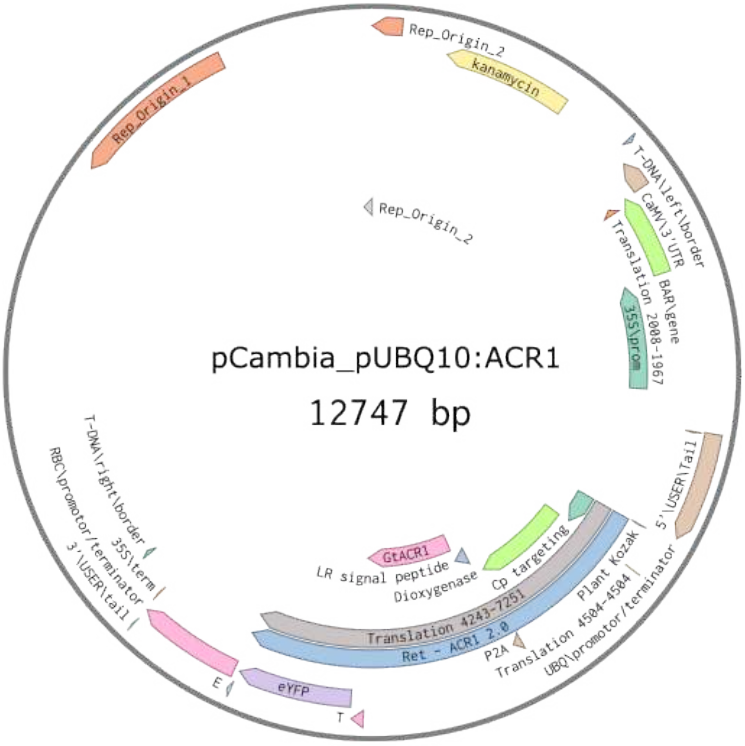
Rep_Origin_2
kanamycin
Rep_Origin_1
T-DNA\left\border
CaMV\3'UTR
Translation 2008-1967
BAR\gene
35S\prom
Rep_Origin_2
pCambia_pUBQ10:ACR1
12747 bp
5'\USER\tail
T-DNA\right\border
35S\term
RBC\promotor/terminator
3'\USER\tail
GtACR1
LR signal peptide
Dioxygenase
Cp targeting
Translation 4243-7251
Ret - ACR1 2.0
P2A
Plant Kozak
Translation 4504-4504
UBQ\promotor/terminator
E
eYFP
T

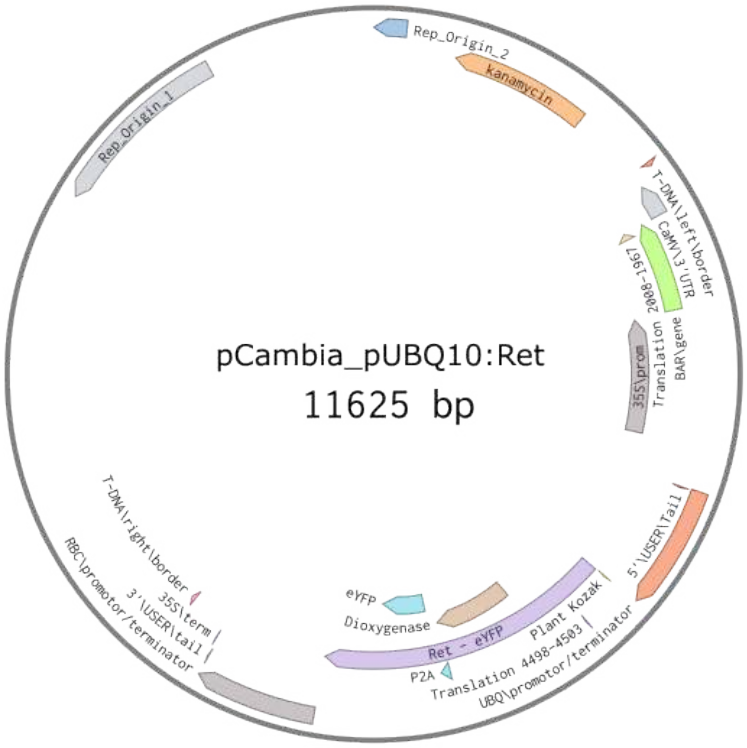
Rep_Origin_2
kanamycin
Rep_Origin_1
T-DNA\left\border
CaMV\3'UTR
2008-1967
BAR\gene
Translation
35S\prom
pCambia_pUBQ10:Ret
11625 bp
5'\USER\tail
T-DNA\right\border
35S\term
3'\USER\tail
RBC\promotor/terminator
eYFP
Dioxygenase
Ret - eYFP
Plant Kozak
P2A
Translation 4498-4503
UBQ\promotor/terminator

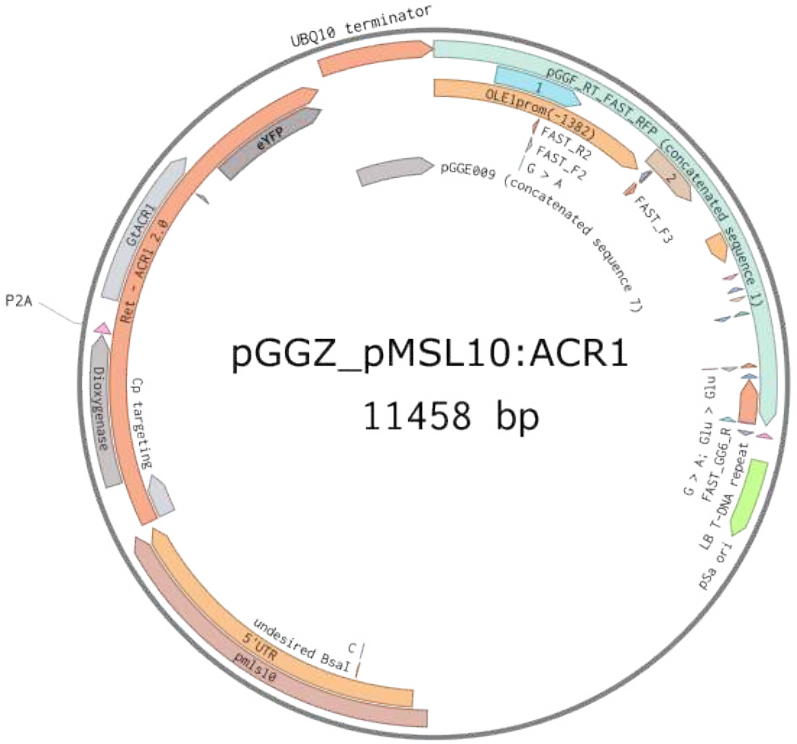
UBQ10 terminator
pGGF_RT_FAST_RFP (concatenated sequence 1)
1
OLE1prom(-1382)
FAST_R2
FAST_F2
G > A
pGGE009 (concatenated sequence 7)
2
FAST_F3
eYFP
GtACR1
Ret - ACR1 2.0
P2A
Dioxygenase
Cp targeting
pGGZ_pMSL10:ACR1
11458 bp
G > A; Glu > Glu
FAST_GG6_R
LB T-DNA repeat
pSa ori
undesired BsaI
5'UTR
pmls10
C

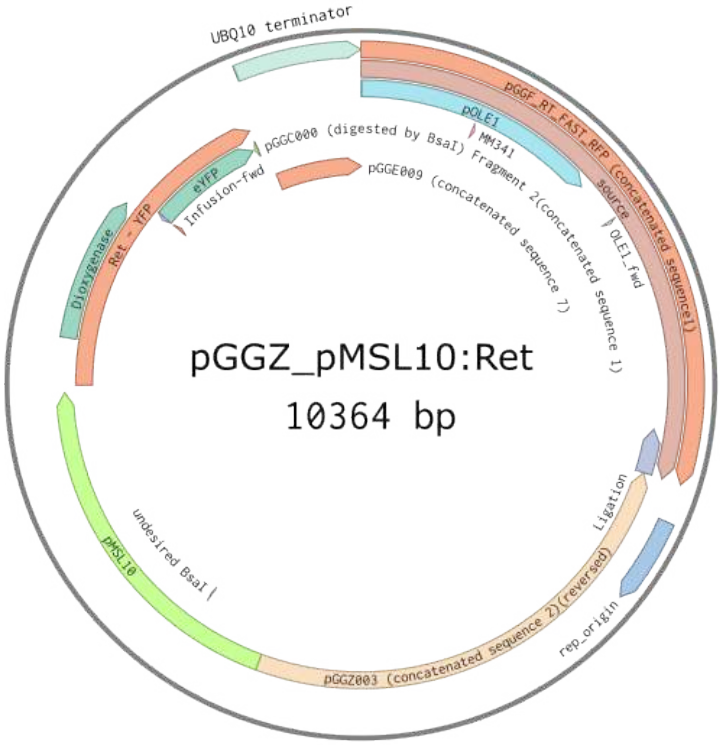
UBQ10 terminator
pGGF_RT_FAST_RFP (concatenated sequence1)
pOLE1
MM341
pGGC000 (digested by BsaI) Fragment 2(concatenated sequence 1)
pGGE009 (concatenated sequence 7)
source
OLE1_fwd
eYFP
Infusion-fwd
Dioxygenase
Ret - YFP
pGGZ_pMSL10:Ret
10364 bp
undesired BsaI
pMSL10
pGGZ003 (concatenated sequence 2)(reversed)
Ligation
rep_origin

References

Ache, P., Becker, D., Ivashikina, N., Dietrich, P., Roelfsema, M.R.G. and Hedrich, R. (2000) GORK, a delayed outward rectifier expressed in guard cells of *Arabidopsis thaliana*, is a K^+-selective, K^+-sensing ion channel. *FEBS Lett*, **486**, 93–98.

Adem, G.D., Chen, G., Shabala, L., Chen, Z.H. and Shabala, S. (2020) GORK Channel: A Master Switch of Plant Metabolism? *Trends Plant Sci*, **25**, 434–445. Available at: https://doi.org/10.1016/j.tplants.2019.12.012.

Alarcon, J.J. and Malone, M. (1994) Substantial hydraulic signals are triggered by leaf-biting insects in tomato. *J Exp Bot*, **45**, 953–957.

Albert, V.A., Williams, S.E. and Chase, M.W. (1992) *Carnivorous Plants: Phylogeny and Structural Evolution*, Available at: https://www.science.org.

Armada-moreira, A., Dar, A.M., Zhao, Z., Cea, C., Gelinas, J., Berggren, M., Costa, A., Khodagholy, D. and Stavrinidou, E. (2023) Plant electrophysiology with conformable organic electronics: Deciphering the propagation of Venus flytrap action potentials.

Bakker, J.M.T. de, Belterman, C.N.W. and Coronel, R. (2021) Excitability and propagation of the electrical impulse in Venus flytrap; a comparative electrophysiological study of unipolar electrograms with myocardial tissue. *Bioelectrochemistry*, **140**, 107810. Available at: https://doi.org/10.1016/j.bioelechem.2021.107810.

Barbosa-Caro, J.C. and Wudick, M.M. (2024) Revisiting plant electric signaling: Challenging an old phenomenon with novel discoveries. *Curr Opin Plant Biol*, **79**, 102528. Available at: https://doi.org/10.1016/j.pbi.2024.102528.

Barish, M.E. (1983) A transient calcium-dependen chloride current in the immature *Xenopus*e oocyte. , 309–325.

Barnett, M.W. and Larkmann, P.M. (2007) The Action Potential. *Pract Neurol*, **7**, 192–197.

Basu, D. and Haswell, E.S. (2020) The Mechanosensitive Ion Channel MSL10 Potentiates Responses to Cell Swelling in *Arabidopsis* Seedlings. *Current Biology*, **30**, 2716-2728.e6. Available at: https://doi.org/10.1016/j.cub.2020.05.015.

Beilby, M.J. (2007) Action Potential in Charophytes. *Int Rev Cytol*, **257**, 43–82.

Bel, A.J.E. Van and Ehlers, K. (2005) Electrical Signalling via Plasmodesmata. *Plasmodesmata*, 263–278.

Bel, A.J.E. Van, Furch, A.C.U., Will, T., Buxa, S. V., Musetti, R. and Hafke, J.B. (2014) Spread the news: Systemic dissemination and local impact of Ca^{2+} signals along the phloem pathway. *J Exp Bot*, **65**, 1761–1787.

Bellandi, A., Papp, D., Breakspear, A., et al. (2022) Diffusion and bulk flow of amino acids mediate calcium waves in plants. , 1–15.

Blatt, M.R. and Thiel, G. (1994) K^+ channels of stomatal guard cells: bimodal control of the K^+ inward-rectifier evoked by auxin. *The Plant Journal*, **5**, 55–68.

Brownlee, C. (2022) Plant physiology: Anatomy of a plant action potential. *Current Biology*, **32**, R1000–R1002. Available at: https://doi.org/10.1016/j.cub.2022.08.024.

Browse, J. (2009) Jasmonate passes muster: A receptor and targets for the defense hormone. *Annu Rev Plant Biol*, **60**, 183–205.

Christenhusz, M.J.M. and Byng, J.W. (2016) The number of known plants species in the world and its annual increase. *Phytotaxa*, **261**, 201–217.

Cuin, T.A., Dreyer, I. and Michard, E. (2018) The role of potassium channels in *Arabidopsis thaliana* long distance electrical signalling: AKT2 modulates tissue excitability while GORK shapes action potentials. *Int J Mol Sci*, **19**, 1–17.

Ding, M., Zhou, Y., Becker, D., et al. (2024) Probing plant signal processing optogenetically by two channelrhodopsins. *Nature*, **633**. Available at: http://dx.doi.org/10.1038/s41586-024-07884-1.

Drechsler, N., Zheng, Y., Bohner, A., Nobmann, B., Wirén, N. von, Kunze, R. and Rausch, C. (2015) Nitrate-dependent control of shoot K homeostasis by NPF7.3/NRT1.5 and SKOR in *Arabidopsis*. *Plant Physiol*, **169**, pp.01152.2015.

Dreyer, I., Gomez-Porras, J.L., Riaño-Pachón, D.M., Hedrich, R. and Geiger, D. (2012) Molecular evolution of slow and quick anion channels (SLACs and QUACs/ALMTs). *Front Plant Sci*, **3**, 1–12.

Dreyer, I., Li, K., Riedelsberger, J., Hedrich, R., Konrad, K.R. and Michard, E. (2022) Transporter networks can serve plant cells as nutrient sensors and mimic transceptor-like behavior. *iScience*, **25**, 104078. Available at: https://doi.org/10.1016/j.isci.2022.104078.

Duan, X., Nagel, G. and Gao, S. (2019) Mutated channelrhodopsins with increased sodium and calcium permeability. *Applied Sciences (Switzerland)*, **9**, 1–11.

Dziubińska, H. (2003) Ways of signal transmission and physiological role of electrical potentials in plants. *Acta Societatis Botanicorum Poloniae*, **72**, 309–318.

Dziubińska, H., Trębacz, K. and Zawadzki, T. (2001) Transmission route for action potentials and variation potentials in *Helianthus annuus L. J Plant Physiol, **158**, 1167–1172.*

Eisenach, C., Papanatsiou, M., Hillert, E.K. and Blatt, M.R. (2014) Clustering of the K^+ channel GORK of *Arabidopsis* parallels its gating by extracellular K^+. *Plant Journal*, **78**, 203–214.

Ellison, A. and Adamec, L. (2018) *Carnivorous Plants: Physiology, ecology and evolution*, Oxford University Press.

Farmer, E.E., Gao, Y., Lenzoni, G., Wolfender, J. and Wu, Q. (2020) Wound- and mechano-stimulated electrical signals control hormone responses. *New Phytologist*.

Fenno, L., Yizhar, O. and Deisseroth, K. (2011) The development and application of optogenetics. *Annu Rev Neurosci*, **34**, 389–412.

Fisahn, J., Herde, O., Willmitzer, L. and Peña-Cortés, H. (2004) *Analysis of the Transient Increase in Cytosolic Ca^{2+} during the Action Potential of Higher Plants with High Temporal Resolution: Requirement of Ca^{2+} Transients for Induction of Jasmonic Acid Biosynthesis and PINII Gene Expression*, Available at: http://pcp.oxfordjournals.org/.

Förster, S., Schmidt, L.K., Kopic, E., et al. (2019) Wounding-Induced Stomatal Closure Requires Jasmonate-Mediated Activation of GORK K^+ Channels by a Ca^{2+} Sensor-Kinase CBL1-CIPK5 Complex. *Dev Cell*, **48**, 87-99.e6.

Fromm, J. and Lautner, S. (2007) Electrical signals and their physiological significance in plants. *Plant Cell Environ*, **30**, 249–257.

Gangwar, S.P., Green, M.N., Michard, E., Simon, A.A., Feijó, J.A. and Sobolevsky, A.I. (2020) Structure of the *Arabidopsis* Glutamate Receptor-like Channel GLR3.2 Ligand-Binding Domain. *Structure*, 1–9.

Gao, Y.-Q., Jimenez-Sandoval, P., Tiwari, S., Stolz, S., Wang, J., Glauser, G., Santiago, J. and Farmer, E.E. (2023) Ricca's factors as mobile proteinaceous effectors of electrical signaling. *Cell*, 1–15. Available at: http://www.ncbi.nlm.nih.gov/pubmed/36870332.

Geiger, D., Scherzer, S., Mumm, P., et al. (2010) Guard cell anion channel SLAC1 is regulated by CDPK protein kinases with distinct Ca^{2+} affinities. *Proc Natl Acad Sci U S A*, **107**, 8023–8028.

Gilroy, S., Białasek, M., Suzuki, N., Górecka, M., Devireddy, A.R., Karpiński, S. and Mittler, R. (2016) ROS, calcium, and electric signals: Key mediators of rapid systemic signaling in plants. *Plant Physiol*, **171**, 1606–1615.

Gilroy, S., Suzuki, N., Miller, G., Choi, W.G., Toyota, M., Devireddy, A.R. and Mittler, R. (2014) A tidal wave of signals: Calcium and ROS at the forefront of rapid systemic signaling. *Trends Plant Sci*, **19**, 623–630. Available at: http://dx.doi.org/10.1016/j.tplants.2014.06.013.

Govorunova, E.G., Sineshchekov, O.A., Janz, R., Liu, X. and Spudich, J.L. (2015) Natural light-gated anion channels: A family of microbial rhodopsins for advanced optogenetics. , **349**, 647–651.

Green, M.N., Gangwar, S.P., Michard, E., et al. (2021) Structure of the *Arabidopsis thaliana* glutamate receptor-like channel GLR3.4. *Mol Cell*, **81**, 3216-3226.e8.

Haswell, E.S., Peyronnet, R., Barbier-Brygoo, H., Meyerowitz, E.M. and Frachisse, J.M. (2008) Two MscS Homologs Provide Mechanosensitive Channel Activities in the *Arabidopsis* Root. *Current Biology*, **18**, 730–734.

Hedrich, R. and Becker, D. (1994) Green circuits - The potential of plant specific ion channels. *Plant Mol Biol*, **26**, 1637–1650.

Hedrich, R. and Geiger, D. (2017) Biology of SLAC1-type anion channels - from nutrient uptake to stomatal closure. *New Phytologist*.

Hedrich, R. and Kreuzer, I. (2023) Demystifying the Venus flytrap action potential. *New Phytologist*, **239**, 2108–2112.

Hedrich, R., Salvador-Recatalà, V. and Dreyer, I. (2016a) Electrical Wiring and Long-Distance Plant Communication. *Trends Plant Sci*, **21**, 376–387. Available at: http://dx.doi.org/10.1016/j.tplants.2016.01.016.

Hedrich, R., Salvador-Recatalà, V. and Dreyer, I. (2016b) Electrical Wiring and Long-Distance Plant Communication. *Trends Plant Sci*, **21**, 376–387. Available at: http://dx.doi.org/10.1016/j.tplants.2016.01.016.

Hosy, E., Vavasseur, A., Mouline, K., et al. (2003) The *Arabidopsis* outward K^+ channel GORK is involved in regulation of stomatal movements and plant transpiration. *Proceedings of the National Academy of Sciences*, **100**, 5549–5554.

Howe, G.A. and Jander, G. (2008) Plant immunity to insect herbivores. *Annu Rev Plant Biol*, **59**, 41–66.

Huang, H., St.-Jean, H., Coady, M.J. and Lapointe, J.Y. (1995) Evidence for coupling between Na^+ pump activity and TEA-sensitive K^+ currents in *Xenopus laevis* oocytes. *J Membr Biol*, **143**, 29–35.

Huang, S., Ding, M., Roelfsema, M.R.G., et al. (2021) Optogenetic control of the guard cell membrane potential and stomatal movement by the light-gated anion channel GtACR1. *Sci Adv*, **7**, 1–12.

Huang, S. and Hedrich, R. (2023) Trigger hair thermoreceptors provide for heat-induced calcium-electrical excitability in Venus flytrap. *Current Biology*, **33**, 3962-3968.e2. Available at: https://doi.org/10.1016/j.cub.2023.07.069.

Iosip, A.L., Bo, J., Id, D.B., Id, I.K., Hedrich, R. and Id, I.D. (2020) The Venus flytrap trigger hair – specific potassium channel KDM1 can reestablish the K^+ gradient required for hapto-electric signaling. , 1–29.

Kew, J.N.C. and Kemp, J.A. (2005) Ionotropic and metabotropic glutamate receptor structure and pharmacology. *Psychopharmacology (Berl)*, **179**, 4–29.

Kim, J.Y., Symeonidi, E., Pang, T.Y., et al. (2021) Distinct identities of leaf phloem cells revealed by single cell transcriptomics. *Plant Cell*, **33**, 511–530.

Kisnieriene, V., Lapeikaite, I., Pupkis, V. and Beilby, M.J. (2019) Modeling the action potential in characeae *Nitellopsis obtusa*: Effect of saline stress. *Front Plant Sci*, **10**, 1–15.

Koselski, M., Trebacz, K., Dziubinska, H. and Krol, E. (2008) Light- and dark-induced action potentials in *Physcomitrella patens*. *Plant Signal Behav*, **3**, 13–18.

Kumari, A., Chételat, A., Nguyen, C.T. and Farmer, E.E. (2019) *Arabidopsis* H^+-ATPase AHA1 controls slow wave potential duration and wound-response jasmonate pathway activation. *Proc Natl Acad Sci U S A*, **116**, 20226–20231.

Kupisz, K., Dziubińska, H. and Trębacz, K. (2017) Generation of action potential-type changes in response to darkening and illumination as indication of the plasma membrane proton pump status in *Marchantia polymorpha*. *Acta Physiol Plant*, **39**.

Kuruma, A. and Hartzell, H.C. (1999) Dynamics of calcium regulation of chloride currents in *Xenopus* oocytes. *Am J Physiol Cell Physiol*, **276**, 161–175.

Lacombe, B. and Achard, P. (2016) Long-distance transport of phytohormones through the plant vascular system. *Curr Opin Plant Biol*, **34**, 1–8. Available at: http://dx.doi.org/10.1016/j.pbi.2016.06.007.

Lapeikaite, I., Dragunaite, U., Pupkis, V., Ruksenas, O. and Kisnieriene, V. (2019) Asparagine alters action potential parameters in single plant cell. *Protoplasma*, **256**, 511–519.

Lapeikaite, I., Pupkis, V., Neniskis, V., Ruksenas, O. and Kisnieriene, V. (2020) Glutamate and NMDA affect cell excitability and action potential dynamics of single cell of macrophyte Nitellopsis obtusa. *Functional Plant Biology*, **47**, 1032–1040.

Lim, C.W., Kim, S.H., Choi, H.W., Luan, S. and Lee, S.C. (2019) The shaker type potassium channel, gork, regulates abscisic acid signaling in *Arabidopsis*. *Plant Pathol J (Faisalabad)*, **35**, 684–691.

Liu, K., Li, L. and Luan, S. (2006) Intracellular K^+ sensing of SKOR, a Shaker-type K^+ channel from *Arabidopsis*. *Plant Journal*, **46**, 260–268.

Maksaev, G. and Haswell, E.S. (2011) Expression and characterization of the bacterial mechanosensitive channel MscS in *Xenopus laevis* oocytes. *Journal of General Physiology*, **138**, 641–649.

Maksaev, G. and Haswell, E.S. (2012) MscS-Like10 is a stretch-activated ion channel from *Arabidopsis thaliana* with a preference for anions. *Proc Natl Acad Sci U S A*, **109**, 19015–19020.

Malone, M. (1996) *Rapid, Long-distance Signal Transmission in Higher Plants* J. A. Callow, ed., Academic Press.

Malone, M. and Stankovic, B. (1991) Surface potentials and hydraulic signals in wheat leaves following localized wounding by heat. *Plant Cell Environ*, **14**, 431–436.

Marhavý, P., Kurenda, A., Siddique, S., et al. (2019) Single-cell damage elicits regional, nematode-restricting ethylene responses in roots. *EMBO J*, **38**.

Meyer, A.J. and Weisenseel, M.H. (1997) Wound-induced changes of membrane voltage, endogenous currents, and ion fluxes in primary roots of maize. *Plant Physiol*, **114**, 989–998.

Meyer, S., Mumm, P., Imes, D., et al. (2010) AtALMT12 represents an R-type anion channel required for stomatal movement in *Arabidopsis* guard cells. *Plant Journal*, **63**, 1054–1062.

Miledi, R. (1982) A calcium -dependent transient outward current in *Xenopus laevis* oocytes. , **497**, 491–497.

Miller, G., Schlauch, K., Tam, R., Cortes, D., Torres, M.A., Shulaev, V., Dangl, J.L. and Mittler, R. (2009) The Plant NADPH Oxidase RBOHD Mediates Rapid Systemic Signaling in Response to Diverse Stimuli. *Sci Signal*, **2**. Available at: https://www.science.org/doi/10.1126/scisignal.2000448 [Accessed January 21, 2025].

Mittler, R., Vanderauwera, S., Suzuki, N., Miller, G., Tognetti, V.B., Vandepoele, K., Gollery, M., Shulaev, V. and Breusegem, F. Van (2011) ROS signaling: The new wave? *Trends Plant Sci*, **16**, 300–309.

Moe-Lange, J., Gappel, N.M., Machado, M., et al. (2021) Interdependence of a mechanosensitive anion channel and glutamate receptors in distal wound signaling.

Mousavi, S.A.R., Chauvin, A., Pascaud, F., Kellenberger, S. and Farmer, E.E. (2013) GLUTAMATE RECEPTOR-LIKE genes mediate leaf-to-leaf wound signalling. *Nature*, **500**, 422–426. Available at: http://dx.doi.org/10.1038/nature12478.

Mumm, P., Imes, D., Martinoia, E., Al-Rasheid, K.A.S., Geiger, D., Marten, I. and Hedrich, R. (2013) C-terminus-mediated voltage gating of *Arabidopsis* guard cell anion channel QUAC1. *Mol Plant*, **6**, 1550–1563. Available at: http://dx.doi.org/10.1093/mp/sst008.

Nagel, G., Ollig, D., Fuhrmann, M., Kateriya, S., Musti, A.M., Bamberg, E. and Hegemann, P. (2002) *Channelrhodopsin-1: A Light-Gated Proton Channel in Green Algae*, Available at: https://www.science.org.

Nguyen, C.T., Stolz, S., Kurenda, A., Chételat, A. and Farmer, E.E. (2018) Identification of cell populations necessary for leaf-to-leaf electrical signaling in a wounded plant. *Proceedings of the National Academy of Sciences*, **115**, 10178–10183.

Papanatsiou, M., Petersen, J., Henderson, L., Wang, Y., Christie, J.M. and Blatt, M.R. (2019) Optogenetic manipulation of stomatal kinetics improves carbon assimilation,water use, and growth. *Science (1979)*, **363**, 1456–1459.

Pavlovič, A., Jakšová, J. and Novák, O. (2017) Triggering a false alarm: Wounding mimics prey capture in the carnivorous venus flytrap (*Dionaea muscipula*). *New Phytologist*, **216**, 927–938.

Procko, C., Murthy, S.E., Keenan, W.T., et al. (2020) Stretch-activated ion channels identified in the touch-sensitive structures of carnivorous Droseraceae plants. *bioRxiv*, 1–24.

Pupkis, V., Lapeikaite, I., Kavaliauskas, J., Trębacz, K. and Kisnieriene, V. (2022) Certain calcium channel inhibitors exhibit a number of secondary effects on the physiological

properties in Nitellopsis obtusa: A voltage clamp approach. *Functional Plant Biology*, **50**, 195–205.

Pyatygin, S.S., Opritov, V.A. and Vodeneev, V.A. (2008) Signaling role of action potential in higher plants. *Russian Journal of Plant Physiology*, **55**, 285–291.

Qi, Z., Stephens, N.R. and Spalding, E.P. (2006) Calcium Entry Mediated by GLR3.3, an *Arabidopsis* Glutamate Receptor with a Broad Agonist Profile. *Plant Physiol*, **142**, 963–971.

Ricca, U. (1926) Transmission of Stimuli in Plants. , **23**, 6–7.

Roelfsema, M.R.G., Hedrich, R. and Geiger, D. (2012) Anion channels: Master switches of stress responses. *Trends Plant Sci*, **17**, 221–229. Available at: http://dx.doi.org/10.1016/j.tplants.2012.01.009.

Salvador-Recatalà, V. (2016) The AKT2 potassium channel mediates NaCL induced depolarization in the root of *Arabidopsis thaliana*. *Plant Signal Behav*, **11**, 1–4. Available at: http://dx.doi.org/10.1080/15592324.2016.1165381.

Sanmartín, M., Rojo, E., Kurenda, A., et al. (2024) GLR-dependent calcium and electrical signals are not coupled to systemic, oxylipin-based wound-induced gene expression in *Marchantia polymorpha*. *New Phytologist*.

Scherzer, S., Böhm, J., Huang, S., et al. (2022) A unique inventory of ion transporters poises the Venus flytrap to fast-propagating action potentials and calcium waves. *Curr Biol*, 1–9. Available at: http://www.ncbi.nlm.nih.gov/pubmed/36087579.

Scherzer, S., Huang, S., Iosip, A., Kreuzer, I., Yokawa, K., AL-Rasheid, K.A.S., Heckmann, M. and Hedrich, R. (2022) Ether anesthetics prevents touch-induced trigger hair calcium-electrical signals excite the Venus flytrap. *Sci Rep*, **12**, 1–10. Available at: https://doi.org/10.1038/s41598-022-06915-z.

Shen, K., Lagrutta, A., Davies, N.W., Standen, N.B., Adelman, J.P. and North, R.A. (1994) [SLo's formation 4 subunits]Tetraethylammonium block about tetrameric channel formation.pdf. , 440–445.

Stanfield, P.R. (1983) Tetraethylammonium ions and the potassium permeability of excitable cells. *Rev Physiol Biochem Pharmacol*, **97**, 1–67.

Stange, A., Hedrich, R. and Roelfsema, M.R.G. (2010) Ca^{2+}-dependent activation of guard cell anion channels, triggered by hyperpolarization, is promoted by prolonged depolarization. *Plant Journal*, **62**, 265–276.

Stanković, B. and Davies, E. (1996) Both action potentials and variation potentials induce proteinase inhibitor gene expression in tomato. *FEBS Lett*, **390**, 275–279.

Stanković, B., Zawadzki, T. and Davies, E. (1997) Characterization of the variation potential in sunflower. *Plant Physiol*, **115**, 1083–1088.

Stephens, N.R., Qi, Z. and Spalding, E.P. (2008) Glutamate Receptor Subtypes Evidenced by Differences in Desensitization and Dependence on the GLR3.3 and GLR3.4 Genes. *Plant Physiol*, **146**, 529–538.

Suda, H., Mano, H., Toyota, M., Fukushima, K., Mimura, T., Tsutsui, I., Hedrich, R., Tamada, Y. and Hasebe, M. (2020) Calcium dynamics during trap closure visualized in transgenic Venus flytrap. *Nat Plants*, **6**, 1219–1224. Available at: http://dx.doi.org/10.1038/s41477-020-00773-1.

Sukharev, S., Akitake, B. and Anishkin, A. (2007) The Bacterial Mechanosensitive Channel MscS: Emerging Principles of Gating and Modulation. *Curr Top Membr*, **58**, 235–267.

Sukhov, V., Akinchits, E., Katicheva, L. and Vodeneev, V. (2013) Simulation of variation potential in higher plant cells. *Journal of Membrane Biology*, **246**, 287–296.

Sukhov, V., Sukhova, E. and Vodeneev, V. (2018) Long-distance electrical signals as a link between the local action of stressors and the systemic physiological responses in higher plants. *Prog Biophys Mol Biol*. Available at: https://doi.org/10.1016/j.pbiomolbio.2018.11.009.

Tabata, T. and Sibaoka, T. (1987) Conduction velocity and blockage of action potential in chara internodal cells. *Plant Cell Physiol*, **28**, 1187–1194.

Tokimasa, T. and North, R.A. (1996) Effects of barium, lanthanum and gadolinium on endogenous chloride and potassium currents in *Xenopus* oocytes. *Journal of Physiology*, **496**, 677–686.

Toyota, M., Spencer, D., Sawai-toyota, S., Jiaqi, W. and Zhang, T. (2018) Glutamate triggers long-distance, calcium-based plant defense signaling. , **6**, 1112–1115.

Tran, D., Dauphin, A., Meimoun, P., et al. (2018) Methanol induces cytosolic calcium variations, membrane depolarization and ethylene production in *Arabidopsis* and tobacco. *Ann Bot*, **122**, 849–860.

Trebacz, K. and Sievers, A. (1998) Action potentials evoked by light in traps of *Dionaea muscipula* ellis. *Plant Cell Physiol*, **39**, 369–372.

Umrath, K. (1932) Der erregungsvorgang bei nitella mucronata.

Vodeneev, V., Akinchits, E. and Sukhov, V. (2015) Variation potential in higher plants: Mechanisms of generation and propagation. *Plant Signal Behav*, **10**, 1–7.

Vodeneev, V., Orlova, A., Morozova, E., Orlova, L., Akinchits, E., Orlova, O. and Sukhov, V. (2012) The mechanism of propagation of variation potentials in wheat leaves. *J Plant Physiol*, **169**, 949–954. Available at: http://dx.doi.org/10.1016/j.jplph.2012.02.013.

Vodeneev, V.A., Opritov, V.A. and Pyatygin, S.S. (2006) Reversible changes of extracellular pH during action potential generation in a higher plant Cucurbita pepo. *Russian Journal of Plant Physiology*, **53**, 481–487.

Vriese, K. De, Costa, A., Beeckman, T. and Vanneste, S. (2018) Pharmacological strategies for manipulating plant Ca^{2+}signalling. *Int J Mol Sci*, **19**.

Wang, F.L., Tan, Y.L., Wallrad, L., et al. (2021) A potassium-sensing niche in *Arabidopsis* roots orchestrates signaling and adaptation responses to maintain nutrient homeostasis. *Dev Cell*, **56**, 781-794.e6.

Watanabe, K., Hashimoto, K., Hasegawa, K., Shindo, H., Kipisz, K., Koselski, M., Wasko, P., Trebacz, K. and Kachitsu, K. (2023) Rapid propagation of Ca^{2+} waves and electrical signals in a liverwort *Marchantia polymorpha*. , 31–41.

Weber, W.M. (1999) Endogenous ion channels in oocytes of *Xenopus laevis*: Recent developments. *Journal of Membrane Biology*, **170**, 1–12.

Wudick, M.M., Portes, M.T., Michard, E., et al. (2018) CORNICHON sorting and regulation of GLR channels underlie pollen tube Ca^{2+} homeostasis. *Science (1979)*.

Yan, C., Gao, Q., Yang, M., Shao, Q., Xu, X., Zhang, Y. and Luan, S. (2024) Ca^{2+}/calmodulin-mediated desensitization of glutamate receptors shapes plant systemic wound signalling and anti-herbivore defence. *Nature Plants* .

Yang, T., Kurenda, A., Farmer, E.E. and Chetelat, A. (2023) Mechanosensation in leaf veins. , 1–13.

Yang, X. and Sachs, F. (1990) Characterizatio of strech-activated ion channels in *Xenopus* oocytes. , 103–122.

Yang, X.C. and Sachs, F. (1989) Block of stretch-activated ion channels in *Xenopus* oocytes by gadolinium and calcium ions. *Science (1979)*, **243**, 1068–1071.

Yu, B., Wu, Q., Li, X., Zeng, R., Min, Q. and Huang, J. (2022) GLUTAMATE RECEPTOR-like gene OsGLR3.4 is required for plant growth and systemic wound signaling in rice (Oryza sativa). *New Phytologist*, **233**, 1238–1256.

Zhou, Y., Ding, M., Gao, S., et al. (2021) Optogenetic control of plant growth by a microbial rhodopsin. *Nat Plants*, **7**. Available at: http://dx.doi.org/10.1038/s41477-021-00853-w.

Chapter 3 – A detailed guide to recording and analysing *Arabidopsis thaliana* leaf surface potential dynamics elicited by mechanical wounding

Status: Published

Journal: bioProtocol

Contribution to this chapter:
Juan Camilo Barbosa-Caro contributed to the entire development of the script for high-throughput data analysis, and to the design of the grip clamps 3D-printed attachments.

A Detailed Guide to Recording and Analysing *Arabidopsis thaliana* Leaf Surface Potential Dynamics Elicited by Mechanical Wounding

Fatiha Atanjaoui[1], Thomas J. Kleist[2,*], Juan Camilo Barbosa-Caro[1], Michael M. Wudick[1,3*]

[1] Heinrich Heine University Düsseldorf, Faculty of Mathematics and Natural Sciences, Institute for Molecular Physiology, 40225 Düsseldorf, Germany
[2] Stowers Institute for Medical Research, Kansas City, USA
[3] Heinrich Heine University Düsseldorf, Faculty of Mathematics and Natural Sciences, Cluster of Excellence on Plant Sciences, 40225 Düsseldorf, Germany
* tkleist@stowers.org, wudick@hhu.de

Abstract

Recordings of electrical potential changes on plant surfaces have been utilized to identify components and mechanisms involved in the formation and transmission of systemic signals elicited by stimuli such as herbivory, wounding, or burning. The recorded responses, commonly referred to as slow wave or variation potentials, exhibit striking variability in waveform. The extent to which this variability is due to differences in experimental procedures or plant biological variability remains unclear. Here, we provide a detailed and robust protocol refined from years of experience in conducting leaf surface potential recordings of *Arabidopsis thaliana* in response to mechanical wounding. This protocol serves as a comprehensive tutorial covering plant growth, procedures for reproducible mechanical wounding, critical aspects of electrophysiological recordings, and statistical analysis of surface potential recordings. It particularly emphasizes the construction and maintenance of electrodes, placement of the reference or ground electrode, mechanism for wounding, as well as data analysis. This protocol aims to promote and facilitate the adoption, standardization, and interoperability of plant surface potential recordings among research groups, thereby increasing the reproducibility and comparability of data within the field.

Key features

- Recording electric potential changes on the petiole of 5-week-old *Arabidopsis* plants using non-invasive surface electrodes, refining [1], in wounding procedure, reproducibility, and data processing
- Genotype-independent method for phenotyping, including parallel recordings from multiple plants.
- Guidelines for plant growth conditions, unambiguous leaf assignment by order of emergence, and detailed instructions for electrode fabrication and maintenance.
- Instructions for constructing devices for standardized, reproducible mechanical wounding along with a custom

script for unbiased and semi-automated data analysis.

Keywords: Surface potential recordings, long distance signaling, leaf numbering, electrode preparation, data analysis pipeline

Background

The first known recorded electrical impulses in plants date back to the 19th century from a modified leaf surface of a Venus Flytrap (*Dionea muscipula*) [2]. Later studies investigated surface potential dynamics in other thigmonastic organs in plants such as *Mimosa pudica*. Inserted electrode measurements in plants were first performed in the 20th century [3] and decades later led to the identification of ion channels as the basis of electrical signals in plants [4]. Modern studies have shown that various environmental stimuli such as light, heat, cold and wounding, trigger electrical signals [5]. Plants can utilize these signals to share information over long distances between organs and to regulate physiological functions [6]. Hence, in order to measure electrical potential changes in plants two methods are commonly used: extracellular and intracellular recordings. Although intracellular recordings offer higher precision and cellular resolution, they are typically only effective for short durations due to factors such as cell damage from electrode insertion. Extracellular recordings on the surface of plants are non-invasive, allowing long-term monitoring, but they do not provide information about the electric potential changes of individual cells or specific tissues. Both intracellular and extracellular recordings help identify and monitor diverse electrical potential changes, such as action potentials (APs) and slow wave potentials (SWPs). APs are short-lasting, self-propagating electrical signals with a fixed amplitude that can be elicited by stimuli such as cold shock. SWPs are long-lasting electrical signals with variable amplitudes and waveforms that are caused by severe local damage. Unlike APs, SWPs do not self-propagate and require chemical and mechanical signals for generation [7]. The method described here provides detailed instructions for reliably detecting these highly variable changes in plant surface potential.

Materials and reagents

Biological materials

1. *Arabidopsis thaliana* (L.) Heynh. (Col-0), available from the European Arabidopsis Stock Centre (NASC), the Arabidopsis Biological Resource Center (ABRC) or similar germline resources

Reagents

1. Murashige & Skoog basal salt mixture incl. MES Buffer (Duchefa, catalog number: M0254.0050)
2. Low Electroendosmosis (LE) Agarose (Biozym, catalog number: 840000)
3. Potassium chloride (KCl) (VWR, catalog number: 26764.3)
4. Silver chloride (AgCl) (Sigma-Aldrich, catalog number: 204382-5G)
5. Ethanol (C_2H_5OH) (Supelco/Merck, catalog number: 1070172511)
6. 13 % Sodium hypochlorite (NaOCl) (Fisher Scientific, catalog number: 10691164)
7. 25 % Ammonium hydroxide (NH_4OH) (Sigma-Aldrich, catalog number: 1336-21-6)
8. Low melt agarose (Biozym, catalog number: 840004)
9. DanKlorix® original (2.8 g/100 mL sodium hypochlorite)

Solutions

1. 50 mM Electrode solution (see recipes)
2. 5 % Sodium hypochlorite (see recipes)
3. 70 % Ethanol (see recipes)
4. ½ Murashige & Skoog (MS) medium (see recipes)

Recipes

1. **50 mM Electrode solution**
   **Note: Depending on whether you prepare the solution for connecting the electrode to the leaf or for the bath electrode you need to use 0.8 % or 3 % LE agarose, respectively.*

Reagent	Final concentration	Quantity or Volume
Potassium chloride	50 mM	0.37 g
milliQ H_2O	n/a	100 mL
Total	n/a	100 mL
LE Agarose	0.8 or 3 % (w/v)	0.8 g or 3 g

2. **5 % Sodium hypochlorite**
   **Note: This solution has to be prepared freshly before every usage.*

Reagent	Final concentration	Quantity or Volume
13 % Sodium hypochlorite	5 %	3.84 mL
milliQ H_2O	n/a	6.16 mL
Total	n/a	10 mL

3. **70 % Ethanol**

Reagent	Final concentration	Quantity or Volume
Ethanol (absolute)	70 %	700 mL
milliQ H_2O	n/a	300 mL
Total	n/a	1000 mL

4. **½ MS (half-strength Murashige & Skoog medium)**
   **Note: To prevent contamination and extend shelf life, autoclave or sterile-filter the solution. Store at room temperature (RT) if sterile; otherwise, keep at 4°C and acclimate to RT before use.*

Reagent	Final concentration	Quantity or Volume
Murashige & Skoog basal salt mix incl. MES buffer	½ strength	2.6 g
milliQ H_2O	n/a	1000 mL
Total	n/a	1000 mL

Laboratory supplies

1. Pipette tips (200 µL, Starlab, catalog number: S1113-1206-C)
2. PCR-tubes (Sarstedt, catalog number: 72.985.002)
3. Parafilm (Carl Roth, catalog number: H666.1)

4. Forceps (Sigma-Aldrich, catalog number: F4517)
5. Trays (Meyer, catalog number: 749112 / 74 91 12)
6. Lids (Meyer, catalog number: 749150 / 74 91 50)
7. Pots 4.5 x 4.5 x 7 cm (Meyer, Göttinger, catalog number:722001 / 72 20 01)
8. BP-Substrate (Baywa, Klasmann-Deilmann, catalog number: 1073986)
9. Vermiculite (Duengerexperte, catalog number: p89)
10. Sand (Lehmann Baustoffe, type: Rheinsand, granulation ≤ 2mm)
11. Container to place the pots containing ½ MS media for recordings

Equipment

1. Insulating tape (Adam Hall 580813RNB10, Conrad Electronic, article number: 5906194000459)
2. Solder (Stannol, model: S-Sn99,3Cu0,7)
3. Soldering iron (Basetech ZD-70D, Conrad Electronic, article number: 4064161149202)
4. Banana plug 2 mm (Amazon, catalog number: GST-2.0MM-SCHR)
5. Optical table with sealed holes (Thorlabs, catalog number: B75120A)
6. Silver wire, >99.99 % purity, 1 mm diameter (World Precision Instruments, catalog number: AGW4010)
7. Amplifier Headstages (NPI Electronic GmbH, model: EXT-02F/2 B, S.Nr° 0180032)
8. Extracellular Amplifier (NPI Electronic GmbH, model: EXT-02F, S.Nr° 0180033)
9. Digitizer (World Precision Instruments, model: Lab-Trax-4/16, 2016 B016N)
10. Micromanipulator (MM33, 3 Axes, Märzhäuser Wetzlar)
11. Grip wrench (C.K. Tools, 000829025)
12. Desiccator (Carl Roth, catalog number: AHL0.1)
13. Microwave
14. Heat plate (IKA C-MAG, -Aldrich: Z672351)
15. Emery paper (Bosch Accessories J45 grit 120, Conrad Electronic, article number: 3165140678421)
16. 3D-printed grids for leaf wounding (self-printed, the design can be found here)
17. Permanent marker pen (Edding 751)

Software and datasets

1. LabScribe: iWorx v4.345, this license is free to use for research purposes
2. LabView NI (23.1001)
3. R Studio (2023.09.0+463 or younger)
4. All codes have been deposited to Github

Procedure

A. Plant growth (start 6-7 weeks before recordings)

**Note: Place a couple of seeds in one pot in case germination rate is low. At 5 days old, thin the seedlings to leave one plant per pot.*

1. Seeding plants
   a. Clean all trays and lids with 70 % ethanol.
   b. Disinfect seeds in a desiccator using chlorine gas method [8].
   c. Prepare soil by mixing BP-Substrate, sand and vermiculite in an 8:1:1 ratio.
   d. Add 125 mL tab water to 500 g of the soil mixture.
   e. Microwave for 10 min at 800 W.
   f. After cooling down, fill the pots with the soil mixture.
   g. Seed the sterilized seeds on the pots filled with room temperature soil.
   h. One plant per pot is needed.
   i. Stratify seeds for 2 days by placing pots containing soil and seeds in a tray closed with a lid at 4 °C.
   j. Transfer pots after those 2 days into the growth chamber.
2. Grow the plants for 5-6 weeks in a growth chamber under short-day photoperiod condition (10 h light/14 h dark cycle) at 22 °C, with 60 % humidity and light intensity of ~ 120 µmol m^2 s^{-1}, water when needed.
   **Note: Avoid overwatering plants to reduce the risk of root anoxia and pest infestations. Older plants should be watered more frequently.*
   a. Growth under short day condition is used to promote vegetative growth and suppress bolting and flowering.
   b. Maintaining pest- and pathogen- free conditions is important for plant vigor and ensuring data reproducibility.
   c. Space plants at sufficient distances to avoid the leaves touching and to prevent leaf damage (Figure 1 A).
   d. After 2-3 weeks, gradually remove the tray lid. Start by propping it ajar for a few days to adjust humidity before fully removing it.
3. Counting leaves (ideally in week 4 of growth)
   **Note: Before counting, each plant should be pre-inspected. Plants showing signs of damage, detached leaves or growth defaults should be excluded. Leaf 13 is usually found between leaf 8 and 5 (which helps as an orientation).*
   a. Cotyledons are excluded from counting or numbering.
   b. Determine whether the order of leaf emergence is clockwise or counterclockwise (from young to old) by determining the spirality of the plant from the top pf the rosette [9].
   c. The leaves usually grow in a 137.5 ° angle, which can be helpful for identifying the next leaf (Figure 1 B).
   d. Count leaves sequentially in reverse chronological order from the oldest leaf towards the newer leaves (Figure 1C, D).

e. Mark the position of your leaves of interest at the pot using a permanent marker (in our case 8 and 13, Figure 1 E).

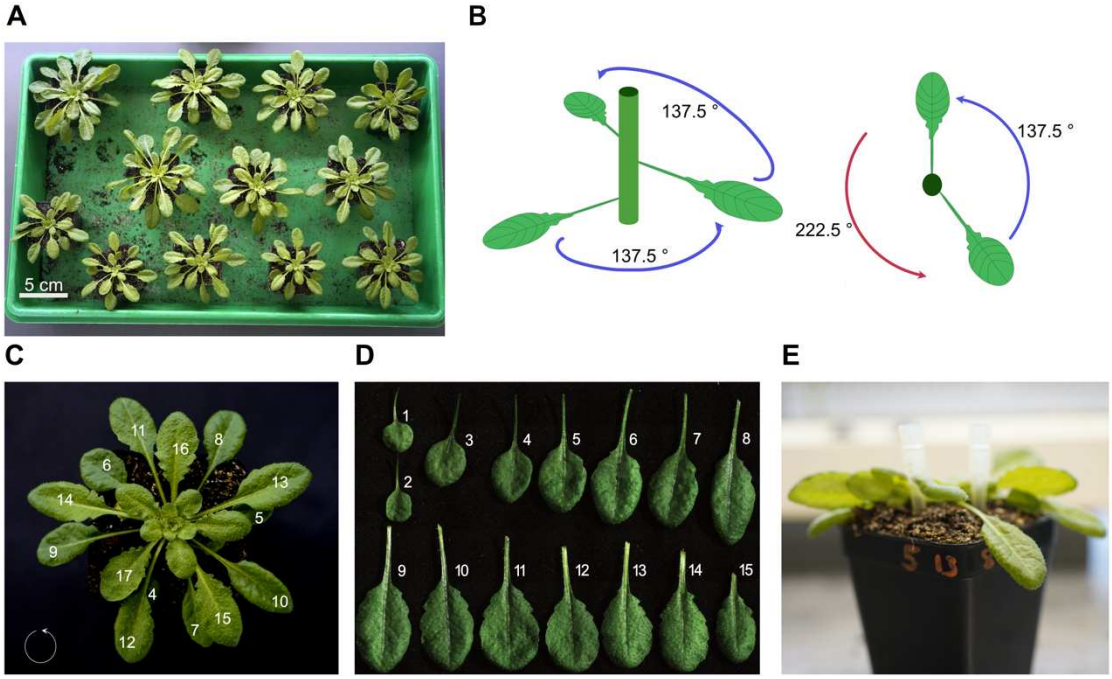

Figure 1. Arrangement and leaf counting of 5-week-old Arabidopsis thaliana for surface potential recordings. A) Plant arrangement in the tray. Each plant has enough space to avoid contact with others. B) Schematic drawing of leaf growth and angle. Starting with the 3rd leaf, all subsequent leaves grow at an angle of ca. 137.5 °. C) Rosette of a 5-week-old Arabidopsis. Growth direction is indicated with a circle in the lower left corner. Leaves are numbered from oldest to youngest. D) Single leaves of a 5-week-old Arabidopsis. E) Example of labelling the leaves of interest (e.g., 13 and 8).

B. Electrode preparation

1. Soldering (Figure 2).
    a. Cut segments of silver wire to desired lengths, depending on the accessibility of your petiole (e.g., 5 cm).
    b. Place an empty 2 mm banana plug in an appropriate holding device.

    Caution: As the soldering iron can reach temperatures up to 200 °C be careful when handling it. During the soldering process both banana plug and silver wire should not be touched to avoid burns

    c. Make a solder bridge from the soldering iron to the banana plug, and heat it up.
    d. Fill the cavity of the banana plug with solder.
    e. Solder the silver wire to banana plugs.
    f. Isolate the solder connection by wrapping with parafilm or electrical tape.
    g. Bend one end to form a hook.

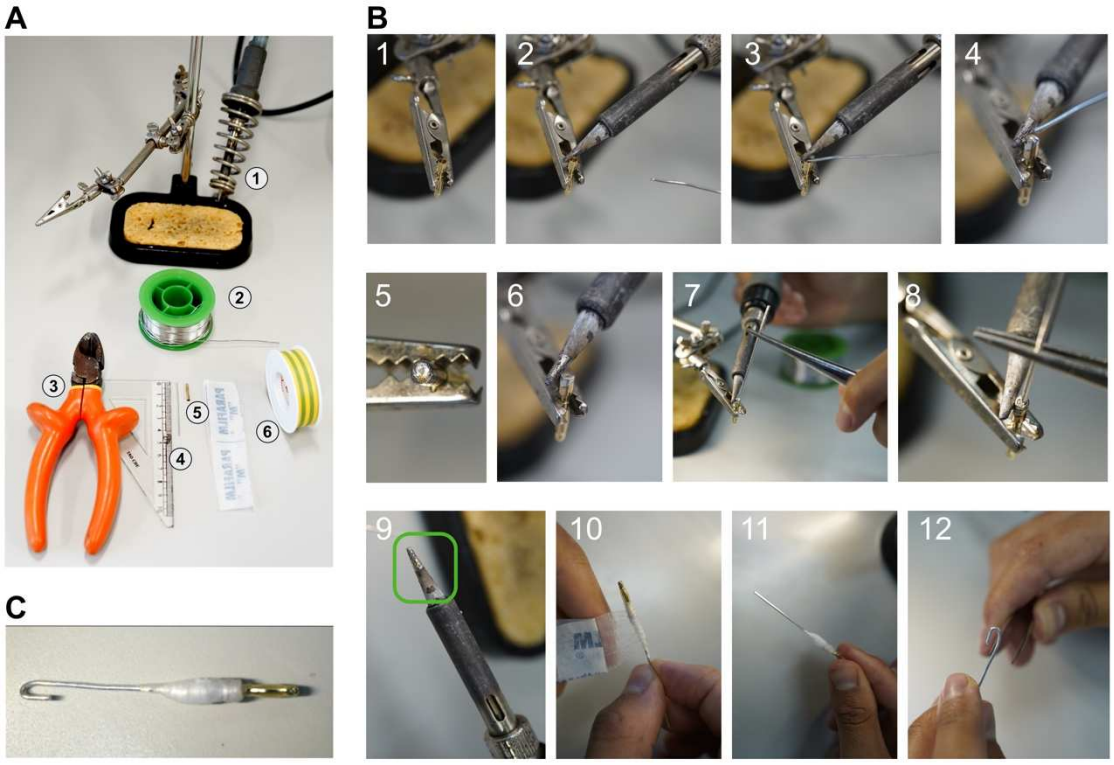

Figure 2. Soldering electrodes for potential recordings. A) Overview of necessary equipment: (1) soldering iron and holding device, (2) solder, (3) pliers and ruler for cutting the silver wire, (4) silver wire, (5) banana plug, (6) parafilm and insulating tape. B) Step-by-step soldering instructions: 1. Place banana plug in the holder. 2. Heat the banana plug with the soldering iron. 3&4. Fill empty banana plug with the solder. 5. Close-up of filled banana plug. 6. Keep the filled banana plug hot to add the silver wire. 7&8. Add the silver wire. 9. Maintain the soldering iron by cleaning it with the solder leaving a thin layer of solder on the tip (green rectangle). 10&11. Wrap the connection of the banana plug and the silver wire with parafilm or insulating tape to isolate it. 12. Bend the tip of the electrode with a forceps into a hook. C) Finished electrode.

2. Chloridization (earliest, a day before the recordings):

   **Note: Chloridize multiple ground and surface electrodes to have enough back up.*

   a. Dip ~1 cm of the hooked electrode end in freshly prepared 5 % sodium hypochlorite (Recipe 2).
   b. Allow reaction to proceed for 30 min.
   c. Rinse with 50 mM electrode solution and dry the electrodes with a paper towel.
   d. The electrodes can typically be used for ~20 recordings or more.

3. Stripping (Figure 3)

   **Note: Stripping is performed on used, chloridized electrodes, prior to properly re-chloridizing them for the next experiment.*

   a. Abrade the used electrodes with emery paper.
   b. Dip the tip of the electrodes in 25 % ammonium hydroxide and scrape with forceps until lustrous. Caution: ammonium hydroxide is hazardous and should only be handled with gloves under the fume hood.
   c. Rinse in 50 mM electrode solution.
   d. Dry electrodes with paper towel.

e. Store in dry and dark conditions (see step 2).

Figure 3. Surface silver chloride electrode. Top: freshly chloridized (see the dark hook), bottom: freshly stripped electrode (see lustrous hook).

C. Setting-up the surface potential rig

**Note: A Faraday cage helps to reduce electric noise but is not strictly necessary. The ground electrode is placed inside the ½ MS solution (Recipe 4). Avoid direct contact of the electrode with the petiole. Use an electric multimeter to confirm that the setup is properly grounded.*

a. Connect digitizer, amplifier, and headstages as described by the manufacturer.
b. Place the headstages in the micromanipulators on the optical table.
c. Set up the Labscribe software as described by the developer.
d. Stick the bath electrode in a PCR tube filled with 3 % LE agar (Recipe 1) and physically secure that connection with parafilm (Figure 4A).
e. Cut the tip of that PCR tube with a scissor and place it in the ½ MS bath solution (Figure 4A).
f. Use enough ½ MS media to be able to immerse the electrode (Figure 4A).
g. Separate the wounding and receiving leaves from each other by using pipet tips (Figure 1E, 4B).
h. Place the pot containing the plant to be recorded in a tray with ½ MS media (Figure 4C).
i. Place the leaf to be wounded inside the wounding device (Figure 4B).
j. Place electrodes on the petioles of leaf 8 and 13 and connect them via an agar bridge using < 20 µL of 0.8 % LE- agar (Recipe 1, Figure 4B).

**Note: Make sure to not burn the plant with the hot agar. Leave the 0.8 % LE-agar on the heat plate to keep it liquid.*

k. Ensure that you have a closed, properly grounded circuit (Figure 4C, D, see Troubleshooting).

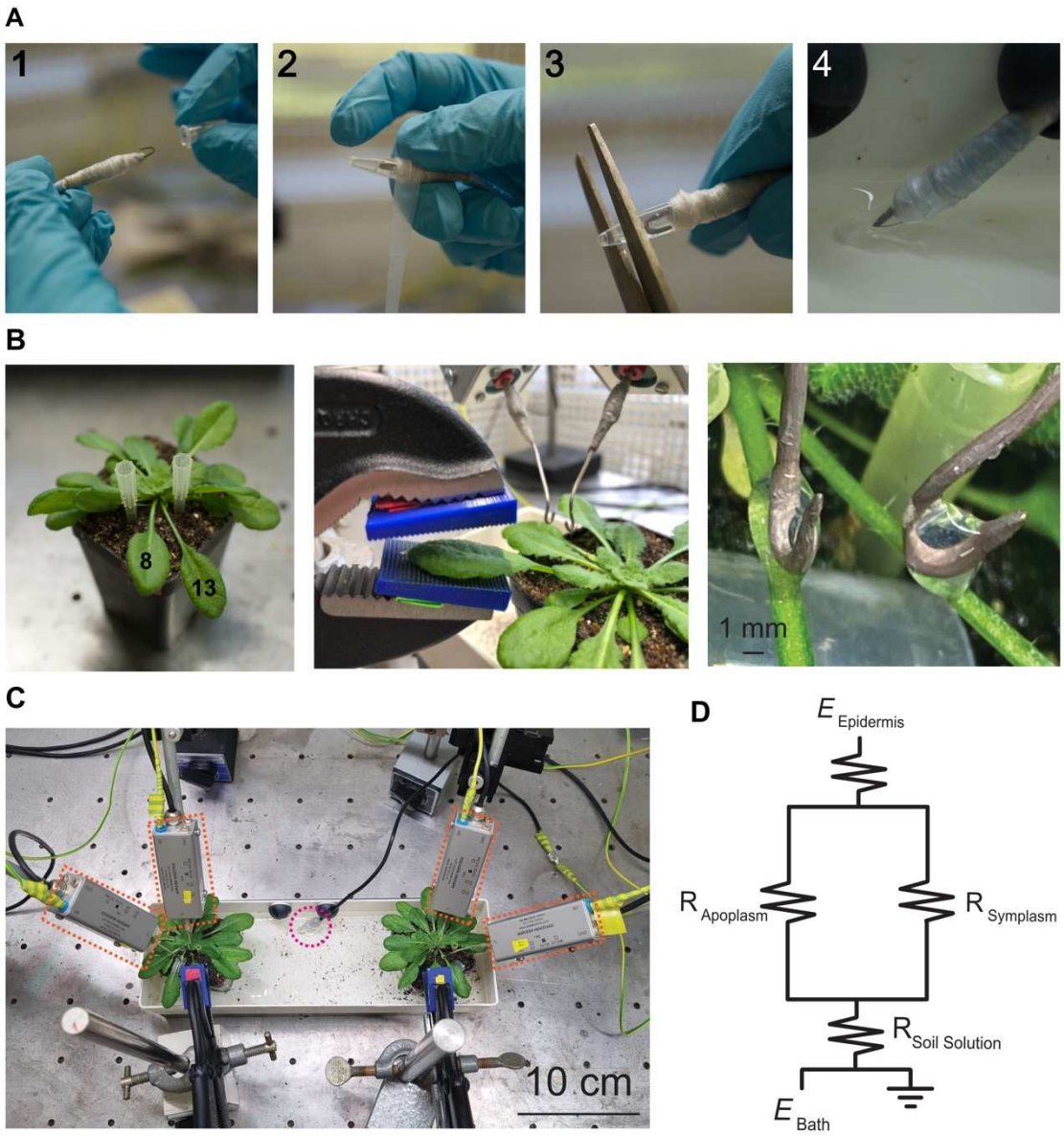

Figure 4. Experimental recording setup and electrode placement. A) To add the bath electrode to the circuit (1) place the electrode into the tube containing the 3% LE electrode solution. (2) Seal the PCR tube on the electrode with parafilm. (3) Cut the tip of the tube to have access to the agar. (4) Position the open tube containing the electrode into the bath solution. B) Shows the separation of leaf 8 and 13 via pipette tips, followed by the placement of leaf 8 inside the clamp. Connect the surface electrode with an 0.8 % agar bridge. C) Overview of the set-up inside the Faraday cage for simultaneous measurement of two plants. Orange rectangles highlight the head stages for each electrode, the pink circle the bath electrode. All electrodes are grounded to the cage. D) Schematic circuit. (R = resistance, E = electrode)

D. Wounding

**Note: Ensure that you can record a stable baseline without drift or noise in Labscribe before starting the actual recording. To properly analyze the data later, mark the end of the wounding (opening of the clamp) with the F1 key in the exported text files. The length of the recording can vary depending on the signal and experiment, and is to be adjusted for your purpose. Avoid letting the clamps jump open to prevent movement of the electrodes and noisy recordings. The closing pressure of the clamp can be adjusted with the screw in the back. Adjust it with the 3D-printed grids in place to a pressure in which the leaf is totally flaccid and translucent, but not severed after wounding Figure 5D). Use similar pressure for all plants.*

a. Ensure that approx. 2/3 of the leaf blade area is placed inside the clamp holding the 3D-printed grids (Figure 4B, 5A, D).
b. Before wounding, record a baseline for 90 sec.
c. Close the clamp completely for 5 sec (Figure 5B).
d. Carefully open the clamp.
e. Record for at least 10 minutes in total (Figure 5C).

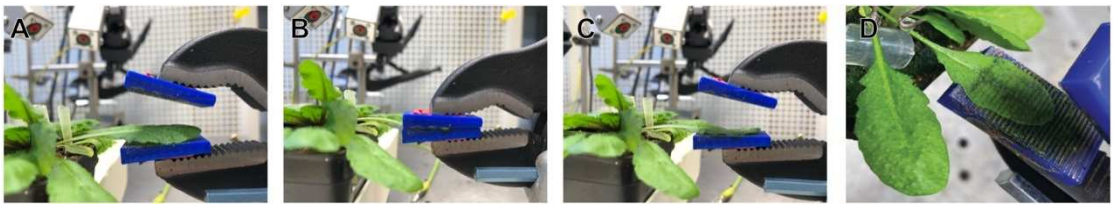

Figure 5. Wounding process during the recoding. A) Placement of the leaf between the clamp. B) Closed clamp on leaf, hold for 5 seconds in this position. C) Opening of clamp. D) Leaf post wounding.

Data analysis

**Note: Consistent annotation of the data set is crucial for the proper execution of the script.*

The SWP typically consists of at least three phases: an initial hyperpolarization, a depolarization, and a re-polarization often followed by a secondary hyperpolarization. Each phase is defined by multiple parameters (Figure 6). These parameters can be analyzed from a single trace. To automate the determination of six different parameters, we developed the R script **SWPanalyzer.Rmd**, which is available on GitHub here.

The script is designed to handle data obtained using the LabScribe and LabView NI software. It can analyze recordings from up to two simultaneously measured plants, with one electrode on the wounded leaf and another on a non-wounded leaf.

1. Annotate files:

All relevant experimental information (e.g., genotype, leaf number, treatments) should be saved in the electrode label that records on leaf 8. Organize this information according to the format specified in the script description.

2. Export .txt Files for analysis:

Once the recording is saved, export it to a .txt file by selecting **File > Export**. In the window that appears, check the box for "Include time of day." The sampling rate can be set to either 10 or 100 Hz, with 100 Hz being sufficient for data visualization. Gather all files in a single folder named after the recording date in the format "yymmdd". The specific name of each file is irrelevant to the script. The folder(s) containing recordings from different days will serve as the initial input for the script.

3. How to use the script:

To run the script, create a new project in R Studio by selecting **File > New Project**. In the window that opens, choose **New Directory > New Project**. Enter a name for the folder (e.g., "home") and select a path where it will be created. This "home" folder will contain the project file (home.Rproj). Place all "yymmdd" folders containing the exported data into this "home" folder. Open the script by selecting **File > Open** and choosing the downloaded **SWPanalyzer.Rmd** file. Read the description and follow the instructions provided in the script.

The first four sections of the script cover the minimum analysis required. After running these sections successfully, the following output files will be generated in the "home" folder:

- A "genotype.csv" file for each genotype measured, containing all recorded traces.
- A "genotypeSummary.csv" file with the calculated parameters for all leaves of all plants.

- A “Mean-genotype-Lxx.pdf” file for each genotype, featuring a mean trace with an overlaid standard error of the mean (±SEM) of all traces (Figure 7A) The traces included in this mean plot can be manually selected in Section 5.
- A “genotype-yymmdd” folder containing plots of each leaf of each plant, with overlays of the calculated parameters and a graphic visualization of the data as a violin plot (Figure 7B), comparing results between genotypes (“yymmdd-parameter.pdf”).

After running the script, visually inspect the quantified parameters by checking the “#.Lxx.pdf” images generated for each trace. If a parameter is wrongly quantified, you can trace it back to the “genotypeSummay.csv” by the date, the #, the leaf, and exclude it from further statistical analysis.

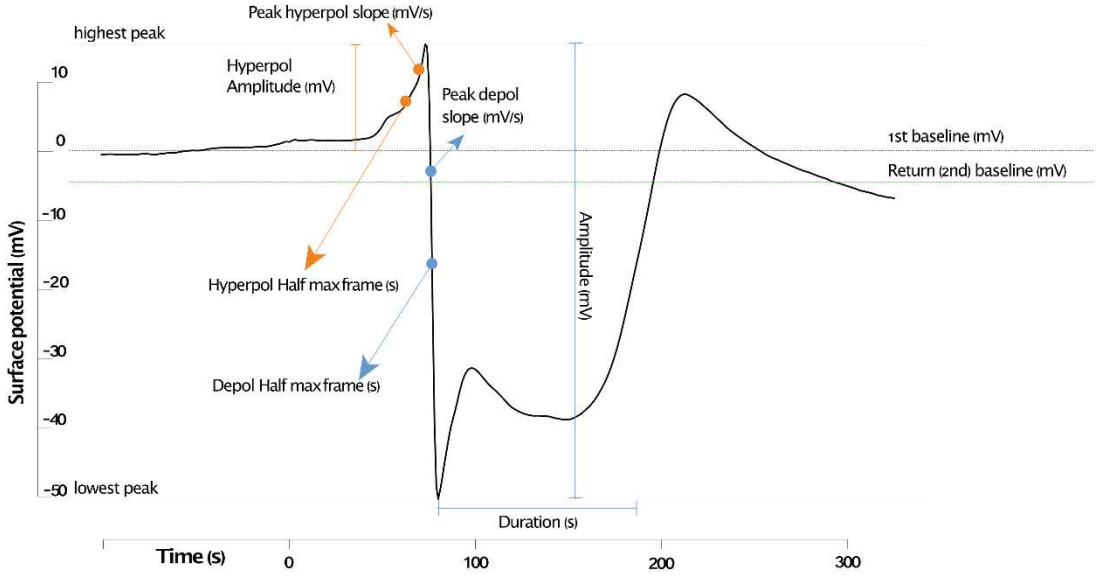

Figure 6. Exemplary Col-0 surface potential curve of leaf 13 with all parameters that are identified using the script. Highlighted in orange are quantified parameters of the 1st hyperpolarization, in blue parameters of the depolarization. The 1st baseline (dashed grey line) is the baseline before wounding, the 2nd is the base line (dashed green line) after repolarization.

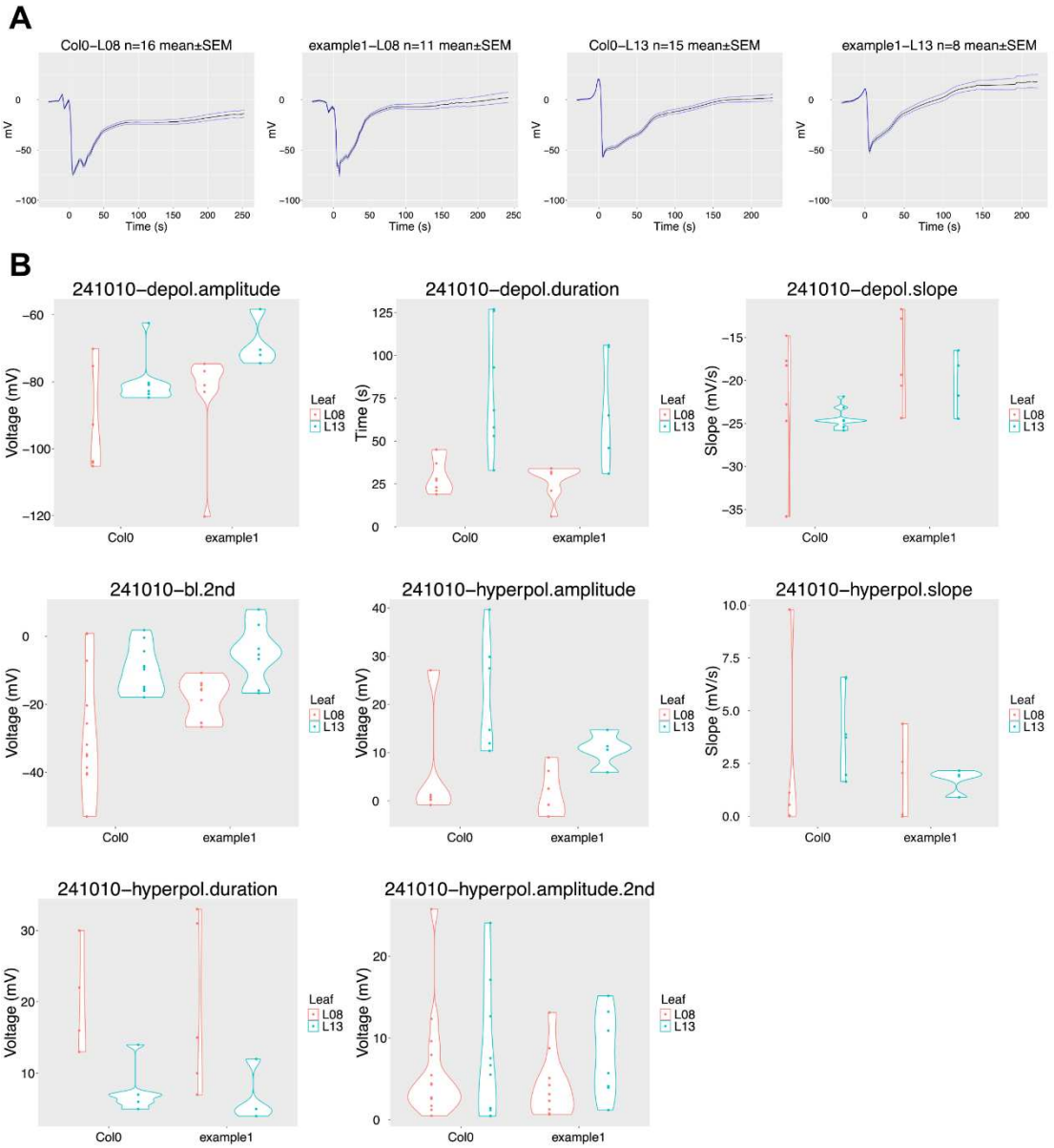

Figure 7. SWPanalyzer.Rmd output of the analyzed exemplary data set from recordings of Col-0 and mutant (example 1) plants. A) Mean traces ± SEM error bands of all analysed traces for leaf (L) 08 and 13. B) Violin plots for each parameter. Depol = depolarization, bl= base line. Each dot represents one recording.

Validation of protocol

This protocol is a robust and reproducible way to study SWPs of plant surfaces. The number of replicates needed is typically ≥10 in order to apply statistical tests (e.g., to compare among genotypes). Parts of this protocol have been used in [10]

Col-0 plants were employed for surface potential recordings (see Figure1, 2, 4, 5). The obtained data was analysed using the **SWPanalyzer.Rmd** (see Data Analysis). The raw data can be found here.

General notes and troubleshooting

General notes

1. Although this protocol uses the *Arabidopsis thaliana* Col-0 ecotype, other ecotypes may be used. However, differences in rosette morphology could affect petiole accessibility for electrode placement.
2. Prior to the measurement, plants should be acclimatized to the new conditions.
3. The raw data, analysis, R script and 3D-design can be found under the following link: https://github.com/jucbca/SWP-data_analysis

Troubleshooting

Recording:

Problem: You are unable to record any changes in electric potentials.

Solution:

a) If you do not detect a signal in the wounded leaf:

1. Use a lighter to burn the leaf from the bottom - this method is the most reliable trigger of SWPs and serves as a positive control for your setup.
2. Check with a multimeter if all connections are properly grounded to the same ground.
3. By visual inspection, ensure the ground electrode is still chloridized. If not, exchange it.
4. Verify that the surface potential electrode is properly connected via an agar bridge. If necessary, exchange the electrodes.

b) If you are able to record a signal in the wounded leaf but not in the distal leaf:

5. Verify that the leaves were counted correctly.

Problem: You are unable to offset the voltage in the amplifier to 0. It is out of range, keeps drifting or presents high noise.

Solution:

a) If the problem occurs for all the electrodes:

1. Increase the volume of ½ MS in the pot container.
2. Ensure the ground electrode is still chloridized. If not, exchange it.

b) If the problem occurs for only one electrode:

3. Ensure the recording electrode is still chloridized. If not, exchange it.
4. Verify that the surface potential electrode is properly connected via an agar bridge. If necessary, exchange the electrodes.

Data analysis:

Section 1: Ensure you run this section every time the project is opened.

Section 2:
Problem: Different folders are created for the same genotype.
Solution: Ensure the spelling of the genotype is consistent across all electrode labels in the .txt files. Variations in spaces, capital letters, or dashes will cause the script to identify them as different genotypes (e.g., Col0, col0, Col 0, Col-0).
Section 3:
Problem: A trace generates aberrant parameters, causing Chunk 3.2 to stop running.
Solution: Re-run Chunk 3.2 and remove the problematic trace. This trace cannot be analyzed due to poor recording quality.

Acknowledgments

This work was funded by grants from Deutsche Forschungsgemeinschaft (DFG, German Research Foundation) under Germany´s Excellence Strategy – EXC-2048/1 – project ID 390686111 (CEPLAS) and under project ID 267205415-CRC) SFB 1208-Project-ID 267205415. We thank Dr. Marriah Green for critical reading of the manuscript and Waldemar Seidel for help in the rig setup.

Competing interests

The authors declare no competing interests.

Ethical considerations

Does not apply.

References

1 Mousavi, S.A.R., Nguyen, C.T., Farmer, E.E. and Kellenberger, S. (2014) Measuring Surface Potential Changes on Leaves. *Nature Protocols*, Nature Publishing Group, **9**, 1997–2004. https://doi.org/10.1038/NPROT.2014.136.
2 Burdon-Sanderson. (1873) I. Note on the Electrical Phenomena Which Accompany Irritation of the Leaf of *Dionæa Muscipula*. *Proceedings of the Royal Society of London*, The Royal Society London, **21**, 495–496. https://doi.org/10.1098/RSPL.1872.0092.
3 Umrath, K. (1930) Untersuchungen über Plasma und Plasmaströmung an Characeen. *Protoplasma* **9**, 576–597 (1930). https://doi.org/10.1007/BF01943373IV. 576–597.
4 Schroeder, J.I., Hedrich, R. and Fernandez, J.M. (1984) Potassium-Selective Single Channels in Guard Cell Protoplasts of *Vicia faba*. *Nature*, **312**, 361–362. https://doi.org/10.1038/312361a0.
5 Lautner, S., Grams, T.E.E., Matyssek, R. and Fromm, J. (2005) Characteristics of Electrical Signals in Poplar and Responses in Photosynthesis. *Plant Physiology*, **138**, 2200–2209. https://doi.org/10.1104/pp.105.064196.
6 Fromm, J. and Lautner, S. (2007) Electrical Signals and Their Physiological Significance in Plants. *Plant, Cell & Environment*, John Wiley & Sons, Ltd, **30**, 249–257. https://doi.org/10.1111/J.1365-3040.2006.01614.X.
7 Vodeneev, V., Akinchits, E. and Sukhov, V. (2015) Variation Potential in Higher Plants: Mechanisms of Generation and Propagation. *Plant Signaling & Behavior*, Taylor & Francis, **10**. https://doi.org/10.1080/15592324.2015.1057365.
8 Doran, L. (2021) Sterilizing the Surface of Seeds by Chlorine Gas V.1le. Protocols.Io. https://doi.org/10.17504/protocols.io.bx8rprv6.

9 Farmer, E., Mousavi, S. and Lenglet, A. (2013) Leaf Numbering for Experiments on Long Distance Signalling in Arabidopsis. *Protocol Exchange*. https://doi.org/10.1038/protex.2013.071.
10 Moe-Lange, J., Gappel, N.M., Machado, M., Wudick, M.M., Sies, C.S.A., Schott-Verdugo, S.N., Bonus, M., Mishra, S., Hartwig, T., Bezrutczyk, M., Basu, D., Farmer, E.E., Gohlke, H., Malkovskiy, A., Haswell, E.S., Lercher, M.J., Ehrhardt, D.W., Frommer, W.B. and Kleist, T.J. (2021) Interdependence of a Mechanosensitive Anion Channel and Glutamate Receptors in Distal Wound Signaling. *Science Advances*, **7**. https://doi.org/10.1126/sciadv.abg4298.

Chapter 4 – Ongoing deciphering of SWP-generating molecular mechanisms

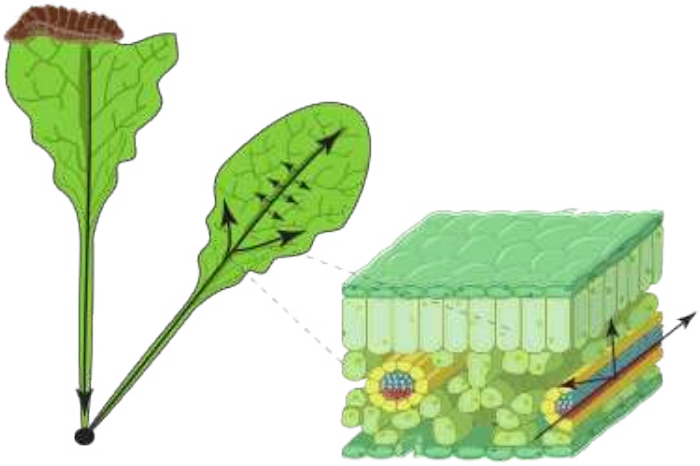

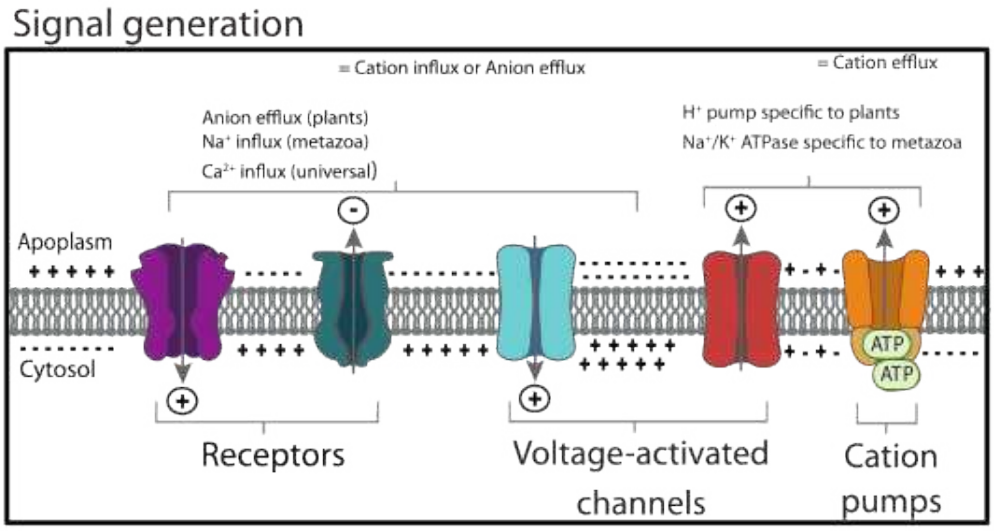

Contribution to this chapter
Juan Camilo Barbosa-Caro contributed entirely to the data acquisition, raw data analysis, statistical analysis, and drafting of this chapter.

Introduction

The previous chapters focused on how the SWP, as a long-distance signaling phenomenon, can be understood from the perspective of propagation and generation. Two phenomena that can be studied separately but are inherently intertwined in the SWP. To this point, my analysis has primarily studied the underlying mechanisms of propagation. The membrane excitability in response to Ca^{2+} can sustain self-propagation, but, in the context of the SWP, this process appears to be dependent on preceding bulk flow and the arrival of propagating chemical cues.

The alleged primacy of chemical transmission in SWP propagation allows a more direct understanding of the electric signal generating mechanisms. Given the likely chemical initiation of the SWP, it becomes possible to delineate the cascade of known signaling events more precisely. The ligand-mediated activation of the Ca^{2+}-permeable channels GLR3.3 and GLR3.6, essential for the initiation of the SWP (Mousavi *et al.*, 2013), temporally aligns with the arrival of the initial chemical cues. This correspondence underscores the likely role of these channels as primary mediators in converting chemical signals (*i.e.*, glutamate and aglycones) into the electrical response characteristic of the initial SWP phase.

In contrast, the mechanism by which the mechanosensitive channel MSL10 sustains a full-length SWP remains elusive (Moe-Lange *et al.*, 2021). It has been proposed that a wound-induced hydraulic wave can be transduced by this channel. However, a hydraulic wave is expected to propagate almost instantaneously throughout the entire plant following a wound event (Malone, 1996; Vodeneev *et al.*, 2015; Sukhov *et al.*, 2013). Despite this, in *Arabidopsis* leaf 13 the wound-induced electric signal does not initiate immediately. This discrepancy, together with the lack of evidence for a mechanical signal, highlights the potential importance of alternative mechanisms. The identification of putative EF-hand Ca^{2+}-binding domains in the structure of MSL10 (Moe-Lange *et al.*, 2021), points to a possible Ca^{2+}-mediated modulation of this protein in SWP generation.

In addition to these known SWP-related proteins, it is expected that voltage-dependent channels are involved in the rapid depolarization and in the repolarization phases of the SWP. The rapid depolarization is likely facilitated by depolarizing, voltage-dependent, anion-permeable channels (Hedrich *et al.*, 2016a; Cuin *et al.*, 2018; Vodeneev *et al.*, 2015). Conspicuous candidates include members of the ALMT (aluminum-activated malate transporter) family, which are voltage-dependent, outward rectifying, anion channels (Dreyer *et al.*, 2012; Roelfsema *et al.*, 2012; Mumm *et al.*, 2013; Meyer *et al.*, 2010). Repolarization is hypothesized to involve depolarization-activated, outwardly rectifying K^+-permeable channels. Proteins such as GORK and members of the AKT family are likely contributors as they have been shown to contribute to repolarization in *Arabidopsis* leaf and roots (Cuin *et al.*, 2018; Adem *et al.*, 2020; Hosy *et al.*, 2003; Salvador-Recatalà, 2016).

Although there is evidence of proteins involved in electric signaling, their specific roles in generating the wound-induced SWP remain elusive. Here we present a preliminary functional screening of voltage-dependent channels in the context of wound-induced, long-distance signaling in *Arabidopsis.* Additionally, we aimed to evaluate the regulatory potential of the putative EF-hand domains in MSL10. Our findings showcase limitations studying $[Ca^{2+}]_{cyt}$ regulation of Cl^- currents using the *Xenopus* oocyte system, due to inherent system constraints, and propose alternative technical approaches to overcome these restrictions.

Results

Functional characterization of the putative MSL10 EF-hand motifs

A well-studied group of mechanosensors is the Mechanosensitive channels of Small conductance (MscS) of the bacteria *Escherichia coli* (Maksaev and Haswell, 2011; Sukharev *et al.*, 2007). In plants, a family of MscS-Like (MSL) genes was identified based on homology to MscS (Maksaev and Haswell, 2012).

Among the 10 MSL members in *Arabidopsis thaliana*, MSL9 and MSL10 are responsible for responding to osmotic stress responses in root cells. MSL10, in particular, has been directly shown to be necessary for initiating an intracellular signaling pathway that leads to increased gene transcription or eventual programmed cell death (Basu and Haswell, 2020; Haswell *et al.*, 2008). Furthermore, MSL10 expressed in the vasculature of *Arabidopsis* petioles has been demonstrated to be crucial in sustaining SWP depolarization, achieving full amplitude of $[Ca^{2+}]_{cyt}$ increase, and for the complete activation of defense response genes in leaves upon distant wounding (Moe-Lange *et al.*, 2021).

The $[Ca^{2+}]_{cyt}$ response mediated by MSL10, observed both in roots and leaves, cannot be fully attributed to the biophysical characteristics of the channel. In other words, MSL10 preferentially facilitates the transport of monovalent anions and cations. Consequently, direct Ca^{2+} flux into the cytosol through MSL10 is unlikely to occur, suggesting indirect effect of MSL10 over Ca^{2+} fluxes.

A possible mechanism for this indirect effect was posited by Moe-Lange et al. (2021). They identified putative Ca^{2+}-interacting domains (EF-hands) in the structural model of the mechanosensor. This interaction could support a feedback mechanisms between $[Ca^{2+}]_{cyt}$ and MSL10 activity, and establish a causal link. Here, I aim to test the EF-hands-mediated Ca^{2+}-dependency of MSL10's electric activity by patch-clamp experiments using *Xenopus laevis* oocytes.

In order to express the channel MSL10 in oocytes, complementary RNA (cRNA) must first be synthesized *in vitro* and subsequently inject it into the cell cytoplasm. Furthermore, recordings of MSL10 characteristic anionic currents, previously characterized by Maksaev et al. (2018), will be attempted in a whole cell configuration using Two-Electrode Voltage Clamp (TEVC). Since MSL10 is a mechanosensitive channel triggered by membrane stretch (Maksaev et al., 2018; Maksaev & Haswell, 2012), it will be co-expressed in with the water-permeable *Arabidopsis* aquaporin TIP1, which is expected to facilitate water flow upon changes in extracellular osmolarity, facilitating cell turgor change, and activation of MSL10.

AtMSL10 and AtTIP1 cRNA synthesis and expression in Xenopus laevis oocytes

*At*MSL10 and *At*TIP1 were tagged with the fluorescent protein mCherry and GFP, respectively, and cloned into the cRNA synthesis-compatible vector pOO2 (Figure 1a). This vector has a SP6 recognition site for transcription initiation upstream of the gene of interest followed by a poly(A) tail of > 100 bp, for efficient translation (Figure 1b). Following the poly-A tail, an *Mlu*I restriction endonuclease cutting site allows linearization of the plasmid template prior to cRNA synthesis, thus interrupting *in vitro* transcription at that point.

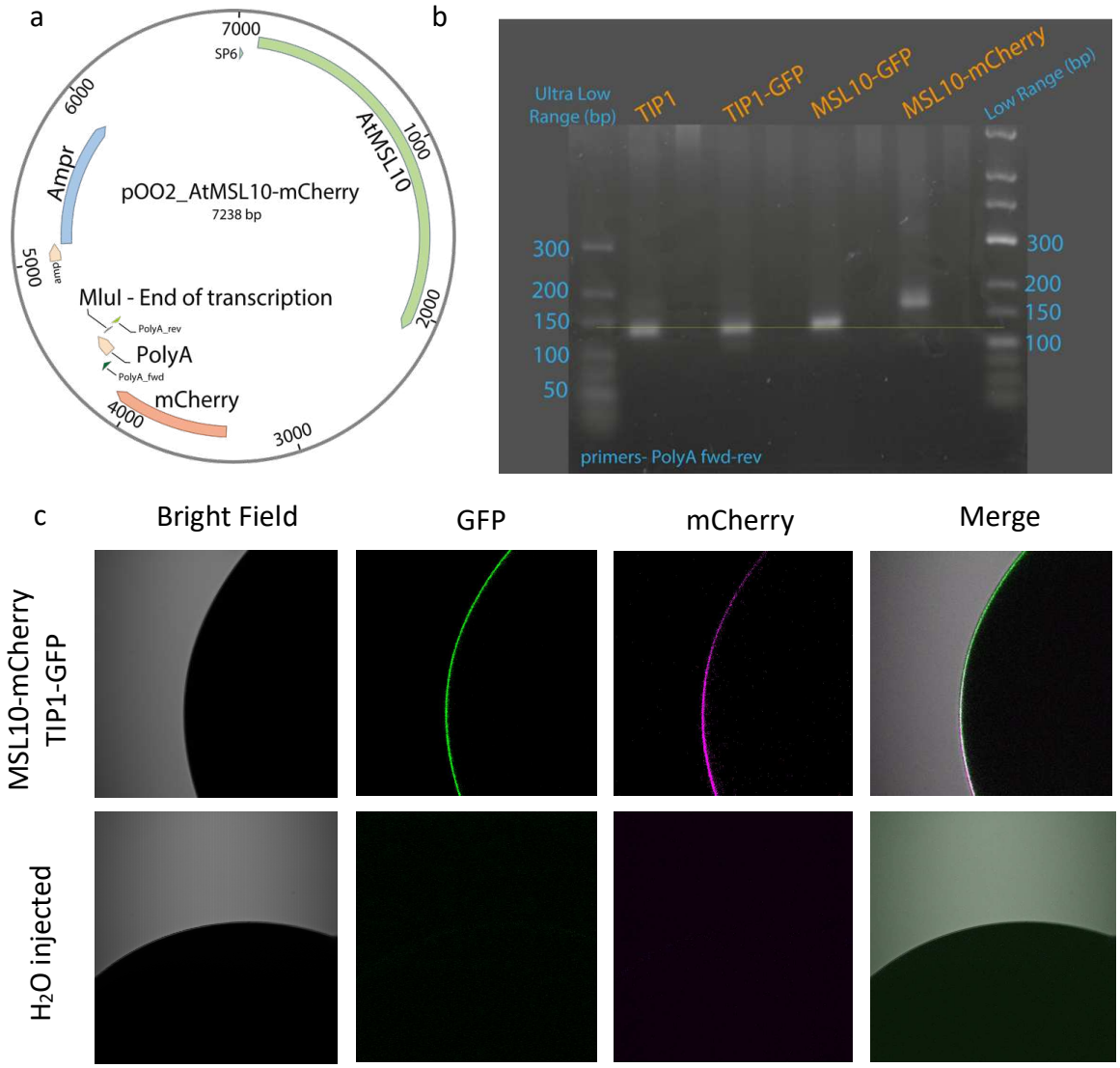

Figure 1. Expression of MSL10-mCherry and TIP1-GFP in *Xenopus* oocytes. (**a**) Vector map of *At*MSL10-mCherry in pOO2. (**b**) PCR amplification of poly(A) tail of various pOO2 plasmids containing the coding sequences of *At*TIP1, *At*MSL10 and their tagged versions. Amplified fragments are ≥ 100 bp. (**c**) Fluorescent signal of oocytes co-injected with *At*TIP1-GFP, *At*MSL10-mCherry, and co-injection of both. GFP imaging filter: Ex-470/40 nm, Em-525/50 nm. mCherry imaging filter Ex-572/25 nm, Em-629/62 nm.

Given the importance of a sufficiently long poly(A) tail for RNA translation into protein, the length of it was determined in the plasmid templates prior to cRNA synthesis and injection (Figure 1b).

cRNA was injected into oocytes, resulting in a detectable fluorescent signal under confocal microscopy as early as 24 h post-injection. Notably, oocytes injected with RNA with an IQ score as low as 6.5 (this is a 1-9 score given by the Qubit 4 genetic material analyzer machine. See materials and methods), also presented membrane fluorescence 48 h after injection (Figure 1c).

Two-Electrode Voltage Clamp recordings of AtMSL10 currents in Oocytes

Oocytes injected with either construct, co-injected with both, or injected with water were kept in an iso-osmotic (235 mOsm) ND96 extracellular solution (Kuruma and Hartzell, 1999). At 24 to 48 h post-injection, oocytes were impaled with two electrodes and the currents across the membrane were measured upon the imposition of multiple voltage steps. The resulting current-voltage (IV) curves, which plot imposed voltage (V) against measured current (I), provide a slope indicative of the membrane ion permeability. This serves as a reliable proxy for the quantity of channels active in that membrane (Figure 2). In order to trigger MSL10 channel opening, a modified hypo-osmotic (100 mOsm) ND solution was perfused and and IV curves were generated at 1-minute intervals for 5 minutes. Subsequently, the initial iso-osmotic solution was perfused once more, and membrane conductivity was recorded over the same intervals.

In iso-osmotic external solution, the reversal potential (where the IV curve intersects the x-axis) of the oocytes was approximately -25 mV. Upon exposure to hypo-osmotic conditions, the reversal potential of the cell shifted to a more negative voltage (-60 mV), accompanied by an increase in outward currents and a decrease in inward currents. This indicates the activation of a membrane conductance selective for ions with a reversal potential more negative than the resting membrane potential.

The change in osmolarity was achieved by altering the concentration of Na^+, while maintaining the theoretical reversal potential of Cl^- and K^+ at 43 and -96 mV, respectively (Table 1). This indicates that the observed current activation to the osmotic stimulus corresponds to a K^+ conductance. Not surprisingly, *Xenopus* oocytes exhibit endogenous, mechanosensitive channels permeable to K^+ (Yang and Sachs, 1990; Weber, 1999). Given the ionic abundance and prominently negative reversal potential of K^+, this K^+ conductance may obscure the activity of *At*MSL10 channels.

To overcome this masking effect of endogenous K^+ conductance, K^+ channel blockers can be used. Ionic gadolinium was shown to inhibit this endogenous conductance (Yang and Sachs, 1989), however, it also blocks the activity of MSL10 (Maksaev and Haswell, 2012). As an alternative, I attempted to inhibit endogenous K^+ currents with the commonly used blocker Tetraethylammonium (TEA) at a concentration of 10 mM (Huang *et al.*, 1995; Tokimasa and North, 1996; Shen *et al.*, 1994).

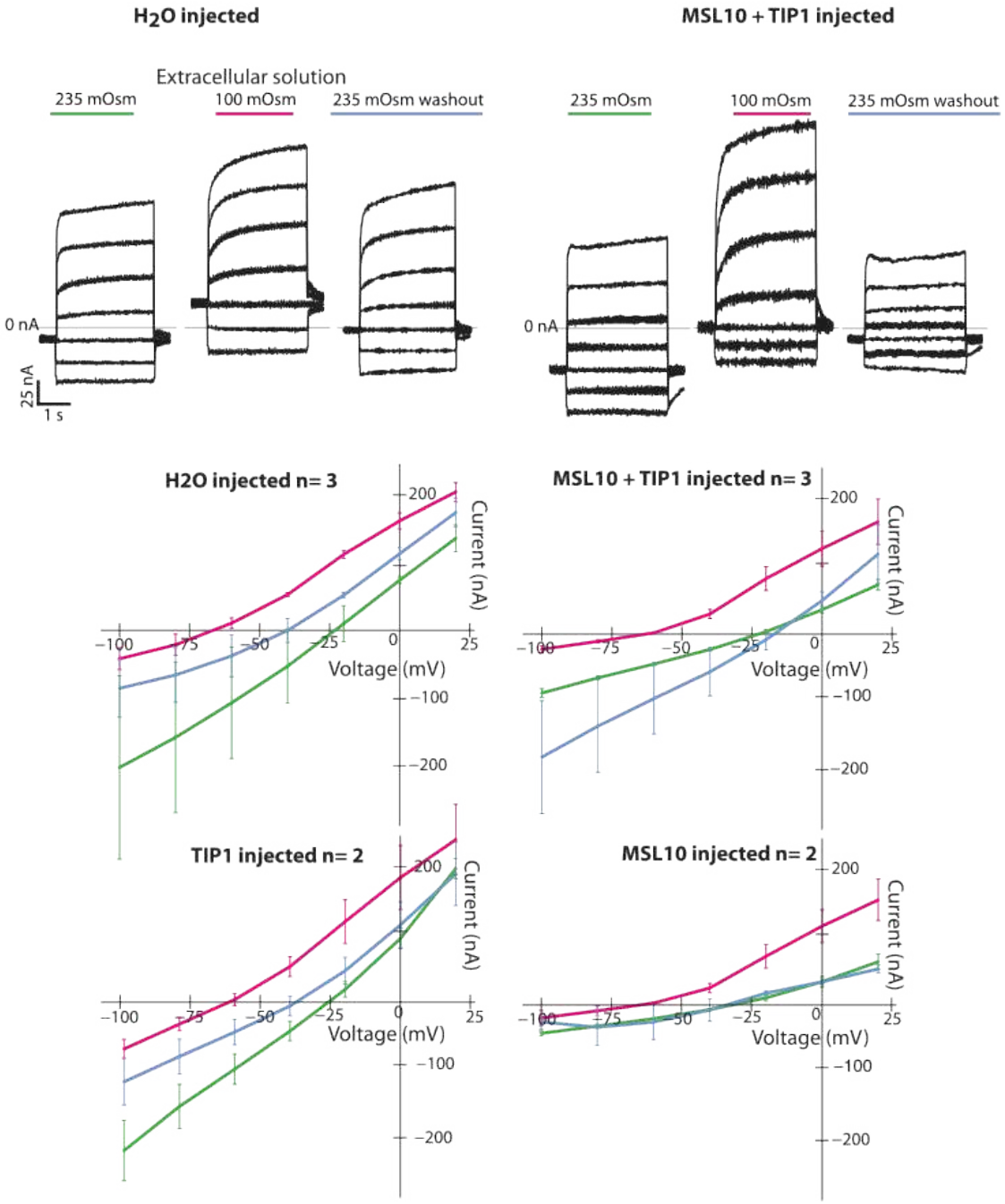

Figure 2. TEVC measurement of hypo-osmotic-activated currents in *Xenopus* oocytes expressing *At*MSL10 and/or *At*TIP1. Above – representative current traces generated by imposed voltage pulses ranging from -100 mV to 20 mV in 20 mV steps. Pulse duration was 1 s and the steady state current was calculated as the average current at the last 500 ms of the pulse. Colors indicate differences in extracellular solutions.

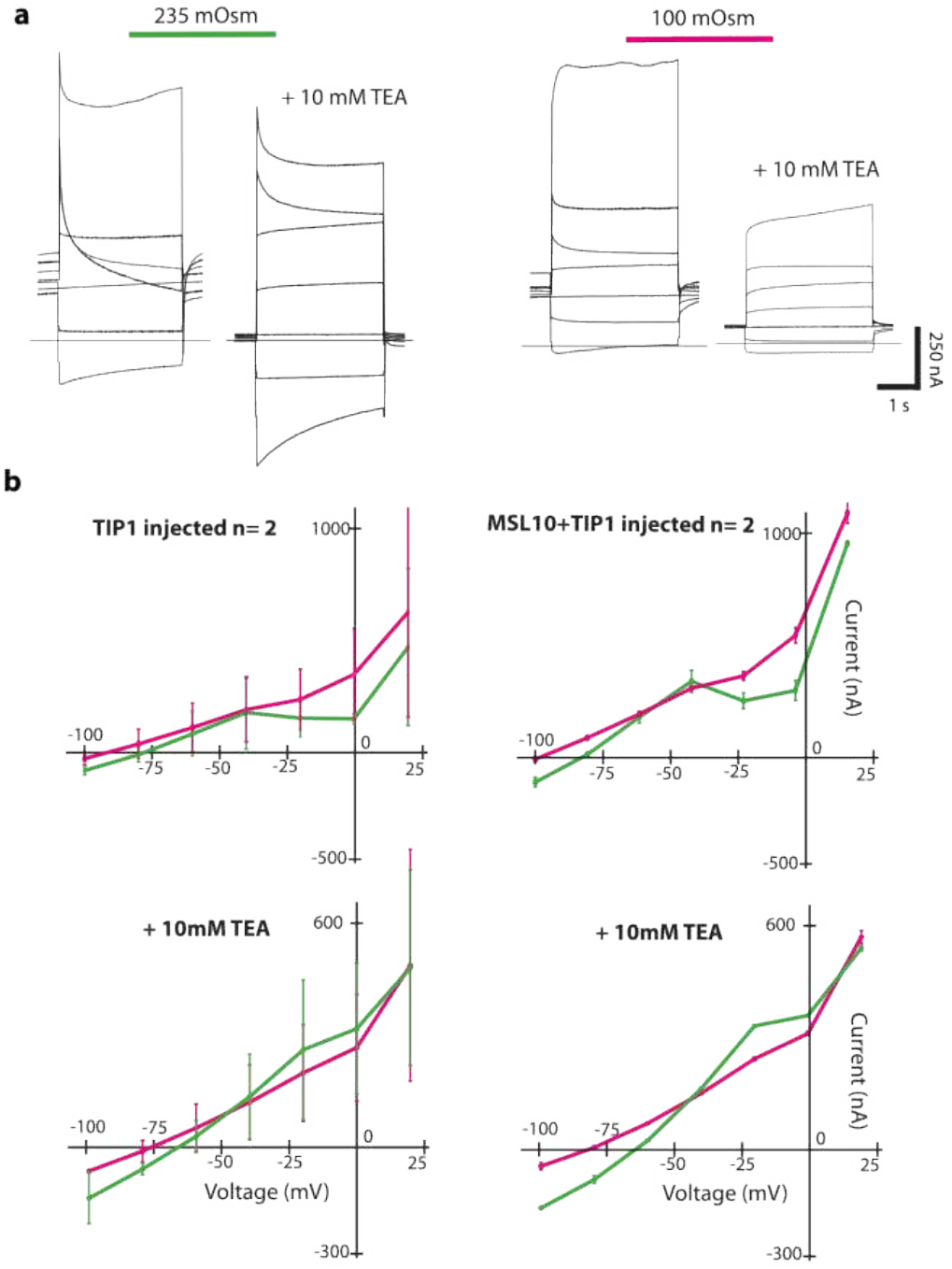

Figure 3. Blockage by 10 mM TEA of endogenous mechanosensitive channels in oocytes. a) Representative current traces in whole-cell configuration, oocytes injected with *At*MSL10 and *At*TIP1. **b)** IV curves of oocytes challenged with an iso-osmotic solution with and without 10 mM TEA.

Perfusion of TEA into the extracellular solution decreased the amplitude of outward currents under both iso- and hypo-osmotic conditions (Figure 3a) and shifted the

reversal potential to more positive in all tested conditions (Figure 3b). However, in oocytes expressing *At*MSL10, the reversal potential shifted only up to -60 mV, a value that is significantly lower than the theoretical reversal potential of Cl^- (16 mV, Table 1).

It can be concluded that TEA blocks, at least partially, the stretch-activated K^+ currents. In spite of this, the reversal potential and current amplitudes were similar between *At*TIP1-only and *At*MSL10 + *At*TIP1-injected oocytes. Two possible explanations for the masking effect to persist are that (1) TEA may not fully block K^+ currents, or (2) other stretch-activated channels might be responsible for the observed effects. These channels could permeate other ions, which are abundant in the cytosol but not in the perfused extracellular medium (Yang and Sachs, 1989; Yang and Sachs, 1990).

Outlook

Besides the masking effect of endogenous stretch-activated channels, there are also Ca^{2+}-activated Cl^- channels, and reciprocally Cl^--activated Ca^{2+} channels (Barish, 1983; Miledi, 1982; Weber, 1999). This endogenous feedback loop represents an unavoidable technical difficulty when investigating the modulation of *At*MSL10-mediated anion conductance by Ca^{2+}. To overcome these technical difficulties inherent to the system, it is necessary to record the activity of *At*MSL10 using excised patches of oocyte membranes. This approach inactivates endogenous K^+ mechanosensitive channels (Maksaev and Haswell, 2012; Maksaev and Haswell, 2011) and allows precise control over the solution on both sides of the membrane. By doing so, it becomes possible to selectively deplete undesired ions, and tightly control [Ca^{+2}] on the intracellular side of the membrane.

Pharmacological inhibition of anionic currents in the *Arabidopsis* SWP

The generation of electric signals in plants is sustained by a combination of depolarizing anionic and Ca^{2+} currents, along with hyperpolarizing K^+ channels and H^+ pumps

(Vodeneev *et al.*, 2015; Brownlee, 2022; Barbosa-Caro and Wudick, 2024). However, the specific contributions of these ions to the complex shape of the SWP in *Arabidopsis* remain unknown. A common approach to functionally dissect the role of individual ions in shaping electrical signals involves blocking specific populations of ion channels (Armada-moreiraet al., 2023; Scherzer, Böhm, et al., 2022; Scherzer, Huang, et al., 2022).

To the date few channels have been identified to participate in the generation of SWPs in *Arabidopsis*. These include GLR3.3 and GLR3.6, which are permeable to Ca^{2+} (Qi *et al.*, 2006; Wudick *et al.*, 2018; Gangwar *et al.*, 2020), MSL10, which is permeable to anions (Maksaev and Haswell, 2012), and the proton pump AHA1, which repolarizes by exporting H^+ (Kumari *et al.*, 2019). Although currently only one anion channel has been identified (MSL10), it is likely that other anion channels also contribute to the SWP (Hedrich *et al.*, 2016a). We hypothesize that, under the effect of the broad anion channel blocker niflumic acid (NiF), the SWP will be more strongly shortened than in *msl10* plants, indicating the involvement of additional anion channels.

To test this hypothesis, we developed a protocol for drug delivery through a cut in leaf 13 that still allows SWP generation (Figure 4a,b). The time required for NiF to reach and act on the tissue was approximately 30-45 min, after which wounding generated a normal signal in leaf 8 but a significantly smaller, shorter, and less steep depolarization in leaf 13 (Figure 4c-f). Notably, the hyperpolarization was unaffected, and the negative control did not differ from untreated Col-0 plants.

Outlook

This set of data demonstrates how pharmacological approaches can be applied to investigate the circuitry of ion channels involved in SWP generation. By applying this method to *msl10* plants, we can assess whether additional anion conductances are implicated in the generation of the SWP. Similarly, the application of other channel or metabolic blockers can be applied to identify the role of Ca^{2+} channels using DNQX or

AP5, K^+ channels by means of TEA^+ or H^+ pumps using the agonist fusicoccin (Kew and Kemp, 2005; De Vriese *et al.*, 2018; Stanfield, 1983; Kumari *et al.*, 2019; Kupisz *et al.*, 2017).

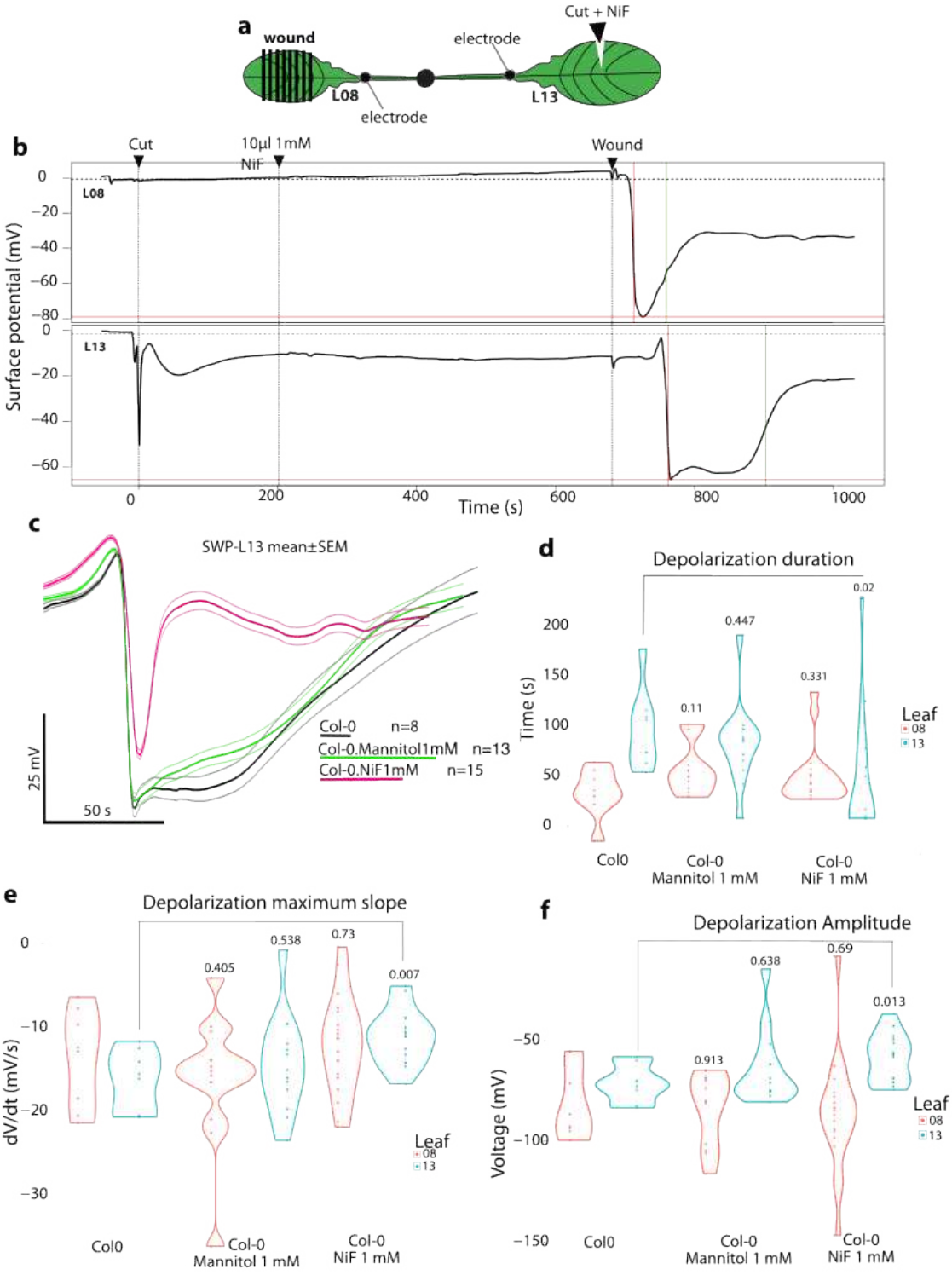

Figure 4. *Arabidopsis* SWP 30-45 min after treatment of leaf 13 with 10 µL of 1mM niflumic acid. (**a**) Illustration of the experimental setup. NiF is added to an incision made in the blade of leaf 13 avoiding cutting through the mid vein. After 30-45 min leaf 8 is wounded by compression. (**b**) Electrophysiological measurements in both leaves during the procedure of sequential drug delivery, indicating no effect of the intervention on the capacity of SWP generation. (**c**) Mean ± SEM traces of Col-0 plants treated with NiF, 1 mM mannitol, and untreated. Quantification of (**d**) duration between half maximum at depolarization and repolarization, (**e**) maximum downward slope at the depolarization, and (**f**) amplitude from peak hyperpolarization to peak depolarization. Parameter quantification was done as in Chapter 2, Figure 4. P-values were calculated with Mann-Whitney U test.

Screening of ion channel knockouts in *Arabidopsis* SWP

Electric signals in plants are sustained by the interplay of multiple ion transporters (Hedrich and Kreuzer, 2023; Hedrich and Becker, 1994). The SWP, in particular, is a highly variable signal that is considered to be sustained by the combinatorial action of receptors, channels and pumps (Hedrich *et al.*, 2016b; Vodeneev *et al.*, 2015; Sukhov *et al.*, 2018). So far, it is known that the GLR3.3/GLR3.6 pair are essential for SWP initiation in *Arabidopsis*, while MSL10 and AHA1, are crucial for its full development and the associated immune response (Mousavi *et al.*, 2013; Moe-Lange *et al.*, 2021; Kumari *et al.*, 2019).

A variety of voltage-sensitive anion and K^+-permeable channels are thought to be involved in the rapid depolarization and the repolarization phases of the SWP (Hedrich *et al.*, 2016b; Cuin *et al.*, 2018). In this study, we aimed to investigate the contribution of diverse ion channels in shaping the SWP in *Arabidopsis*, focusing on the ALMT anion channel family, due to their rapid response to voltage changes (Dreyer *et al.*, 2012; Roelfsema *et al.*, 2012; Mumm *et al.*, 2013; Meyer *et al.*, 2010). We hypothesize that these channels could contribute to the rapid depolarization phase through a depolarization-activated, depolarizing activity. Our investigation focuses on ALMTs that are expressed in the vascular tissue (Kim et al., 2021).

We also focused on the K^+ channel GORK because it is outwardly rectifying and depolarization-activated, which could generate a hyperpolarization that drives the SWP back to baseline (Cuin *et al.*, 2018; Hosy *et al.*, 2003; Adem *et al.*, 2020; Lim *et al.*, 2019;

Eisenach *et al.*, 2014; Ache *et al.*, 2000; Förster *et al.*, 2019). Additionally, we investigated the SKOR K^+ channel, which is also outwardly rectifying but regulated by intracellular K^+ concentration rather than voltage. Furthermore, SKOR has been suggested to be implicated in signal repolarization in *Dionaea* (Liu *et al.*, 2006; Drechsler *et al.*, 2015; Scherzer, Huang, *et al.*, 2022; Scherzer, Böhm, *et al.*, 2022).

We developed a high-throughput setup for stimulation and analysis to facilitate the mutant screening process (Atanjaoui, submitted). The experiments were conducted in batches of mutants and Col-0 as the wild-type SWP reference.
Prior to electrphysiological recordings, mutant lines were genotyped and confirmed homozygous using T-DNA specific primers (Table 3). The screening of two alleles of *almt13* and one allele of *almt9* revealed no significant differences in any of the seven parameters quantified (Figure 5). However, only two traces were obtained for the Col-0 reference, rendering the comparison unreliable. For the *almt5* mutant, detailed analysis of one allele showed no significant difference compared to Col-0 (Figure 6).

We also investigated the *gork/skor* double mutant, hypothesizing a prolonged repolarization, observable as an extended depolarization duration. However, this parameter, along with all the others quantified, were not significantly different from the Col-0 SWP (Figure 7).

Outlook

The SWP phenotype of the *almt5* and *gork*/*skor* mutants is not significantly different from that of Col-0, suggesting that these proteins may not be involved in the signal generation. However, it is not discarded that the specific insertional mutants used here do not completely abolish protein expression. Hence, screening other available insertional mutants or a newly generated, CRISPR/Cas9-based deletion mutants might provide a more definitive conclusion.

The data acquired for the *amlt13* and *amlt9* mutants is currently incomplete. Repetition of this experiment with an increased sample size is necessary to determine whether these insertional mutants exhibit a significantly different SWP compared to Col-0.

Overall, the screening of ion channels presented here is the beginning of an ambitious and promising project that can further unveil the diversity of molecular actors underlying the *Arabidopsis* SWP.

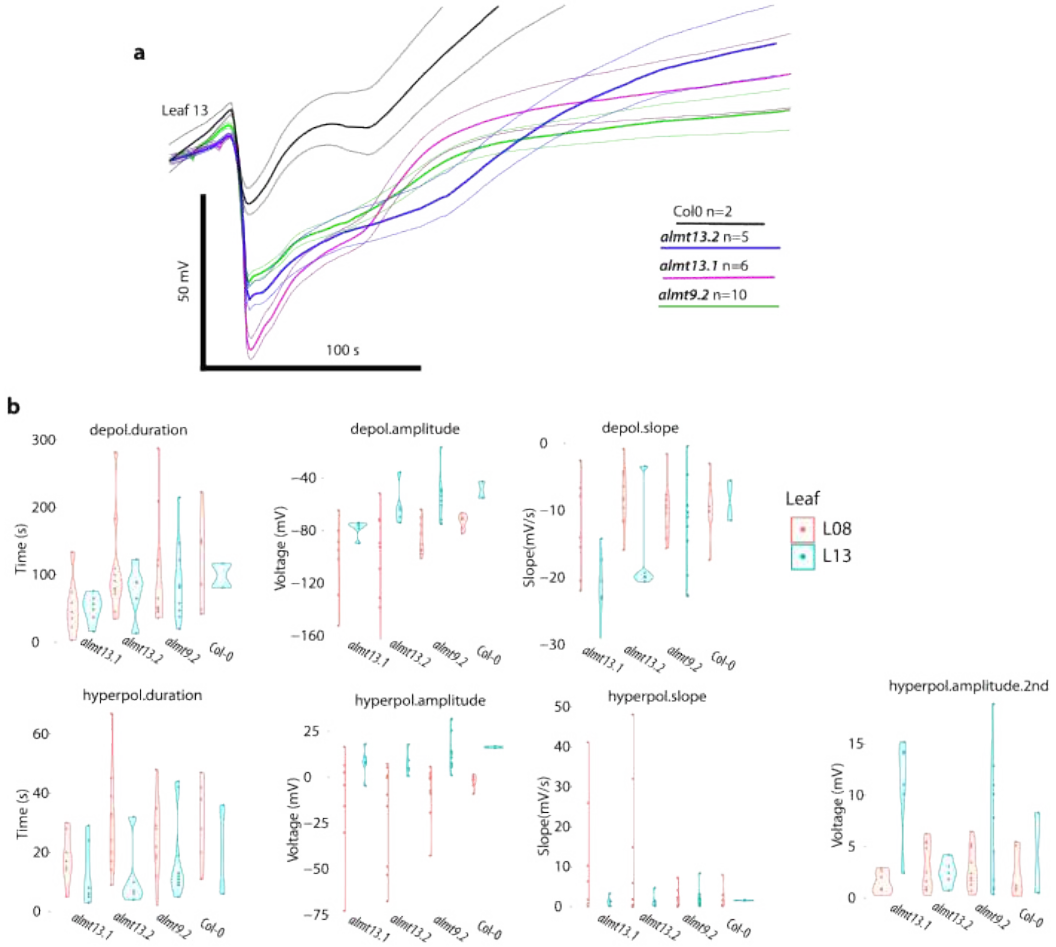

Figure 5. SWP quantification of *almt13.1, almt13.2, almt9.2* mutant plants. (**a**) Mean ± SEM traces of Col-0 and different mutants. (**b**) Quantification of SWP parameters in leaf 8 and 13 for the traces summarized in (a). Parameter quantification was done as in Chapter 2, Figure 4.

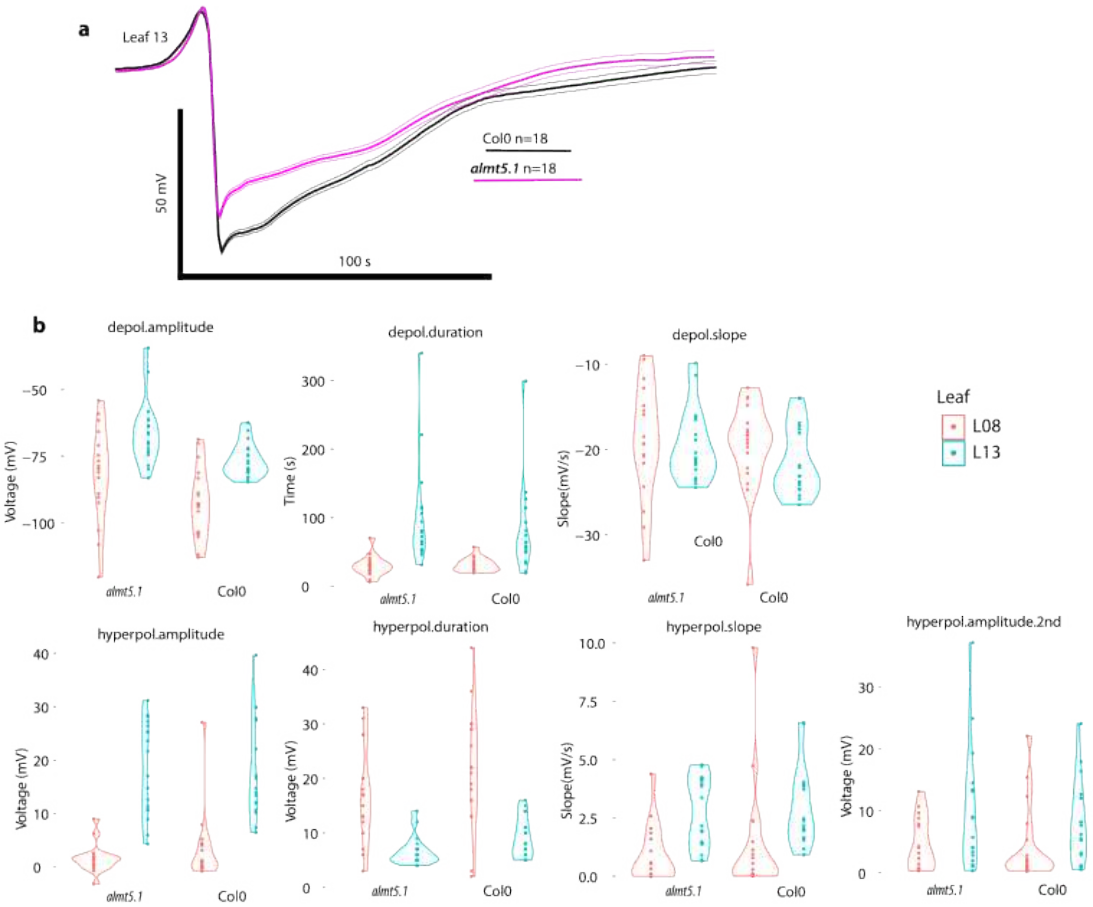

Figure 6. SWP quantification of *almt5.1* mutant plants. (**a**) Mean ± SEM traces of Col-0 and the mutant. (**b**) Quantification of SWP parameters in leaf 8 and 13 for the traces summarized in (a). Parameter quantification was done as in Chapter 2, Figure 4.

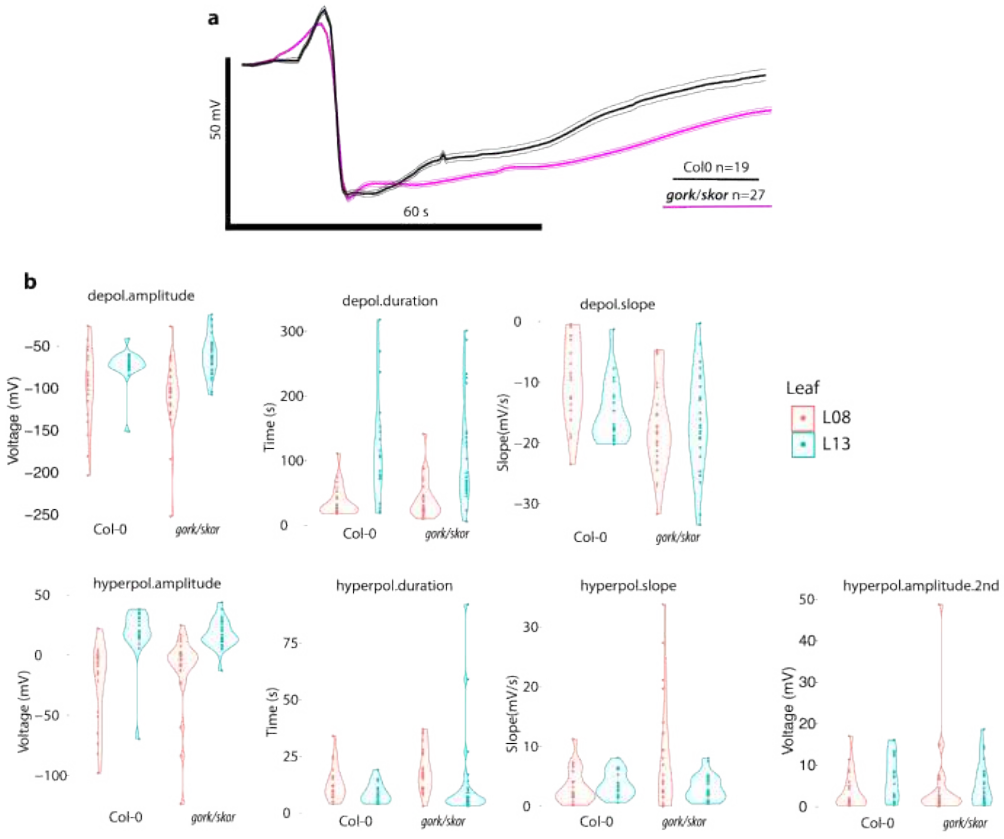

Figure 7. SWP quantification of *gork/skor* double mutant plants. (**a**) Mean ± SEM traces of Col-0 and the mutant. (**b**) Quantification of SWP parameters in leaf 8 and 13 for the traces summarized in (a). Parameter quantification was done as in Chapter 2, Figure 4.

Potential hyperpolarization phenotype in the *mslΔ5*, and *msl10* plants

The SWP can be analytically divided into multiple, distinct phases (Moe-Lange *et al.*, 2021). Notable phenotypic differences are observed in the SWP traces of the *msl10* single mutant and the *mslΔ5* quintuple mutant published by Moe-Lange *et al*. These differences are most evident in the initial hyperpolarization phase, where the amplitude is reduced in the single and the averaged traces shown (Moe-Lange *et al.*, 2021).

Given that the phenotype of diminished hyperpolarization amplitude was not addressed by Moe-Lange *et al.* (2021), we aimed to quantify and statistically validate

the difference observed in the few traces published. Using a custom-made, high-throughput pipeline designed for enhanced analytical resolution of SWP signals in *Arabidopsis* (Atanjaoui *et al.*, submitted), we reanalyzed the published data. Our results provided quantitative evidence that the leaf 13 SWP hyperpolarization amplitude in *msl10* is significantly smaller than in the wild type. Additionally, the peak depolarization slope is significantly shallower in the *msl10* mutant (Figure 8a,b).

To independently replicate this unresolved phenotype, we performed the same experiment with one allele each of *msl10* and *mslΔ5.* In this single experiment, the SWP of these mutants was shorter than in Col-0, consistent with the published results. However, the phenotype of diminished hyperpolarization amplitude could not be reproduced (Figure 8c,d).

Outlook

Although no statistical difference was observed in the hyperpolarization phase between *msl10*, *mslΔ5* and Col-0, repeating this experiment with a larger sample size may provide more robust results, since the sample size for the wild type control was too small for proper statistical analysis. The initial hyperpolarization phase of the SWP is a cryptic phenomenon that biophysically is thought to only occur by the activity of outward pumping ATPases (Brownlee, 2022; Vodeneev *et al.*, 2015; Barbosa-Caro and Wudick, 2024). Previous studies largely overlooked this phase, focusing instead on the depolarization phase during SWP phenotypic characterization (Moe-Lange *et al.*, 2021; Kumari *et al.*, 2019; Mousavi *et al.*, 2013; Farmer *et al.*, 2020; Yan *et al.*, 2024; Gao *et al.*, 2023). The analytical tool developed in this study offers the potential to investigate the role of proteins across multiple phases of the *Arabidopsis* SWP, enabling a more comprehensive understanding of this complex signal.

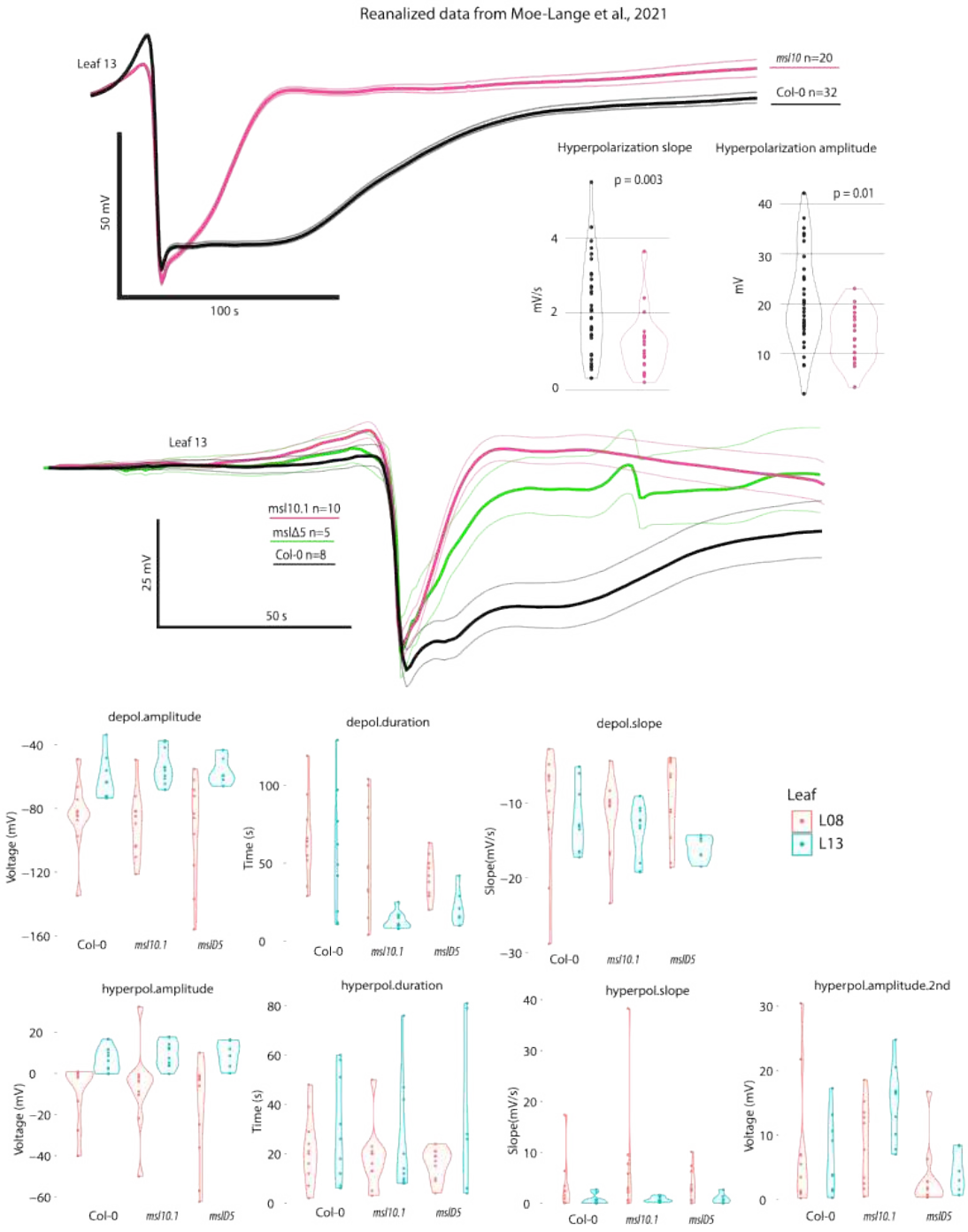

Figure 8. SWP quantification of *msl10* and mslΔ5 mutant plants. (**a**) Mean ± SEM traces of reanalyzed Col-0 and *msl10* mutant data published in Moe-Lange *et al.* (2021). (**b**) Quantification of SWP parameters in leaf 13 for the traces summarized in (a). (**c**) Mean ± SEM traces of Col-0, *msl10* and *mslΔ5* mutants. (**d**) Quantification of SWP parameters in leaf 13 for the traces summarized in (**c**). Parameter quantification was done as in Chapter 2, Figure 4. P-values were calculated with the Mann-Whitney U test.

Materials and methods

cRNA synthesis

pOO2 plasmids were used as template, with the SP6 promoter and *Mlu*I restriction site at the end of the poly(A) tail. Linearization of the pOO2 plasmid was done with *Mlu*I (New England Biolabs). Synthesis protocol was performed with the mMessage mMachine® kit (Thermo Fisher Scientific). cRNA concentration was determined with the NanoDrop One (Thermo Fisher Scientific), and the integrity was determined with as the IQ index of the Qubit 4 (Thermo Fisher Scientific). The IQ index is equivalent to the proportion of complete (long) over degraded (short) fragments of RNA. cRNA with an IQ index above 7 and concentration between 0.5-1 µg/µL was aliquoted and stored at -80 °C.

Xenopus oocyte transfection

Oocytes obtained from Ecocyte (Germany) were placed in Nunc 96-well, V-bottom plates (Thermo Fisher Scientific, Germany), submerged in modified Barth solution (Table 2), with the animal pole upwards, and left to rest at -4 °C for 1-2 h. The plate was placed in the Roboinject (Multichannel Systems, Germany), in which each oocyte was injected with 70 nl of 0.5-1 µg/µL of freshly thawed cRNA. Protein expression was checked every 24 h under the LSM 900 Airyscan confocal microscope (Zeiss, Germany).

Two electrode voltage-clamp

Intracellular patch clamp recordings were performed with the Roboocyte I (Multichannel Systems, Germany). Voltage steps ranging from -100 to +20 mV were imposed for 1 second and the steady state current was determined as the average current in the 500 ms. This protocol was run every 30 s during 5 minutes for each perfusion. This voltage protocol was coded in the roboocyte's coding language, and used as a .rsl file. Design of the protocols and manipulation of the roboocyte was done with PC running a Windows 7 operating system. The raw data from the roboocyte was extracted as .dat files and manipulated with a custom-made script in R (version 4.3.2).

Drug delivery for SWP pharmacology

Niflumic acid (Tocris bio-techne, USA) was initially diluted to 100 mM in DMSO and stored at -20 °C. The working solution (niflumic acid 1 mM, DMSO 1 %, Silwet 0.25 %, pH 5 with HEPES) was used for the experiments. For negative control the drug is replaced by Mannitol (mannitol 1 mM, DMSO 1 %, Silwet 0.25 %, pH5 with HEPES). Drug delivery was done through a transversal cut was done in the leaf blade avoiding cutting the mid vein.

Plant genotyping

T-DNA insertional knockout plants were obtained from the Nottingham *Arabidopsis* Stock Centre (NASC). Only genotyped plants, confirmed to be homozygous were used for surface potential recordings. The primers used for genotyping can be found in Table 3.

Surface potential recordings

Plants were acclimated for a minimum of 1 hour in the recording room under 120 µmol $m^{-2}s^{-1}$ white light for Col-0 plants, red light (600 nm) for Col-0 plants expressing channelrhodopsins, at ~22°C. The pot was submerged 3-4 cm deep in half strength Murashige & Skoog basal salt solution solution. An Ag/AgCl electrode was chloridized and used as ground electrode placed in the solution. Recording was done with 1 mm diameter Ag/AgCl electrodes (World Precision Instruments, USA). To bridge the electrodes and the tissue, an agar-salt bridge was used - consisting of 2 % (w/v) agar (Sigma-Aldrich, A9799) and 3 M KCl saturated with AgCl. Experiments were initiated only after a stable baseline of at least 5 minutes was observed. Data acquisition was done with dual-channel amplifiers (NPI Instruments EXT-02F amplifiers, World Precision Instruments LabTrax data acquisition digital converter, iWorx LabScribe 4 data acquisition software). Gain was set to the minimum for all experiments, and offset was manually adjusted to zero after mounting electrodes.

Surface potential data manipulation and statistical analysis

The SWP signal parameters are quantified by a custom-made algorithm. Initially, the recorded voltage vector, at 1 Hz sample rate, is smoothed with a Savitzky-Golay filter, with a moving window of 3 points and a fitting polynomial of order 1. From that filtered signal the parameters are automatically calculated as follows:

Reference parameters

- **first baseline** - average voltage from the beginning of the trace to the stimulus mark (inputted as an F1 during recording).
- **depol.peak** – minimum voltage of the complete trace.
- **first.hyperpol.peak** – maximum voltage between stimulus mark and **depol.peak**
- **second.hyperpol.peak** – maximum voltage between **depol.peak** and the recording end.
-

Hyperpolarization phase

- **hyperpol.amplitude** – the voltage difference between the **first baseline** and the **first.hyperpol.peak**.
- **hyperpol.slope** – the maximum point of the first derivative of the trace between the stimulus mark and the **first.hyperpol.peak**.
- **hyperpol.duration** – Time difference between **hyperpol.slope** and **depol.slope** (see below).

Depolarization phase

- **depol.slope** – minimum point of the first derivative of the trace between **first.hyperpol.peak** and **depol.peak**.
- **depol.amplitude** – Voltage difference between **first.hyperpol.peak** and **depol.peak**.
- **depol.duration** – time difference between the points where voltage equals (**first.hyperpol.peak** - **depol.peak**)/2 and (**second.hyperpol.peak** - **depol.peak**)/2.

Repolarization phase

- **bl.2nd** (second baseline) – average voltage in the final 60 s of the recording.
- **hyperpol.amplitude.2nd** – voltage difference between **second.hyperpol.peak** and **bl.2nd.**

Modified ND solutions				
	235 mOsm		100 mOsm	
ion	Concentration (mM)	Reversal potential (mV)	Concentration (mM)	Reversal potential (mV)
Cl^-	6	43	6	43
Na^+	111,5	73,8	44,5	50,6
K^+	2	-96,8	2	-96,8
Modified ND solution + 10 mM TEA-Cl				
	235 mOsm		100 mOsm	
ion	Concentration (mM)	Reversal potential (mV)	Concentration (mM)	Reversal potential (mV)
Cl^-	16	18,3	17	16,7
Na^+	34,5	44,2	101,5	71,4
K^+	2	-96,8	2	-96,8

Table 1. Extracellular solutions used to perfuse *Xenopus* oocytes in TEVC experiments

Component	mM
NaCl	88,00
KCl	1,00
$Ca(NO_3)_2$	0,33
$CaCl_2$	0,41
$MgSO_4 \cdot 7H_2O$	0,82
$NaHCO_3$	2,40
HEPES	5,00

Table 2. Modified Barth solution for *Xenopus* oocytes maintenance. The solution was balanced to pH 7.5 using HEPES buffer. Then autoclaved and stored at 4 C.

Code	name	5' to 3' sequence	gene identifier/info
JB001	SALK_082581_LP	GGTTTGATCGAATCTGAAACG	ALMT 4-1 At1g25480
JB002	SALK_082581_RP	ACAAACCACAACCAGTTCTCG	ALMT 4-1 At1g25480
JB003	SALK_086236C_LP	TGAATTTCCGAAAGAATGCAG	ALMT 4-2 At1g25480
JB004	SALK_086236C_RP	TTTTTGAAGGAGCAACATTGG	ALMT 4-2 At1g25480
JB005	SALK_071319.53_LP	GCACAATGTTAGCTGGAGGAC	ALMT 5-1 At1g68600
JB006	SALK_071319.53_RP	CCCGGTTATTCAATTCATGTG	ALMT 5-1 At1g68600
JB007	SALK_070728_LP	GCACAATGTTAGCTGGAGGAC	ALMT 5-2 At1g68600
JB008	SALK_070728_RP	CCCGGTTATTCAATTCATGTG	ALMT 5-2 At1g68600
JB009	SALK_117912_LP	GAGAATTAGGGTTCGATTCCG	ALMT 9-1 At3g18440
JB010	SALK_117912_RP	TGAATACATCAGTGTAGCGCG	ALMT 9-1 At3g18440
JB011	SALK_072016_LP	TCAGTTTCATACATGCCTCCC	ALMT 10-3 At4g00910
JB012	SALK_072016_RP	CACAATCAGGAAAAGCTGAGG	ALMT 10-3 At4g00910
JB013	SALK_119894_LP	TCAGTTTCATACATGCCTCCC	ALMT 10-1 At4g00910
JB014	SALK_119894_RP	CACAATCAGGAAAAGCTGAGG	ALMT 10-1 At4g00910
JB015	SAIL_533_F01_LP	TCAGGACGAGAATATTGCGAC	ALMT9-2 At3g18440
JB016	SAIL_533_F01_RP	ACACCATCAATGCCTTCAGTC	ALMT9-2 At3g18440
JB017	SAIL_827_G12_LP	TGTAGTTCCTCCACGTCATCC	ALMT10-2 At4g00910
JB018	SAIL_827_G12_RP	TCAGCTGCTGTCACATGTACC	ALMT10-2 At4g00910
JB019	SAILSEQ_517_F03_ LP	TAATAAAGCGGAATTGGAACG	ALMT13-1. At5g46600
JB020	SAILSEQ_517_F03_RP	GGCGGATTTAGAATCCAAAAC	ALMT13-1. At5g46600
JB021	SAILSEQ_627_B08_LP	CACGAAAGTCTTACGCGTCTC	ALMT13-2. At5g46600
JB022	SAILSEQ_627_B08_RP	ATCATCGATCGGCTCATATTG	ALMT13-2. At5g46600
JB028	SALKseq_117912.3_LP	CGAACTCAATGAGGAGAGACG	ALMT 9-1 At3g18440
JB029	SALKseq_117912.3_RP	TTATGAATGTTGCGACTTCCC	ALMT 9-1 At3g18440
JB030	SAILseq_533_F01.1_LP	TGGAATGGAATGAATAATCACG	ALMT9-2 At3g18440
JB031	SAILseq_533_F01.1_RP	TCCCAGTCACCGAATAAAGTG	ALMT9-2 At3g18440
JB032	SAILseq_827_G12.0_LP	CTCGAAAAACTTGCTGATTCG	ALMT10-2 At4g00910
JB033	SAILseq_827_G12.0_RP	TTAAAAGTTGAAACCATGCCG	ALMT10-2 At4g00910
JB040	GABI_575H12-LP	AGGAAGTGTCCCACCAATTTC	gork/skor double mutant N2103490
JB041	GABI_575H12-RP	AACAGAGAAGCAGCTCTCGTG	gork/skor double mutant N2103490
JB042	GABI_391G12_LP	ACACGATCATTCCCATTCTTG	gork/skor double mutant N2103489
JB043	GABI_391G12_RP	TATGAACCGAAACAAACTCGG	gork/skor double mutant N2103489
JB044	WiscDsLox386E04-LP	CCCGGTTATTCAATTCATGTG	almt5-3 At1g68600
JB045	WiscDsLox386E04-RP	GCACAATGTTAGCTGGAGGAC	almt5-3 At1g68600
JB046	SALK_071319.53.00.x_LP	GCACAATGTTAGCTGGAGGAC	almt5-4 At1g68600
JB047	SALK_071319.53.00.x_RP	CCCGGTTATTCAATTCATGTG	almt5-4 At1g68600

JB066	SALK_097435_LP	CCCATATCTCACTGGTTCACC	skor1
JB067	SALK_097435_RP	CCAAACTTCAGCGAAACAGAG	skor1
JB068	SALK_144737_LP	GGAGACATCTCCATCATTTGC	gork2
JB069	SALK_144737_RP	GTTTCTTGTTTCCGCACAATC	gork2
JB070	SALK_082258_LP	TGCATCACCTAGAAACGAACC	gork3
JB071	SALK_082258_RP	TTATTTGCAGCCGACCTATTG	gork3
JB072	GK-391G12_LP	GGATTCTAGTTGCTTAATCCGGAC	skor2
JB073	GK-391G12_RP	TCGATCTCTGGACTCGATACACTA	skor2
JB074	GK-865F05_LP	ACAAATGATCCACGACGTTTC	gork1
JB075	GK-865F05_RP	TTTTGGTTCTGATTCGGTTTG	gork1
JB081	GABI_513D02_LP	ATACTCTGCGTGGGTTTACCC	akt2-1
JB082	GABI_513D02_RP	GACGCTGCTTCAATGCTATTC	akt2-1
JB083	GABI_152C05_LP	CATTGTGGCATTGTCTTGTTG	akt2-2
JB084	GABI_152C05_RP	TTTGGTGTTGTTTTAGGCTCG	akt2-2
JB085	SALK_017212_LP	TGATAGAAGTCGAAAGCAGCG	akt2-3
JB086	SALK_017212_RP	AGCATCGAGGAAAAGGAAGAG	akt2-3

Table 3. List of primer for genotyping T-DNA insertional *Arabidopsis thaliana* mutants.

References

Ache, P., Becker, D., Ivashikina, N., Dietrich, P., Roelfsema, M.R.G. and Hedrich, R. (2000) GORK, a delayed outward rectifier expressed in guard cells of *Arabidopsis thaliana*, is a K^+-selective, K^+-sensing ion channel. *FEBS Lett*, **486**, 93–98.

Adem, G.D., Chen, G., Shabala, L., Chen, Z.H. and Shabala, S. (2020) GORK Channel: A Master Switch of Plant Metabolism? *Trends Plant Sci*, **25**, 434–445. Available at: https://doi.org/10.1016/j.tplants.2019.12.012.

Alarcon, J.J. and Malone, M. (1994) Substantial hydraulic signals are triggered by leaf-biting insects in tomato. *J Exp Bot*, **45**, 953–957.

Albert, V.A., Williams, S.E. and Chase, M.W. (1992) *Carnivorous Plants: Phylogeny and Structural Evolution*, Available at: https://www.science.org.

Armada-moreira, A., Dar, A.M., Zhao, Z., Cea, C., Gelinas, J., Berggren, M., Costa, A., Khodagholy, D. and Stavrinidou, E. (2023) Plant electrophysiology with conformable organic electronics : Deciphering the propagation of Venus flytrap action potentials.

Bakker, J.M.T. de, Belterman, C.N.W. and Coronel, R. (2021) Excitability and propagation of the electrical impulse in Venus flytrap; a comparative electrophysiological study of unipolar electrograms with myocardial tissue. *Bioelectrochemistry*, **140**, 107810. Available at: https://doi.org/10.1016/j.bioelechem.2021.107810.

Barbosa-Caro, J.C. and Wudick, M.M. (2024) Revisiting plant electric signaling: Challenging an old phenomenon with novel discoveries. *Curr Opin Plant Biol*, **79**, 102528. Available at: https://doi.org/10.1016/j.pbi.2024.102528.

Barish, M.E. (1983) A transient calcium-dependen chloride current in the immature *Xenopus*e oocyte. , 309–325.

Barnett, M.W. and Larkmann, P.M. (2007) The Action Potential. *Pract Neurol*, **7**, 192–197.

Basu, D. and Haswell, E.S. (2020) The Mechanosensitive Ion Channel MSL10 Potentiates Responses to Cell Swelling in *Arabidopsis* Seedlings. *Current Biology*, **30**, 2716-2728.e6. Available at: https://doi.org/10.1016/j.cub.2020.05.015.

Beilby, M.J. (2007) Action Potential in Charophytes. *Int Rev Cytol*, **257**, 43–82.

Bel, A.J.E. Van and Ehlers, K. (2005) Electrical Signalling via Plasmodesmata. *Plasmodesmata*, 263–278.

Bel, A.J.E. Van, Furch, A.C.U., Will, T., Buxa, S. V., Musetti, R. and Hafke, J.B. (2014) Spread the news: Systemic dissemination and local impact of Ca^{2+} signals along the phloem pathway. *J Exp Bot*, **65**, 1761–1787.

Bellandi, A., Papp, D., Breakspear, A., et al. (2022) Diffusion and bulk flow of amino acids mediate calcium waves in plants. , 1–15.

Blatt, M.R. and Thiel, G. (1994) K^+ channels of stomatal guard cells: bimodal control of the K^+ inward-rectifier evoked by auxin. *The Plant Journal*, **5**, 55–68.

Brownlee, C. (2022) Plant physiology: Anatomy of a plant action potential. *Current Biology*, **32**, R1000–R1002. Available at: https://doi.org/10.1016/j.cub.2022.08.024.

Browse, J. (2009) Jasmonate passes muster: A receptor and targets for the defense hormone. *Annu Rev Plant Biol*, **60**, 183–205.

Christenhusz, M.J.M. and Byng, J.W. (2016) The number of known plants species in the world and its annual increase. *Phytotaxa*, **261**, 201–217.

Cuin, T.A., Dreyer, I. and Michard, E. (2018) The role of potassium channels in *Arabidopsis thaliana* long distance electrical signalling: AKT2 modulates tissue excitability while GORK shapes action potentials. *Int J Mol Sci*, **19**, 1–17.

Ding, M., Zhou, Y., Becker, D., et al. (2024) Probing plant signal processing optogenetically by two channelrhodopsins. *Nature*, **633**. Available at: http://dx.doi.org/10.1038/s41586-024-07884-1.

Drechsler, N., Zheng, Y., Bohner, A., Nobmann, B., Wirén, N. von, Kunze, R. and Rausch, C. (2015) Nitrate-dependent control of shoot K homeostasis by NPF7.3/NRT1.5 and SKOR in *Arabidopsis*. *Plant Physiol*, **169**, pp.01152.2015.

Dreyer, I., Gomez-Porras, J.L., Riaño-Pachón, D.M., Hedrich, R. and Geiger, D. (2012) Molecular evolution of slow and quick anion channels (SLACs and QUACs/ALMTs). *Front Plant Sci*, **3**, 1–12.

Dreyer, I., Li, K., Riedelsberger, J., Hedrich, R., Konrad, K.R. and Michard, E. (2022) Transporter networks can serve plant cells as nutrient sensors and mimic transceptor-like behavior. *iScience*, **25**, 104078. Available at: https://doi.org/10.1016/j.isci.2022.104078.

Duan, X., Nagel, G. and Gao, S. (2019) Mutated channelrhodopsins with increased sodium and calcium permeability. *Applied Sciences (Switzerland)*, **9**, 1–11.

Dziubińska, H. (2003) Ways of signal transmission and physiological role of electrical potentials in plants. *Acta Societatis Botanicorum Poloniae*, **72**, 309–318.

Dziubińska, H., Trębacz, K. and Zawadzki, T. (2001) Transmission route for action potentials and variation potentials in *Helianthus annuus* L. *J Plant Physiol*, **158**, 1167–1172.

Eisenach, C., Papanatsiou, M., Hillert, E.K. and Blatt, M.R. (2014) Clustering of the K^+ channel GORK of *Arabidopsis* parallels its gating by extracellular K^+. *Plant Journal*, **78**, 203–214.

Ellison, A. and Adamec, L. (2018) *Carnivorous Plants: Physiology, ecology and evolution*, Oxford University Press.

Farmer, E.E., Gao, Y., Lenzoni, G., Wolfender, J. and Wu, Q. (2020) Wound- and mechano-stimulated electrical signals control hormone responses. *New Phytologist*.

Fenno, L., Yizhar, O. and Deisseroth, K. (2011) The development and application of optogenetics. *Annu Rev Neurosci*, **34**, 389–412.

Fisahn, J., Herde, O., Willmitzer, L. and Peña-Cortés, H. (2004) *Analysis of the Transient Increase in Cytosolic Ca^{2+} during the Action Potential of Higher Plants with High Temporal Resolution: Requirement of Ca^{2+} Transients for Induction of Jasmonic Acid Biosynthesis and PINII Gene Expression*, Available at: http://pcp.oxfordjournals.org/.

Förster, S., Schmidt, L.K., Kopic, E., et al. (2019) Wounding-Induced Stomatal Closure Requires Jasmonate-Mediated Activation of GORK K^+ Channels by a Ca^{2+} Sensor-Kinase CBL1-CIPK5 Complex. *Dev Cell*, **48**, 87-99.e6.

Fromm, J. and Lautner, S. (2007) Electrical signals and their physiological significance in plants. *Plant Cell Environ*, **30**, 249–257.

Gangwar, S.P., Green, M.N., Michard, E., Simon, A.A., Feijó, J.A. and Sobolevsky, A.I. (2020) Structure of the *Arabidopsis* Glutamate Receptor-like Channel GLR3.2 Ligand-Binding Domain. *Structure*, 1–9.

Gao, Y.-Q., Jimenez-Sandoval, P., Tiwari, S., Stolz, S., Wang, J., Glauser, G., Santiago, J. and Farmer, E.E. (2023) Ricca's factors as mobile proteinaceous effectors of electrical signaling. *Cell*, 1–15. Available at: http://www.ncbi.nlm.nih.gov/pubmed/36870332.

Geiger, D., Scherzer, S., Mumm, P., et al. (2010) Guard cell anion channel SLAC1 is regulated by CDPK protein kinases with distinct Ca^{2+} affinities. *Proc Natl Acad Sci U S A*, **107**, 8023–8028.

Gilroy, S., Białasek, M., Suzuki, N., Górecka, M., Devireddy, A.R., Karpiński, S. and Mittler, R. (2016) ROS, calcium, and electric signals: Key mediators of rapid systemic signaling in plants. *Plant Physiol*, **171**, 1606–1615.

Gilroy, S., Suzuki, N., Miller, G., Choi, W.G., Toyota, M., Devireddy, A.R. and Mittler, R. (2014) A tidal wave of signals: Calcium and ROS at the forefront of rapid systemic signaling. *Trends Plant Sci*, **19**, 623–630. Available at: http://dx.doi.org/10.1016/j.tplants.2014.06.013.

Govorunova, E.G., Sineshchekov, O.A., Janz, R., Liu, X. and Spudich, J.L. (2015) Natural light-gated anion channels: A family of microbial rhodopsins for advanced optogenetics. , **349**, 647–651.

Green, M.N., Gangwar, S.P., Michard, E., et al. (2021) Structure of the *Arabidopsis thaliana* glutamate receptor-like channel GLR3.4. *Mol Cell*, **81**, 3216-3226.e8.

Haswell, E.S., Peyronnet, R., Barbier-Brygoo, H., Meyerowitz, E.M. and Frachisse, J.M. (2008) Two MscS Homologs Provide Mechanosensitive Channel Activities in the *Arabidopsis* Root. *Current Biology*, **18**, 730–734.

Hedrich, R. and Becker, D. (1994) Green circuits - The potential of plant specific ion channels. *Plant Mol Biol*, **26**, 1637–1650.

Hedrich, R. and Geiger, D. (2017) Biology of SLAC1-type anion channels - from nutrient uptake to stomatal closure. *New Phytologist*.

Hedrich, R. and Kreuzer, I. (2023) Demystifying the Venus flytrap action potential. *New Phytologist*, **239**, 2108–2112.

Hedrich, R., Salvador-Recatalà, V. and Dreyer, I. (2016a) Electrical Wiring and Long-Distance Plant Communication. *Trends Plant Sci*, **21**, 376–387. Available at: http://dx.doi.org/10.1016/j.tplants.2016.01.016.

Hedrich, R., Salvador-Recatalà, V. and Dreyer, I. (2016b) Electrical Wiring and Long-Distance Plant Communication. *Trends Plant Sci*, **21**, 376–387. Available at: http://dx.doi.org/10.1016/j.tplants.2016.01.016.

Hosy, E., Vavasseur, A., Mouline, K., et al. (2003) The *Arabidopsis* outward K^+ channel GORK is involved in regulation of stomatal movements and plant transpiration. *Proceedings of the National Academy of Sciences*, **100**, 5549–5554.

Howe, G.A. and Jander, G. (2008) Plant immunity to insect herbivores. *Annu Rev Plant Biol*, **59**, 41–66.

Huang, H., St.-Jean, H., Coady, M.J. and Lapointe, J.Y. (1995) Evidence for coupling between Na^+ pump activity and TEA-sensitive K^+ currents in *Xenopus laevis* oocytes. *J Membr Biol*, **143**, 29–35.

Huang, S., Ding, M., Roelfsema, M.R.G., et al. (2021) Optogenetic control of the guard cell membrane potential and stomatal movement by the light-gated anion channel GtACR1. *Sci Adv*, **7**, 1–12.

Huang, S. and Hedrich, R. (2023) Trigger hair thermoreceptors provide for heat-induced calcium-electrical excitability in Venus flytrap. *Current Biology*, **33**, 3962-3968.e2. Available at: https://doi.org/10.1016/j.cub.2023.07.069.

Iosip, A.L., Bo, J., Id, D.B., Id, I.K., Hedrich, R. and Id, I.D. (2020) The Venus flytrap trigger hair – specific potassium channel KDM1 can reestablish the K + gradient required for hapto-electric signaling. , 1–29.

Kew, J.N.C. and Kemp, J.A. (2005) Ionotropic and metabotropic glutamate receptor structure and pharmacology. *Psychopharmacology (Berl)*, **179**, 4–29.

Kim, J.Y., Symeonidi, E., Pang, T.Y., et al. (2021) Distinct identities of leaf phloem cells revealed by single cell transcriptomics. *Plant Cell*, **33**, 511–530.

Kisnieriene, V., Lapeikaite, I., Pupkis, V. and Beilby, M.J. (2019) Modeling the action potential in characeae Nitellopsis obtusa: Effect of saline stress. *Front Plant Sci*, **10**, 1–15.

Koselski, M., Trebacz, K., Dziubinska, H. and Krol, E. (2008) Light- and dark-induced action potentials in *Physcomitrella patens. Plant Signal Behav*, **3**, 13–18.

Kumari, A., Chételat, A., Nguyen, C.T. and Farmer, E.E. (2019) *Arabidopsis* H^+-ATPase AHA1 controls slow wave potential duration and wound-response jasmonate pathway activation. *Proc Natl Acad Sci U S A*, **116**, 20226–20231.

Kupisz, K., Dziubińska, H. and Trębacz, K. (2017) Generation of action potential-type changes in response to darkening and illumination as indication of the plasma membrane proton pump status in *Marchantia polymorpha*. *Acta Physiol Plant*, **39**.

Kuruma, A. and Hartzell, H.C. (1999) Dynamics of calcium regulation of chloride currents in *Xenopus* oocytes. *Am J Physiol Cell Physiol*, **276**, 161–175.

Lacombe, B. and Achard, P. (2016) Long-distance transport of phytohormones through the plant vascular system. *Curr Opin Plant Biol*, **34**, 1–8. Available at: http://dx.doi.org/10.1016/j.pbi.2016.06.007.

Lapeikaite, I., Dragunaite, U., Pupkis, V., Ruksenas, O. and Kisnieriene, V. (2019) Asparagine alters action potential parameters in single plant cell. *Protoplasma*, **256**, 511–519.

Lapeikaite, I., Pupkis, V., Neniskis, V., Ruksenas, O. and Kisnieriene, V. (2020) Glutamate and NMDA affect cell excitability and action potential dynamics of single cell of macrophyte *Nitellopsis obtusa*. *Functional Plant Biology*, **47**, 1032–1040.

Lim, C.W., Kim, S.H., Choi, H.W., Luan, S. and Lee, S.C. (2019) The shaker type potassium channel, gork, regulates abscisic acid signaling in *Arabidopsis*. *Plant Pathol J (Faisalabad)*, **35**, 684–691.

Liu, K., Li, L. and Luan, S. (2006) Intracellular K^+ sensing of SKOR, a Shaker-type K^+ channel from *Arabidopsis*. *Plant Journal*, **46**, 260–268.

Maksaev, G. and Haswell, E.S. (2011) Expression and characterization of the bacterial mechanosensitive channel MscS in *Xenopus laevis* oocytes. *Journal of General Physiology*, **138**, 641–649.

Maksaev, G. and Haswell, E.S. (2012) MscS-Like10 is a stretch-activated ion channel from *Arabidopsis thaliana* with a preference for anions. *Proc Natl Acad Sci U S A*, **109**, 19015–19020.

Malone, M. (1996) *Rapid, Long-distance Signal Transmission in Higher Plants* J. A. Callow, ed., Academic Press.

Malone, M. and Stankovic, B. (1991) Surface potentials and hydraulic signals in wheat leaves following localized wounding by heat. *Plant Cell Environ*, **14**, 431–436.

Marhavý, P., Kurenda, A., Siddique, S., et al. (2019) Single-cell damage elicits regional, nematode-restricting ethylene responses in roots. *EMBO J*, **38**.

Meyer, A.J. and Weisenseel, M.H. (1997) Wound-induced changes of membrane voltage, endogenous currents, and ion fluxes in primary roots of maize. *Plant Physiol*, **114**, 989–998.

Meyer, S., Mumm, P., Imes, D., et al. (2010) AtALMT12 represents an R-type anion channel required for stomatal movement in *Arabidopsis* guard cells. *Plant Journal*, **63**, 1054–1062.

Miledi, R. (1982) A calcium -dependent transient outward current in *Xenopus laevis* oocytes. , **497**, 491–497.

Miller, G., Schlauch, K., Tam, R., Cortes, D., Torres, M.A., Shulaev, V., Dangl, J.L. and Mittler, R. (2009) The Plant NADPH Oxidase RBOHD Mediates Rapid Systemic Signaling in Response to Diverse Stimuli. *Sci Signal*, **2**. Available at: https://www.science.org/doi/10.1126/scisignal.2000448 [Accessed January 21, 2025].

Mittler, R., Vanderauwera, S., Suzuki, N., Miller, G., Tognetti, V.B., Vandepoele, K., Gollery, M., Shulaev, V. and Breusegem, F. Van (2011) ROS signaling: The new wave? *Trends Plant Sci*, **16**, 300–309.

Moe-Lange, J., Gappel, N.M., Machado, M., et al. (2021) Interdependence of a mechanosensitive anion channel and glutamate receptors in distal wound signaling.

Mousavi, S.A.R., Chauvin, A., Pascaud, F., Kellenberger, S. and Farmer, E.E. (2013) GLUTAMATE RECEPTOR-LIKE genes mediate leaf-to-leaf wound signalling. *Nature*, **500**, 422–426. Available at: http://dx.doi.org/10.1038/nature12478.

Mumm, P., Imes, D., Martinoia, E., Al-Rasheid, K.A.S., Geiger, D., Marten, I. and Hedrich, R. (2013) C-terminus-mediated voltage gating of *Arabidopsis* guard cell anion channel QUAC1. *Mol Plant*, **6**, 1550–1563. Available at: http://dx.doi.org/10.1093/mp/sst008.

Nagel, G., Ollig, D., Fuhrmann, M., Kateriya, S., Musti, A.M., Bamberg, E. and Hegemann, P. (2002) Channelrhodopsin-1: A Light-Gated Proton Channel in Green Alga*e*, Available at: https://www.science.org.

Nguyen, C.T., Stolz, S., Kurenda, A., Chételat, A. and Farmer, E.E. (2018) Identification of cell populations necessary for leaf-to-leaf electrical signaling in a wounded plant. *Proceedings of the National Academy of Sciences*, **115**, 10178–10183.

Papanatsiou, M., Petersen, J., Henderson, L., Wang, Y., Christie, J.M. and Blatt, M.R. (2019) Optogenetic manipulation of stomatal kinetics improves carbon assimilation,water use, and growth. *Science (1979)*, **363**, 1456–1459.

Pavlovič, A., Jakšová, J. and Novák, O. (2017) Triggering a false alarm: Wounding mimics prey capture in the carnivorous venus flytrap (*Dionaea muscipula*). *New Phytologist*, **216**, 927–938.

Procko, C., Murthy, S.E., Keenan, W.T., et al. (2020) Stretch-activated ion channels identified in the touch-sensitive structures of carnivorous Droseraceae plants. *bioRxiv*, 1–24.

Pupkis, V., Lapeikaite, I., Kavaliauskas, J., Tręb acz, K. and Kisnieriene, V. (2022) Certain calcium channel inhibitors exhibit a number of secondary effects on the physiological properties in *Nitellopsis obtusa*: A voltage clamp approach. *Functional Plant Biology*, **50**, 195–205.

Pyatygin, S.S., Opritov, V.A. and Vodeneev, V.A. (2008) Signaling role of action potential in higher plants. *Russian Journal of Plant Physiology*, **55**, 285–291.

Qi, Z., Stephens, N.R. and Spalding, E.P. (2006) Calcium Entry Mediated by GLR3.3, an *Arabidopsis* Glutamate Receptor with a Broad Agonist Profile. *Plant Physiol*, **142**, 963–971.

Ricca, U. (1926) Transmission of Stimuli in Plants. , **23**, 6–7.

Roelfsema, M.R.G., Hedrich, R. and Geiger, D. (2012) Anion channels: Master switches of stress responses. *Trends Plant Sci*, **17**, 221–229. Available at: http://dx.doi.org/10.1016/j.tplants.2012.01.009.

Salvador-Recatalà, V. (2016) The AKT2 potassium channel mediates NaCL induced depolarization in the root of *Arabidopsis thaliana*. *Plant Signal Behav*, **11**, 1–4. Available at: http://dx.doi.org/10.1080/15592324.2016.1165381.

Sanmartín, M., Rojo, E., Kurenda, A., et al. (2024) GLR-dependent calcium and electrical signals are not coupled to systemic, oxylipin-based wound-induced gene expression in *Marchantia polymorpha*. *New Phytologist*.

Scherzer, S., Böhm, J., Huang, S., et al. (2022) A unique inventory of ion transporters poises the Venus flytrap to fast-propagating action potentials and calcium waves. *Curr Biol*, 1–9. Available at: http://www.ncbi.nlm.nih.gov/pubmed/36087579.

Scherzer, S., Huang, S., Iosip, A., Kreuzer, I., Yokawa, K., AL-Rasheid, K.A.S., Heckmann, M. and Hedrich, R. (2022) Ether anesthetics prevents touch-induced trigger hair calcium-electrical signals excite the Venus flytrap. *Sci Rep*, **12**, 1–10. Available at: https://doi.org/10.1038/s41598-022-06915-z.

Shen, K., Lagrutta, A., Davies, N.W., Standen, N.B., Adelman, J.P. and North, R.A. (1994) [SLo's formation 4 subunits] Tetraethylammonium block about tetrameric channel formation.pdf. , 440–445.

Stanfield, P.R. (1983) Tetraethylammonium ions and the potassium permeability of excitable cells. *Rev Physiol Biochem Pharmacol*, **97**, 1–67.

Stange, A., Hedrich, R. and Roelfsema, M.R.G. (2010) Ca^{2+}-dependent activation of guard cell anion channels, triggered by hyperpolarization, is promoted by prolonged depolarization. *Plant Journal*, **62**, 265–276.

Stanković, B. and Davies, E. (1996) Both action potentials and variation potentials induce proteinase inhibitor gene expression in tomato. *FEBS Lett*, **390**, 275–279.

Stanković, B., Zawadzki, T. and Davies, E. (1997) Characterization of the variation potential in sunflower. *Plant Physiol*, **115**, 1083–1088.

Stephens, N.R., Qi, Z. and Spalding, E.P. (2008) Glutamate Receptor Subtypes Evidenced by Differences in Desensitization and Dependence on the GLR3.3 and GLR3.4 Genes. *Plant Physiol*, **146**, 529–538.

Suda, H., Mano, H., Toyota, M., Fukushima, K., Mimura, T., Tsutsui, I., Hedrich, R., Tamada, Y. and Hasebe, M. (2020) Calcium dynamics during trap closure

visualized in transgenic Venus flytrap. *Nat Plants*, **6**, 1219–1224. Available at: http://dx.doi.org/10.1038/s41477-020-00773-1.

Sukharev, S., Akitake, B. and Anishkin, A. (2007) The Bacterial Mechanosensitive Channel MscS: Emerging Principles of Gating and Modulation. *Curr Top Membr*, **58**, 235–267.

Sukhov, V., Akinchits, E., Katicheva, L. and Vodeneev, V. (2013) Simulation of variation potential in higher plant cells. *Journal of Membrane Biology*, **246**, 287–296.

Sukhov, V., Sukhova, E. and Vodeneev, V. (2018) Long-distance electrical signals as a link between the local action of stressors and the systemic physiological responses in higher plants. *Prog Biophys Mol Biol*. Available at: https://doi.org/10.1016/j.pbiomolbio.2018.11.009.

Tabata, T. and Sibaoka, T. (1987) Conduction velocity and blockage of action potential in chara internodal cells. *Plant Cell Physiol*, **28**, 1187–1194.

Tokimasa, T. and North, R.A. (1996) Effects of barium, lanthanum and gadolinium on endogenous chloride and potassium currents in *Xenopus* oocytes. *Journal of Physiology*, **496**, 677–686.

Toyota, M., Spencer, D., Sawai-toyota, S., Jiaqi, W. and Zhang, T. (2018) Glutamate triggers long-distance, calcium-based plant defense signaling. , **6**, 1112–1115.

Tran, D., Dauphin, A., Meimoun, P., et al. (2018) Methanol induces cytosolic calcium variations, membrane depolarization and ethylene production in *Arabidopsis* and tobacco. *Ann Bot*, **122**, 849–860.

Trebacz, K. and Sievers, A. (1998) Action potentials evoked by light in traps of *Dionaea muscipula* ellis. *Plant Cell Physiol*, **39**, 369–372.

Umrath, K. (1932) Der erregungsvorgang bei nitella mucronata.

Vodeneev, V., Akinchits, E. and Sukhov, V. (2015) Variation potential in higher plants: Mechanisms of generation and propagation. *Plant Signal Behav*, **10**, 1–7.

Vodeneev, V., Orlova, A., Morozova, E., Orlova, L., Akinchits, E., Orlova, O. and Sukhov, V. (2012) The mechanism of propagation of variation potentials in wheat leaves. *J Plant Physiol*, **169**, 949–954. Available at: http://dx.doi.org/10.1016/j.jplph.2012.02.013.

Vodeneev, V.A., Opritov, V.A. and Pyatygin, S.S. (2006) Reversible changes of extracellular pH during action potential generation in a higher plant Cucurbita pepo. *Russian Journal of Plant Physiology*, **53**, 481–487.

Vriese, K. De, Costa, A., Beeckman, T. and Vanneste, S. (2018) Pharmacological strategies for manipulating plant Ca^{2+} signalling. *Int J Mol Sci*, **19**.

Wang, F.L., Tan, Y.L., Wallrad, L., et al. (2021) A potassium-sensing niche in *Arabidopsis* roots orchestrates signaling and adaptation responses to maintain nutrient homeostasis. *Dev Cell*, **56**, 781-794.e6.

Watanabe, K., Hashimoto, K., Hasegawa, K., Shindo, H., Kipisz, K., Koselski, M., Wasko, P., Trebacz, K. and Kachitsu, K. (2023) Rapid propagation of Ca^{2+} waves and electrical signals in a liverwort *Marchantia polymorpha*. , 31–41.

Weber, W.M. (1999) Endogenous ion channels in oocytes of *Xenopus laevis*: Recent developments. *Journal of Membrane Biology*, **170**, 1–12.

Wudick, M.M., Portes, M.T., Michard, E., et al. (2018) CORNICHON sorting and regulation of GLR channels underlie pollen tube Ca^{2+} homeostasis. *Science (1979)*.

Yan, C., Gao, Q., Yang, M., Shao, Q., Xu, X., Zhang, Y. and Luan, S. (2024) Ca^{2+}/calmodulin-mediated desensitization of glutamate receptors shapes plant systemic wound signalling and anti-herbivore defence. *Nature Plants* .

Yang, T., Kurenda, A., Farmer, E.E. and Chetelat, A. (2023) Mechanosensation in leaf veins. , 1–13.

Yang, X. and Sachs, F. (1990) Characterizatio of strech-activated ion channels in *Xenopus* oocytes. , 103–122.

Yang, X.C. and Sachs, F. (1989) Block of stretch-activated ion channels in *Xenopus* oocytes by gadolinium and calcium ions. *Science (1979)*, **243**, 1068–1071.

Yu, B., Wu, Q., Li, X., Zeng, R., Min, Q. and Huang, J. (2022) GLUTAMATE RECEPTOR-like gene OsGLR3.4 is required for plant growth and systemic wound signaling in rice (Oryza sativa). *New Phytologist*, **233**, 1238–1256.

Zhou, Y., Ding, M., Gao, S., et al. (2021) Optogenetic control of plant growth by a microbial rhodopsin. *Nat Plants*, **7**. Available at: http://dx.doi.org/10.1038/s41477-021-00853-w.

Final remarks

In the current work I delve into plant long-distance, electric signaling in response to wounding from its fundamental composing mechanisms: signal propagation and generation. Initially I present the physiological framework to understand how these two mechanisms can function independently, or be tightly interlinked in the form of self-generating signals. Next, I present the experimental work done in the group for testing the main, current hypotheses regarding electric signaling in the context of leaf wounding.

Focusing on signal propagation, we challenged the hypothesis that *Arabidopsis* leaves can sustain voltage-dependent electric signals as a mean of sustaining a self-propagating electric signal. For this we characterized and used the optogenetic tools recently developed in plants. The evidence shows that leaves cannot sustain a voltage-activated, but rather can sustain a Ca^{2+}-activated, self-propagating electric signal. This finding hints a lack of functional, voltage-dependent Ca^{2+} conductance, and rather posits the existence of a Ca^{2+} -dependent molecular circuitry that can sustain actively self-propagating signals. It is possible that the propagating signal we observed is sustained by the ROS-Ca^{2+}-pH feedback loop, originally described by Miller *et al*. (2009). This ought to be experimentally tested.

Furthermore, we tested how the propagation of molecular flow in the leaves coincide with the propagation of the electric signal. With this approach we aimed to shed light on how the propagation of chemical cues necessary to activate the wound-induced SWP is related to the occurrence of the electric signal. The arrival of that molecular flow to the non-wounded leaf closely coincides with the first voltage deflection. The implication of this early arrival of chemical cues can conduct to hypothesize the existence of a relay that delays the hydraulic wave in the interleaf node; and also, the occurrence of chemical modulation of the Ca^{2+} -dependent self-propagating signal presented earlier.

In the process of testing these main hypotheses, we also contributed to the general understanding of plant electric signaling. We showed how the plant tissue is conductive

to externally generated electric signals, but tissue-generated electric signals are tightly compartmentalized by a yet unknown mechanism. We also visualize for the first time that the different components of the SWP propagate at different speeds, probably indicating the parallel function of different propagating mechanisms. Equally important, we developed an experimental and analytical framework for high-throughput screening of SWP generation-related genes.

Overall, this work sheds light on the propagation mechanisms of electric signals in general, and of *Arabidopsis* wound-induced SWP in particular. Moreover, it provides the field with a subtly clearer framework, and a set of questions and tools to progress in the pursue of understanding the physiology of plant electric, and long distance signaling.

Acknowledgements

I am deeply thankful for all the masterful teachers I found. This work is fruit of their expertise, patience and teachings.

Special mention to Micha for infinite ideas, dedication, and genetic crosses, to Fatiha for helping me hit the ground running, to Eleni for the guidance and Manan for the fun collaboration, to Manolo the GreenGate master, to Nora for fair advices, to Moritz my ephys buddy, to Diana, Britta, Melissa, Ronja, Nicoline and Lisa for actually running this lab, to Waldemar and Marcel for their art, to Kirill for the memes and precious questions, to Laurita, Tom and Meik for the h^5u, to Haoyu for learning so fast, to Susanne für die Deutschübungen, to Yuuma for the wisdom and discussions, to Eliza for the sharp eye, to Jona for defending first, to Wolf for funding and round tables, to Ana for saving me from biochemistry, to Marriah for the energy and the bread, to Jacob for the rice, and Andrea for the chicken, to Hiroko for managing everything, everywhere, all at once, and all those who I might forget now.